

Department of Neurology

Faculty2: Medicine Clinical Medicine

Saarland University Medical Center, Homburg/Saar

**The role and mechanism of innate immune molecules in
Alzheimer's disease and cerebrovascular disorders**

Dissertation for the degree of

Doctor of Medicine and Natural Sciences (MD/PhD)

Faculty of Medicine

SAARLAND UNIVERSITY

2021

Submitted by Wenqiang Quan

Born on August 22, 1985 in Shaanxi, P. R. China

Aus der Klinik für Neurologie

Klinische Medizin der Medizinischen Fakultät

Universitätsklinikum des Saarlandes (UKS), Homburg/Saar

*Dissertation zur Erlangung des Grades eines
Doktors der Medizin und der Naturwissenschaften (MD/PhD)*
der Medizinischen Fakultät

der UNIVERSITÄT DES SAARLANDES

2021

vorgelegt von Wenqiang Quan

geb. Am 22. August 1985 in in Shaanxi, V. R. China

To

My Dear wife Ying Zheng



Daughter Zhenghao Quan

Declaration

I hereby declare that this thesis is my own original work and effort. All experiments, except for those specified, were exclusively performed by me. Except for the publications written by myself listed in the publication list, the data presented here have not been submitted anywhere else for any award. Where other sources of information and help have been used, they have been indicated and acknowledged.

Homburg/Saar, 05.07.2021

Wenqiang Quan

Wenqiang Quan

Tag der Promotion: 16.11.2021

Dekan: Prof. Dr. M. D. Menger

Berichterstatter: Prof. M. Laschke

Prof. K. Faßbender

ABBREVIATIONS

A β	Amyloid β -peptide
ABCA7	ATP binding cassette subfamily A member 7
ABCB1	ATP binding cassette subfamily B member 1
ACE	Angiotensin-converting enzyme
AD	Alzheimer's disease
AKT	Protein kinase B, PKB
ALK5	Activin-like kinase-5
AMPA	α -Amino-3-hydroxy-5-methyl-4-isoxazolepropionic acid
ANOVA	Analysis of Variance
APP	Amyloid precursor protein
APOE	Apolipoprotein E
ARE	AU-rich element
BACE	β -site APP-cleaving enzyme
BBB	Blood-brain barrier
bFGF	basis fibroblast growth factor
BMDM	Bone marrow derived macrophages
bp	Base pair
BSA	Bovine serum albumin
BLC10	B-cell lymphoma/leukemia 10
CAA	Cerebral amyloid angiopathy
CARMA1	CARD-containing MAGUK protein 1
CCL-2	Chemokine (C-C motif) ligand 2
CCR-2	Chemokine (C-C motif) receptor 2
Clec7a	C-type lectin domain family 7 member A
CD	Cluster of differentiation
CD13/APN	Aminopeptidase N
CD33	Myeloid Cell Surface Antigen CD33
cDNA	Complementary deoxyribonucleic acid
Chi3l3	Chitinase-like 3
CNS	Central nervous system
Ct	Threshold cycle
CTF	C-terminal fragment
Cx3cr1	CX3C chemokine receptor 1
Da	Dalton
DAM	Disease-associated microglia
DMEM	Dulbecco's Modified Eagle Medium
DMSO	Dimethyl sulfoxide
DNA	Deoxyribonucleic acid
dsDNA	Double-strand deoxyribonucleic acid
dsRNA	Double-stranded RNA
<i>e.g.</i>	<i>exempli gratia</i> , for example
ECE	Endothelin-converting enzyme
EDTA	Ethylene diamine tetraacetic acid

ELISA	Enzyme-linked immunosorbent assay
ERK	Extracellular-signal-regulated kinase
FACS	Fluorescence-activated cell sorting
FBS	Fetal bovine serum
g	Gram
GAPDH	Glyceraldehyde 3-phosphate dehydrogenase
GFP	Green fluorescence protein
Gua-HCl	Guanidine chloride buffer
GSK-3 β	Glycogen synthase kinase-3 β
HBPC	Human primary brain vascular pericytes
HBSS	Hanks' balanced salt solution
H ₂ O ₂	Hydrogen peroxide
Iba-1	Ionized calcium-binding adaptor molecule 1
IDE	Insulin-degrading enzyme
IgG	Immunoglobulin G
IGF-1	Insulin growth factor
IL-10	Interleukin-10
IL-18	Interleukin-18
IL-1 β	Interleukin-1 β
IKK	I- κ B kinase
iNOS	Inducible nitric oxide synthase
IP3R	Inositol trisphosphate receptor
IRAK	Interleukin-1 Receptor-Associated Kinase
IRS1	Insulin-receptor substrate-1
IS	Immunological synapse
kb	Kilo base pairs
kDa	Kilodalton
KO/ ko	knock out
KPI	Kunitz-type protease inhibitor
LAL	Limulus Amebocyte Lysate
LPS	Lipopolysaccharides
LTD	Long-term depression
LTP	Long-term potentiation
L-VGCC	L-type voltage-gated Ca ²⁺ channels
m	Micro
M	Molar
MAL	MyD88-adaptor-like
MAPKs	Mitogen Activated Protein (MAP) kinases
MCC950	NLRP3 inflammasome inhibitor
MEKK	MAP kinase kinase kinase
mFI	Mean fluorescence intensity
min	Minute
MMP	Matrix metalloproteinase
mrc1	Mannose receptor C type 1
mTOR	The mammalian target of rapamycin
MUNC18-1	Mammalian uncoordinated18-1

MyD88	Myeloid Differentiation Factor 88
NC	Nitrocellulose
NEP	Neprilysin
NF- κ B	Nuclear Factor kappa B
NLRP3	NOD-like receptor family, pyrin domain containing 3
NMDA	N-Methyl-D-aspartic acid
NO	Nitric oxide
O. D.	Optical density
PAMPs	Pathogen-associated molecular patterns
PBS	Phosphate-Buffered Saline
PCR	Polymerase chain reaction
PDGFR β	Platelet-derived growth factor receptor beta
PEG	Polyethylene glycol
PET	Positron emission tomography
PFA	Paraformaldehyde
PKC	Protein kinase C
PLC	Phosphoinositide phospholipase C
PLCG2	Phospholipase C gene 2
PLC γ 2	Phospholipase C gamma 2
PMSF	Phenylmethylsulfonyl fluoride
p2ry12	Purinergic receptor P2Y12
PPAR	Peroxisome proliferator-activated receptor
PRRs	Pattern recognition receptors
PPIA	Peptidyl-prolyl cis-trans isomerase A
PSD-95	Postsynaptic density protein-95
PVDF	Polyvinylidene difluoride
RAGE	Receptor for advanced glycation end products
RIP1	Receptor-Interacting Protein kinase 1
RNA	Ribonucleic acid
RNase	Ribonuclease
ROS	Reactive oxygen species
rpm	Revolution(s) per minute
PrP	Prion Protein
RT-PCR	Reverse transcription PCR
SD	Standard deviation
SDS-PAGE	Sodium dodecyl sulfate-polyacrylamide gel electrophoresis
sec	Second
SEM	Standard error of the mean
SMADs	Sma and Mad related proteins
SNAP-25	synaptosome-associated protein 25
SR-A	Scavenger receptors, Class A
TAB	TAK binding protein
TAK	Transforming-growthfactor- β -activated kinase
Taq	Thermus aquaticus
TBS	Tris buffer with salt
TCR	T-cell receptor

TEMED	Tetramethylethylenediamine
TFP	Tomato fluorescent protein
TGF	Transforming growth factor
TGF β	Transforming-growth factor- β
TGF β R1	Transforming growth factor β receptor 1
TIRAP	TIR-associated protein
TLRs	Toll-like receptors
TNF- α	Tumor necrosis factor- α
TNFR	TNF- α receptor
TPP	Tristetraprolin
TRADD	TNF receptor type 1-associated death domain protein
TRAF	TNF receptor-associated factor
TRAM	TRIF-related adaptor molecule
TREM2	Triggering receptor expressed on myeloid cells 2
TRIF	TIR-domain-containing adaptor inducing IFN- β
Tris	Tris-(hydroxymethyl)-aminomethane
TSC	Tuberous sclerosis
UV	Ultraviolet
V	Volt
VEGF	Vascular endothelial growth factor
WB	Western blot
WT/wt	Wild type
% (v/v)	Volume/volume percentage solution
% (w/v)	Weight/volume percentage solution

CONTENT

ABSTRACT	1
ZUSAMMENFASSUNG	3
PART I Haploinsufficiency of microglial MyD88 ameliorates Alzheimer’s pathology and vascular disorders in APP/PS1-transgenic mice	6
1. INTRODUCTION	7
1.1. <i>Alzheimer’s disease: Overview</i>	7
1.2. <i>Pathophysiology of AD and Aβ</i>	9
1.3. <i>Microglia in AD pathogenesis</i>	17
1.4. <i>Innate immune signalling in AD</i>	21
2. AIM OF THIS WORK	26
3. MATERIALS AND METHODS	27
3.1. <i>Materials</i>	27
3.1.1. <i>Instruments</i>	27
3.1.2. <i>Experimental material</i>	28
3.1.3. <i>Chemicals</i>	30
3.1.4. <i>Kits</i>	32
3.1.5. <i>Oligonucleotides</i>	33
3.1.6. <i>Antibody</i>	33
3.1.7. <i>Buffer</i>	36
3.1.8. <i>Mice and Cross-breeding</i>	38
3.2. <i>Methods</i>	39
3.2.1. <i>Culture of pericytes</i>	39
3.2.2. <i>Pericyte treatments</i>	40
3.2.3. <i>Positive selection of CD11b-positive microglia in the adult mouse brain</i>	40
3.2.4. <i>Morris water maze test</i>	42
3.2.5. <i>Tissue collection</i>	43
3.2.6. <i>Isolation blood vessels of mice brain</i>	44
3.2.7. <i>Quantify vasculature of mice brain</i>	48

3.2.8. Immunohistochemistry for A β staining.....	49
3.2.9. Immunofluorescent staining.....	51
3.2.10. Brain homogenates.....	53
3.2.11. Bio-Rad Protein Assay.....	53
3.2.12. Western blot analysis.....	53
3.2.13. Protein detection using immunoblotting.....	55
3.2.14. Purification of membrane components and β - and γ -secretase activity assays.....	56
3.2.15. Reverse transcription and quantitative PCR for analysis of gene transcripts.....	57
4. RESULTS.....	62
4.1. Establishment of APP/PS1-transgenic mice with haploinsufficiency of MyD88 in microglia.....	62
4.2. Haploinsufficiency of microglial MyD88 improves cognitive function of APP/PS1-transgenic mice....	63
4.3. Haploinsufficiency of microglial MyD88 preserves synaptic proteins in APP/PS1-transgenic mice....	65
4.4. Haploinsufficiency of microglial MyD88 reduces A β load in the brain parenchyma of APP/PS1-transgenic mice.....	66
4.5. Haploinsufficient expression of MyD88 in microglia reduces A β load in the brain blood vessels of APP/PS1-transgenic mice.....	68
4.6. Haploinsufficient expression of MyD88 in microglia inhibits pro-inflammatory activation in APP/PS1-transgenic mouse brain.....	69
4.7. Haploinsufficient expression of MyD88 suppressed pro-inflammatory activation in microglia but enhanced microglial responses to A β in APP/PS1-transgenic mouse brain.....	71
4.8. Haploinsufficiency of microglial MyD88 in microglia increases cerebral vasculature of APP/PS1-transgenic mice.....	73
4.9. Haploinsufficiency of microglial MyD88 increases cerebral vasculature of APP/PS1-transgenic mice	74
4.10. Haploinsufficiency of MyD88 in microglia increases LRP1 at BBB of APP/PS1-transgenic mice.....	75
4.11. IL-1 β treatment decreases LRP1 in cultured pericytes.....	76
5. DISCUSSION.....	80
PART II NLRP3 deficiency differently regulates cerebral vasculature under physiological and pathological conditions.....	86
1. INTRODUCTION.....	87
1.1 The vascular pathogenesis of Alzheimer's disease.....	87
1.2 The function of cerebrovascular pericytes in the pathogenesis of AD.....	88
1.3 NLRP3 inflammasome.....	89
1.4 NLRP3 is involved in AD pathogenesis.....	91

1.5 NLRP3 and Pericytes.....	92
2. MATERIALS AND METHODS.....	94
2.1 Materials.....	94
2.2 Methods.....	94
2.1.1. Mice and Cross-breeding.....	94
2.1.2. Tissue collection and isolation of blood vessels.....	94
2.1.3. Histological image acquisition and analysis.....	95
2.1.4. Western blot analysis of PDGFR β and CD13 in cerebral blood vessels.....	95
2.1.5. Culture of pericytes.....	96
2.1.6. Analysis of pericyte proliferation and apoptosis.....	96
2.1.7. Treatments of pericytes for detection of PDGFR β and CD13 and phosphorylated AKT, ERK and NF κ B p65.....	97
2.1.8. Flow cytometric analysis of innate immune receptors in pericytes.....	97
2.1.9. Statistics.....	98
3. RESULTS.....	99
3.1 NLRP3 deficiency reduces pericyte cell coverage and decreases protein levels of PDGFR β and CD13 in the Brain.....	99
3.2 NLRP3 deficiency reduces vasculature in the brain.....	101
3.3 NLRP3 inhibition attenuates cell proliferation in cultured pericytes.....	102
3.4 NLRP3 inhibition attenuates expression of PDGFR β and CD13 in cultured pericytes.....	103
3.5 IL-1 β increases protein expression of PDGFR β and CD13 in cultured pericytes.....	104
3.6 Deficiency of NLRP3 increases pericytes and vasculature in the brain of Tau-transgenic AD mice....	106
3.7 Deletion of MyD88 specifically in pericytes attenuates amyloid pathology in APP/PS1-transgenic mice108	
3.8 Deficiency of MyD88 in pericytes attenuates AD-associated pathology in APP-transgenic mice.....	109
4. DISCUSSION.....	111
REFERENCES.....	114
LIST OF FIGURES AND COOPERATIONS.....	139
ACKNOWLEDGEMENTS.....	145

ABSTRACT

Alzheimer's disease (AD) is characterized by extracellular amyloid- β (A β) deposits, intracellular accumulation of tau filaments and microglia-dominated inflammatory activation. Growing evidence indicates that innate immune signaling (including MyD88 or NLRP3-mediated signaling cascade), controls microglial inflammatory activities and A β clearance. However, their effects on amyloid pathology and neurodegeneration remain inconclusive and the underlying pathogenic mechanisms are still unclear.

This thesis research mainly consists of two parts:

1) Haploinsufficiency of microglial MyD88 ameliorates Alzheimer's pathology and vascular disorders in APP/PS1-transgenic mice. We conditionally knocked out *myd88* gene specifically in microglia of APP/PS1-transgenic mice by 6 months and analyzed AD-associated pathologies by 9 months. We observed that deletion of MyD88 in microglia reduced the number of microglia in the brain and transcription of pro-inflammatory genes, e.g. *tnf- α* and *il-1 β* , in both brain tissues and individual microglia, which was correlated with a decrease of cerebral A β load and improvement of cognitive function. As potential mechanisms, MyD88 deficiency in microglia increased microglial recruitment toward A β deposits, increased vasculature and elevated protein expression of LRP1 in cerebral capillaries in APP/PS1-transgenic mice. Cell culture experiments further showed that treatments with interleukin-1 β decreased LRP1 expression in pericytes, a group of cells wrapping around endothelial cells in capillaries. In summary, deletion of MyD88 in microglia at a late disease stage attenuates pro-inflammatory activation and amyloid pathology, and perhaps prevents the impairment of microvasculature and LRP1-mediated A β clearance in the brain of APP/PS1-transgenic mice, all of which protects neurons and improves cognitive function of AD mice.

2) NLRP3 regulates the coverage and activation of pericytes. There is growing evidence showing that cerebral circulation is impaired in AD and cerebrovascular disorders contribute to AD pathogenesis. Pericytes play a central role in regulating structure and function of capillaries in the brain and are damaged in AD. However, molecular mechanisms which drive pericyte proliferation and activation are unclear. In our study, we first investigated the physiological function of NLRP3 in pericytes. We immunostained 9-month-old NLRP3-deficient and wild-

type littermate mice and observed that NLRP3 deficiency reduced PDGFR β -positive pericytes and collagen type IV-immunoreactive vasculature in the brain. In Western blot analysis, NLRP3 deficiency decreased PDGFR β and CD13 proteins in isolated cerebral microvessels. We further treated cultured pericytes with NLRP3 inhibitor, MCC950, and observed that NLRP3 inhibition attenuated cell proliferation. NLRP3 inhibition also decreased protein levels of PDGFR β and CD13 in cultured pericytes. On the contrary, treatments with IL-1 β , the major product of NLRP3-contained inflammasome, increased protein levels of PDGFR β and CD13 in pericytes. The alteration of PDGFR β and CD13 protein levels was correlated with phosphorylation of AKT and inhibition of AKT reduced both protein markers in pericytes. Thus, NLRP3 activation might be essential to maintain pericytes in the brain under a physiological condition.

Interestingly, after we mated human Tau-transgenic mice with NLRP3 knockout mice, we found that deficiency of NLRP3 increased pericytes and vasculature in the brain of Tau-transgenic AD mice, which suggests that NLRP3 might mediate the pathologic changes of pericytes and vasculature under a pathological condition.

In summary, deficiency of microglial MyD88 at a late disease stage inhibits neuroinflammation and improves cognitive function of APP-transgenic AD mice. We have a novel finding that neuroinflammation potentially regulates pericyte proliferation and behaviour through activating innate immune signalling pathways, e.g. NLRP3. Thus, our results contribute to a better understanding of AD pathogenesis and could even offer a new therapeutic target for AD patients.

ZUSAMMENFASSUNG

(Thank Miss Laura Schnöder for translating the English abstract to German)

Die Alzheimer-Krankheit (AD) ist durch extrazelluläre Amyloid- β (A β) Ablagerungen, intrazelluläre Akkumulation von Tau-filamenten und durch Mikroglia-dominierte Aktivierung der Inflammation charakterisiert. Es gibt zunehmend Hinweise darauf, dass Signalwege des angeborenen Immunsystems (einschließlich der MyD88 oder NLRP3-vermittelten Signalkaskade), die inflammatorische Aktivität der Mikroglia und den Abbau von A β kontrollieren. Allerdings ist dabei der Effekt auf die Amyloid Pathologie und Neurodegeneration nicht eindeutig entschlüsselt und die zugrundeliegenden pathogenen Mechanismen sind immer noch unklar.

Diese wissenschaftliche Arbeit fokussiert sich auf zwei Hauptaspekte:

1) Haploinsuffizienz des mikroglialen MyD88 mildert die Alzheimer-Pathologie und vaskuläre Störungen in APP/PS1-transgenen Mäusen. Wir haben das Gen *myd88* spezifisch in Mikroglia von APP/PS1-transgenen Mäusen in einem Alter von sechs Monaten konditionell ausgeschaltet und die AD-assoziierte Pathologie in einem Alter von neun Monaten analysiert. Wir konnten beobachten, dass die mikrogliale Deletion von MyD88 die Anzahl der Mikroglia im Gehirn und die Transkription der pro-inflammatorischen Gene wie *tnf- α* und *il-1 β* , sowohl im Hirngewebe als auch in einzelnen Mikroglia, reduziert. Dies korrelierte mit einer Reduktion des zerebralen A β Gehalts und einer Verbesserung der kognitiven Funktion. Als möglicher Mechanismus konnten wir zeigen, dass eine mikrogliale MyD88 Defizienz die Rekrutierung der Mikroglia zu den A β Ablagerungen erhöht, das Gefäßsystem hinsichtlich Verzweigung der Blutgefäße, Länge und Dichte verbessert und die Proteinexpression von LRP1 in zerebralen Kapillaren der APP/PS1-transgenen Mäuse erhöht. Experimente in Zellkulturen zeigten zudem, dass die Behandlung mit Interleukin-1 β die LRP1 Expression in Perizyten, einer Zellgruppe welche in Kapillaren die Endothelzellen umhüllt, mindert. Zusammenfassend zeigt diese Studie, dass die Deletion von MyD88 in Mikroglia, im späten Krankheitsstadium die pro-inflammatorische Aktivierung und die Amyloid Pathologie mildert und möglicherweise sowohl die Beeinträchtigung der Mikrovaskulatur, als auch die in AD reduzierte LRP1-vermittelte A β

Reinigung, im Gehirn von APP/PS1-transgenen Mäusen aufhebt. Zusammengenommen schützen diese Effekte die Neurone und verbessern die kognitive Funktion der AD Mäuse.

2) NLRP3 reguliert die besiedelte Fläche und Aktivierung von Perizyten. Immer mehr Hinweise deuten darauf hin, dass die zerebrale Zirkulation in AD geschädigt ist und dass zerebrovaskuläre Schädigungen zur AD Pathogenese beitragen. Perizyten spielen bei der Regulierung von Struktur und Funktion der Hirnkapillaren eine zentrale Rolle und sind in AD geschädigt. Die molekularen Mechanismen welche Proliferation und Aktivierung der Perizyten beeinflussen sind allerdings noch unklar. In unserer Studie haben wir zunächst die physiologische Rolle von NLRP3 in Perizyten untersucht. Wir haben Immunfärbungen an neun Monate alten NLRP3-defizienten und Wildtyp-Geschwistermäusen durchgeführt und dabei beobachtet, dass eine Defizienz von NLRP3 die PDGFR β -positiven Perizyten und Collagen Typ IV-positive Gefäße im Hirn reduziert. Western blot Analysen zeigen einen verringerten Proteingehalt von PDGFR β und CD13 in isolierten zerebralen Mikrogefäßen nach Defizienz von NLRP3.

Des Weiteren haben wir kultivierte Perizyten mit dem NLRP3 Inhibitor MCC950 behandelt und konnten beobachten, dass die Inhibition von NLRP3 die Zellproliferation mindert. Zudem verringert eine Inhibition von NLRP3 den Proteingehalt von PDGFR β und CD13 in kultivierten Perizyten. Im Gegensatz dazu erhöhte die Behandlung mit IL-1 β , dem Hauptprodukt der NLRP3-beinhaltenden Inflammasomen, den Proteingehalt von PDGFR β und CD13 in Perizyten. Der veränderte Proteingehalt von PDGFR β und CD13 korrelierte mit der Phosphorylierung von AKT. Die Inhibition von AKT wiederum reduzierte beide Proteinmarker in Perizyten. Daher ist die Aktivierung von NLRP3 möglicherweise notwendig, um Perizyten unter physiologischen Bedingungen im Gehirn zu erhalten.

Interessanterweise konnten wir nach der Verpaarung von NLRP3 defizienten Mäusen mit Mäusen die das humane Tau Protein exprimieren feststellen, dass die Defizienz von NLRP3 die Anzahl der Perizyten sowie die Länge und Dichte der Gefäße im Gehirn der Tau-transgenen AD Mäuse erhöht. Dies lässt vermuten, dass NLRP3 möglicherweise die pathogenen Veränderungen der Perizyten und Gefäße unter pathologischen Bedingungen vermittelt.

Zusammenfassend konnten wir zeigen, dass eine mikrogliale Defizienz von MyD88 im späteren Krankheitsstadium die Neuroinflammation mildert und kognitive Funktion der APP-transgenen Mäuse verbessert. Zudem konnten wir erstmals zeigen, dass die Neuroinflammation die Proliferation der Perizyten und deren Eigenschaft durch Aktivierung der Signalwege des angeborenen Immunsystems wie beispielsweise über NLRP3 reguliert.

Daher tragen unsere Ergebnisse zu einem besseren Verständnis der AD Pathogenese bei wodurch möglicherweise neue therapeutische Ziele für die AD Therapie identifiziert werden können.

**PART I Haploinsufficiency of microglial MyD88 ameliorates
Alzheimer's pathology and vascular disorders in APP/PS1-
transgenic mice**

1. INTRODUCTION

1.1. Alzheimer's disease: Overview

Alzheimer's disease (AD) is a type of irreversible, neurodegenerative disorder that is fast becoming one of the most costly, deadly, and burdensome diseases of this century. Its pathology can progress from asymptomatic to the phase of subjective cognitive decline (SCD), via a stage of mild cognitive impairment (MCI) and eventually leading to overt dementia, and the process may stretch over 15-25 years (Bintener C 2020). In healthy aging, with some degree of brain atrophies but does not lose neurons significantly; however, the damage is extensive in the AD brain as many neurons stop functioning, lose connections to other neurons or even die. AD disrupts processes vital to neurons and their neural networks, including communication, metabolism, and repair. It contributes to the damage or death of neurons involved in memory, learning, and thinking. As a result, losing neurons and their connections leads to the characteristic clinical manifestations of AD, such as difficulties with memory, language, problem-solving, and other thinking skills, which can affect a person's ability to carry out everyday activities (McKhann 2011, figures 2019).

AD is also the most common form of dementia, with someone developing it every 3 seconds in the world. An estimated 50 million people, mostly older than 60 years, live with AD or other dementias worldwide (1.7 million in Germany) (figures 2020). Since the leading risk factor for dementia is age, the continued increase in life expectancy increases the likelihood that more people will develop AD. According to the latest data, the prevalence of dementia will double in Europe and triple worldwide by 2050 (Bintener C 2020). Nowadays, despite a wealth of research available providing detailed information about molecular pathogenic events of AD, yet no curative treatments are available, and we should do more to develop efficient strategies to slow down or halt this dementia.

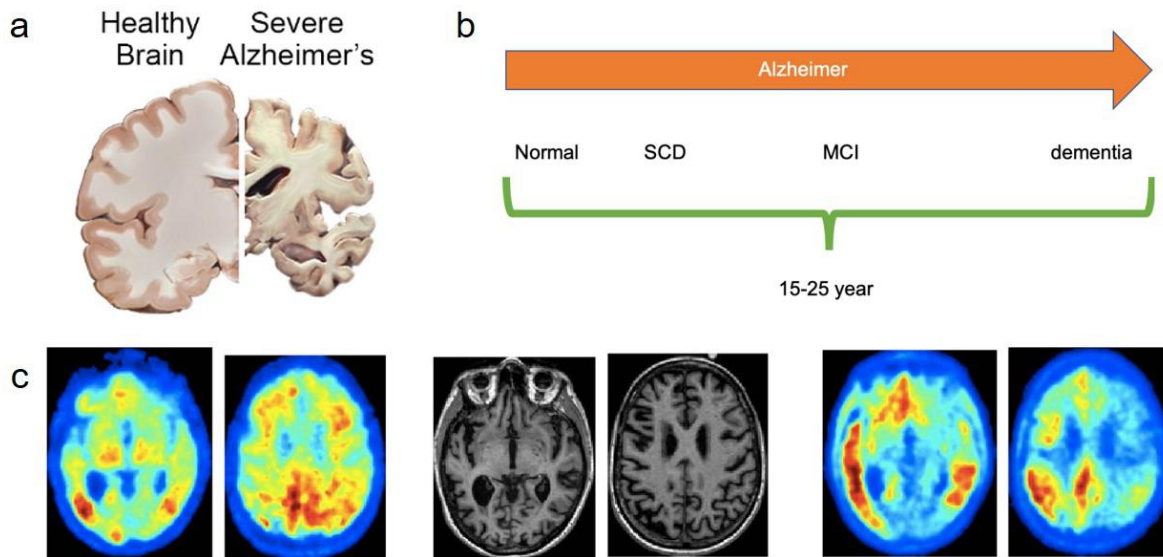


Figure 1.1 Imaging of AD patients. (a) Comparison between normal brain and AD brain. (b) AD is a continuum, stretching over a period of 15-25 years. (c) The T1 weighted MRI images (middle) show generalized cortical atrophy, left >right; Amyloid PET scan using PIB shows amyloid deposition mainly in the posterior cingulate region (left); TAU-PET image using AV1451 tracer showing left inferior temporal lobe, parietal lobe and mild posterior cingulate deposition of tau (right). (Scheltens, De Strooper et al. 2021).

Aging is the most important causative factor in AD. The majority of cases occur after age 65 and are known as late-onset AD (LOAD), while cases that occur between age 30 and mid-60 are pretty rare, just accounting for less than 5% of all cases and are referred to as early-onset AD. The likelihood of developing AD doubles every five years after the age of 65 (Corrada, Brookmeyer et al. 2010). Approximately 70% of the risk of developing AD can be attributed to genetics, and causative genes include PSEN1, PSEN2, APP and Sor11 (Ballard, Gauthier et al. 2011). Genome-wide association studies (GWASs) have identified more than 40 risk genes, which are mostly associated with lipid metabolism (APOE4, CLU, ABCB7), immune response (CR1, CD33, TREM2), and regulation of endocytosis (SORL1, BIN1) (Cacace, Sleegers et al. 2016). Significantly, the APOE ϵ 4 allele, is the most potent genetic risk factor of LOAD. Approximately 25% to 30% of the population carry the APOE ϵ 4 allele, of which the presence of ϵ 4 in heterozygotes increases the risk of AD development 3-fold, while in homozygosis it increased the risk 12-fold. Similarly, variation in the TREM2 gene elevated the risk ratio by 2.9% for AD development. In addition, as AD develops over a long preclinical period of several decades, that a host of acquired factors may play an important role in the development and

course of AD, of particular importance among these factors are cerebrovascular disease, hypertension, as well as metabolic conditions such as diabetes and obesity. Strong evidence showed that the incidence of AD might have decreased as a result of effective interventions for cardiovascular risk in both healthy and cognitively impaired individuals. Based on the Rotterdam study, the seven most important modifiable risk factors eliminated, overweight, hypertension, diabetes mellitus, cholesterol, smoking, and education, would lead to a 30% reduction in the incidence of dementia(de Bruijn, Heeringa et al. 2015).

1.2. Pathophysiology of AD and A β

From the preclinical phase, basic scientists also coin this phase as the cellular phase of AD, widespread neuronal degeneration and synaptic loss discovered in the brain, affecting areas of the brain such as the hippocampus and cortex, eventually resulting in diffuse brain atrophy. A series of molecular and cellular changes in the brain has driven the latent progression of the disease before cognitive impairment is observed, such as the typical pathology of AD: extracellular amyloid β peptide (A β) deposition as neurotic plaques, hyperphosphorylated Tau protein aggregation coalesces to form intracellular neurofibrillary tangles (NTF) along with microglia-dominated inflammatory activation in the brain parenchyma. The predominant view of AD pathogenesis is that the accumulation of A β precipitates the disease process and triggers a deleterious cascade involving tau pathology and neurodegeneration. The buildup of A β in the brain is mainly attributed to increased production or reduced clearance, and in most cases of LOAD there is an imbalance between the intracerebral production of A β and its removal.

1.2.1. Production of A β

In 1985, Masters et al. first identified the A β peptide as the core protein of amyloid plaques (Masters, Multhaup et al. 1985). The produce of A β following sequential cleavage of a larger precursor protein, a large type-I integral membrane protein of 695–770 aa that is APP, by β -secretase (also known as BACE1) and γ -secretase. In nonpathological conditions, APP is degraded by α -secretase, the cleavage between residues 16 and 17, which produce a secreted fragment of 612 aa (sAPP α) along with a cellular fragment of 83 aa residue C-terminal fragment (C83/CTF α) in the membrane, preventing the formation of A β (Bayer, Cappai et al. 1999). While in the amyloidogenic pathway, the APP is subjected to BACE1 cleavage at the N-terminus of A β

sequence, releasing secreted APP β (sAPP β) and the membrane-bound a 99-residue CTF (C99/CTF β) fragment. An intramembrane protease, γ -secretase, following cleavage by BACE1 cleaves CTF β to 4 kDa A β and CTF α to a smaller 3 kDa fragment named P3 or A α (Cole and Vassar 2007). The γ -secretase complex then continues to process the A β C-terminus producing soluble monomeric A β , and the most common subtypes of A β in the human body are A β 1-38, A β 1-40, and A β 1-42. The C-terminus of A β 42 has increased hydrophobicity and therefore a greater propensity for aggregation than other form peptides, A β 42 is considered being especially toxic(Long and Holtzman 2019).

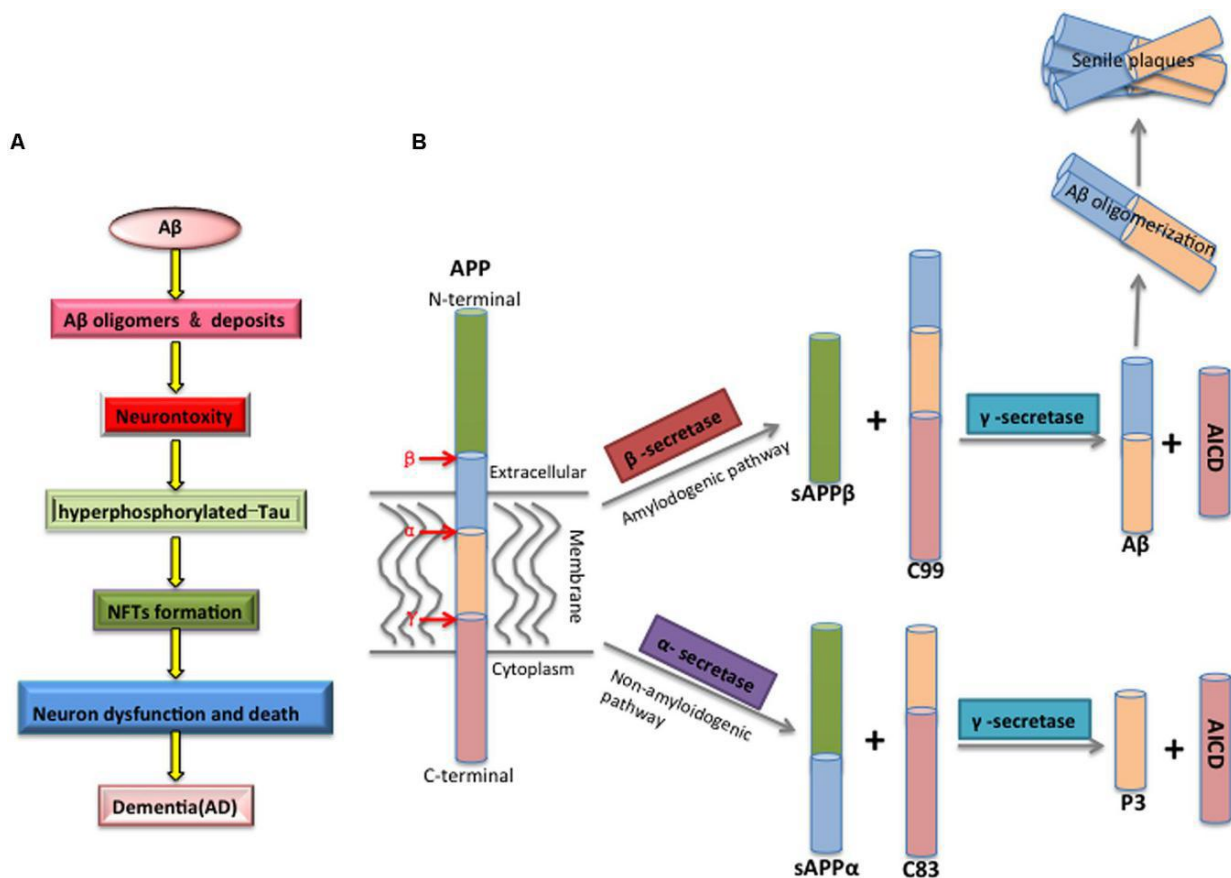


Figure 1.2 APP processing and A β toxicity. (A) Mechanisms of A β toxicity. (B) APP processed through non-amyloidogenic and amyloidogenic pathways In nonpathological conditions, APP is cleaved by α -secretase to produce sAPP- α and C83, c83 is further cleaved by γ -secretase to produce AICD and p3; in the amyloidogenic pathway, APP Cleavage by beta- secretase generates sAPP-beta and C99, then C99 is cleaved by gamma-secretase, generating AICD and A β .(Sun, Chen et al. 2015).

1.2.2. Clearance of A β

A β accumulation is thought to be a trigger, or even a driver, for the pathological process of AD. In general, the production and degradation of A β are in a dynamic equilibrium. Recent studies strongly showed that A β clearance, but not its production, is impaired in AD patients (Wildsmith, Holley et al. 2013). Then the deficient clearance of A β in AD patients can, thus, contribute to its aggregation within the brain. It is now recognized that misfolded or other abnormally modified proteins in the brain, such as A β and Tau, can be eliminated by different clearance mechanisms. The principal pathways that are involved in clearing soluble A β from the brain include 1) enzymatic degradation (Leissring 2016), 2) internalization by glial cells (Tarasoff-Conway, Carare et al. 2015), 3) transportation to the periphery by the blood-brain barrier (BBB) (Zhao, Nelson et al. 2015), and 4) washing-away by interstitial fluid (ISF) bulk-flow along the perivascular space and thereafter by drainage of the meningeal lymphatic system (Engelhardt, Carare et al. 2016, Da Mesquita, Louveau et al. 2018) and cerebrospinal fluid absorption (Baranello, Bharani et al. 2015, Tarasoff-Conway, Carare et al. 2015).

1.2.2.1. Degradation clearance

The majority of intracellular A β is degraded by two main protein clearance mechanisms of the proteostasis network, the ubiquitin-proteasome pathway (UPS) and the autophagy-lysosomal system (Ihara, Morishima-Kawashima et al. 2012). The UPS is a complex enzymatic pathway that is a key component of the proteostasis network to remove damaged proteins. Evidence suggests that the accumulation of hyperphosphorylated tau oligomers at human AD synapses is correlated with an increase in ubiquitinated substrates and proteasomal components, in line with dysfunction of the ubiquitin-proteasome system (Vilchez, Saez et al. 2014, Bellia, Lanza et al. 2019). Both intracellular A β oligomers and aggregated tau proteins inhibit proteasome activity, as evidenced by the significantly lower proteasome activity in AD patients compared to age-matched controls (Keller, Hanni et al. 2000). The autophagic degradation system is an intracellular catabolic process that internalize most extracellular and some cell surface proteins and degraded within lysosomes. Autophagy declines as AD disease progresses, accompanied by maturation of autophagosomes and transport impairment, which results in a large number of autophagic vesicles containing high levels of A β in AD neurons (Yu, Cuervo et al. 2005) Loss-

of-function experiments have shown that autophagy deficiency decimated extracellular A β plaque burden, this reduction was because of the impaired exocytosis which inhibits A β secretion, leading to the accumulation of A β in intracellular vesicles ultimately inducing cell damage and death(Nixon and Yang 2011, Nilsson, Loganathan et al. 2013). In addition, protein aggregation-induced activation of proteasomes or autophagy can further activate macroautophagy, implying there exists an interaction between proteasomes and autophagy(Massey, Kaushik et al. 2006).

Proteases secreted by neurons or astrocytes can also clear extracellular A β , include neprilysin (NEP), insulin-degrading enzyme (IDE), matrix metalloproteinases (MMPs), angiotensin-converting enzyme (ACE), endothelin-converting enzyme (ECE), and plasmin(Miners, Baig et al. 2008). Of these, the most widely studied enzymes are NEP and IDE. NEP, a membrane-bound zinc metalloendopeptidase, is the most efficient hydrolytic enzyme degrading A β (Bulloj, Leal et al. 2008). The fact that the decline in NEP in the brain was associated with increased A β deposition notably supported the role of NEP for the degradation of A β , especially in vulnerable regions such as the hippocampus and mid-temporal gyrus (Yasojima, McGeer et al. 2001, Wang, Iwata et al. 2003). IDE, a zinc-endopeptidase, was initially recognized as the significant proteolysis enzyme for insulin and was the first identified A β -degrading proteases. Both A β and insulin are ligands of IDE, and hyperinsulinemia may induce A β accumulation through competition between them to result in reduced clearance of A β (Gasparini and Xu 2003, Sims-Robinson, Kim et al. 2010). Although IDE is mainly located in the intracellular, reports suggest it may be membrane-associated in neurons and even secreted into the intercellular fluid. Its activity was detected in the medium, implying that it may be also degrade secreted A β (McDermott and Gibson 1997). Wang et al. (Wang, He et al. 2015) demonstrated a link between the IDE gene's polymorphisms and LOAD susceptibility in the Xinjiang Han population. Research in IDE deficiency animals showed a >50% decrease in A β degradation and a chronic elevation of cerebral accumulation of endogenous A β (Farris, Mansourian et al. 2003).

1.2.2.2. Blood-brain barrier clearance

Interstitial proteins also can be cleared to peripheral circulation directly through the BBB. The BBB is mainly composed of endothelial cells and mural perivascular pericyte, and it is a

highly selective barrier between blood and CNS that prevents AD-related proteins such as A β and tau from free into the peripheral circulation(Abbott, Patabendige et al. 2010). Transport A β from the brain to blood must instead be through specialized transporters. High-resolution MRI analysis of regional BBB permeability in the living human brain shown that age-dependent early BBB breakdown in the hippocampus and its CA1 is accelerated in individuals with mild dementia(Montagne, Barnes et al. 2015). Post-mortem human studies have observed the accumulation of blood-derived proteins (e.g., IgG, albumin, fibrin, and thrombin) in the hippocampus and cortex, particularly in individuals carrying APOE4 gene(Halliday, Rege et al. 2016, Montagne, Nation et al. 2020), and degeneration of BBB-associated pericytes(Sengillo, Winkler et al. 2013), suggesting the BBB is damaged in AD. Specifically, some evidence suggests that the low-density lipoprotein receptor-related protein 1 (LRP1), an apolipoprotein E (apoE) receptor, is expressed at the abluminal membrane of the BBB and is a leading efflux transporter that mediates soluble A β clearance through the BBB(Liebner, Dijkhuizen et al. 2018, Ma, Zhao et al. 2018). However, some studies revealed that LRP1 not only acts as an essential mediator for the clearance of extracellular A β , but it also enhances the generation of A β through internalization of the APP, and hence it is amyloidogenic processing(Van Gool, Storck et al. 2019). Another system involved in local soluble A β efflux is ATP-binding cassette (ABC) transporters(Miller 2015, Zhao, Nelson et al. 2015), of which ABCB1 (also known as P-glycoprotein 1 or MDR1) is the main protein responsible for the efflux of A β , which directly exports A β into the circulation. Conversely, free A β in the bloodstream can reenter the brain interstitium via RAGE receptor (advanced glycosylation end product-specific receptor)(Deane, Singh et al. 2012). Studies have revealed that the expression of the blood efflux transporters LRP1(Sweeney, Sagare et al. 2018) and ABCB1(Gil-Martins, Barbosa et al. 2020) is decreased in AD, whereas the blood influx transporter RAGE(Byun, Yoo et al. 2017) is upregulated, these results suggest that removal of A β through BBB is impaired in AD.

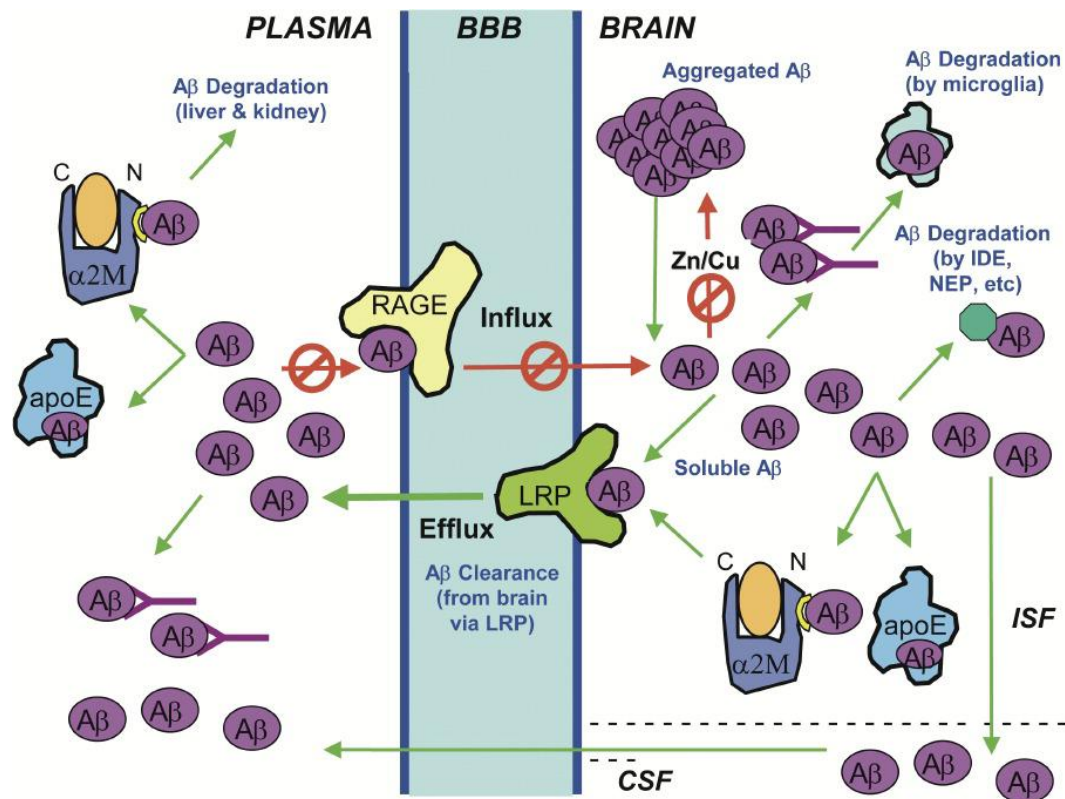


Figure 1.3 Various pathways involved in removal of Aβ in the brain. Soluble Aβ can be cleared from the brain via two main pathways: degradation (phagocytic degradation by activated microglia and peptidase degradation) or transport across the BBB and exported out of the brain into the blood stream. (Tanzi, Moir et al. 2004).

1.2.2.3. Microglial clearance (Discussed in detail in the following sections 1.3)

1.2.2.4. Glymphatic clearance

Although there are no lymphatic vessels lined with endothelial cells in the central nervous system, the lymphatic drainage in the brain clearly exists, which is of great significance for maintaining the physiological functions of the brain. Compared with other organs in the human body, the lymphatic clearance pathway of the brain is different. This is a topic that people have been discussing (Yoo HS, et al. 2020; Thomas JL, et al. 2019). Because of the complex etiology and pathogenesis of AD, the current related research has not made breakthrough progress.

Therefore, new perspectives have been given more attention to the research on the lymphatic drainage pathways in the brain (Natale G, et al. 2021; Silva I, et al. 2021).

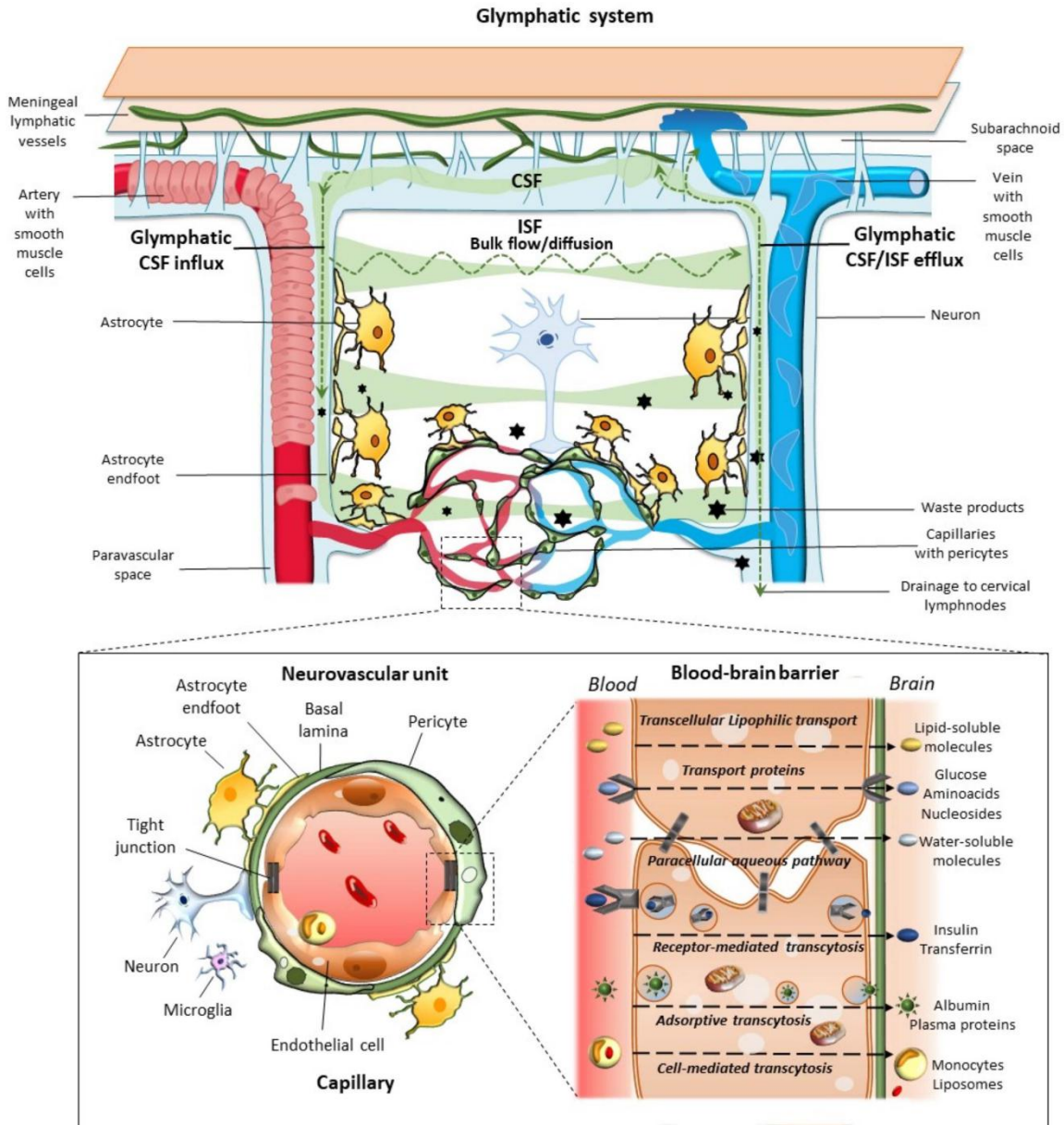


Figure 1.4 Glymphatic system, neurovascular unit (NVU), and the blood-brain-barrier (BBB). The glymphatic system contributes to the transport of nutrients and signaling molecules into the brain parenchyma meanwhile promoting the clearance of proteins and interstitial waste solutes out of the brain. (Natale G, Limanaqi F, Busceti CL, et al. Glymphatic System as a Gateway to Connect Neurodegeneration From Periphery to CNS. *Front Neurosci.* 2021;15:639140.)

Under normal circumstances, the soluble A β produced in the central nervous system can enter the bloodstream, enzyme clearance, cell phagocytosis, and clearance of the perivascular space through receptor-mediated pathways and clear out of the brain in time, without causing A β deposition. When A β is excessively produced or obstructed in removal, it will cause abnormal aggregation to form neurotoxic insoluble fibers. The transport of abnormally aggregated A β fibers across endothelial cells is blocked. At this time, cerebral lymphatic circulation becomes the main way to clear it (Liu Q et al. 2020). In recent years, there has been heated discussion about the lymphatic circulation of the central nervous system. Researchers believed that the discovery of the meningeal lymphatic system is a new development in neurophysiology (Da Mesquita S, et al. 2018). With the increase of age, meningeal lymphatic function damage or obstruction is considered to be an aggravating factor of A β accumulation (Goodman JR, et al. 2018). To clarify the relationship between meningeal lymphatic circulation and cerebrospinal fluid and interstitial fluid, and to start research on related targeted drugs from the protection and repair of damaged meningeal lymphatic system, may be a potential target for the prevention and treatment of AD.

Recent studies indicate that the molecular tracers in the cerebrospinal fluid are mainly discharged from the lymphatic vessels of the meninges, emphasizing the importance of draining lymphatic pathways for clearing molecules from the brain (Satoh JI, et al. 2018; De Luca C, et al. 2018). This research challenges the traditional concept of cerebrospinal fluid homeostasis. It believes that meningeal lymphatic vessels can contact cerebrospinal fluid, under healthy conditions, continuously discharge their molecules and cell contents into the cervical lymph nodes (Cervical lymphnode, CLNs). The reduction in the production and clearance of cerebrospinal fluid is considered to be a contributing factor to the severity of different neuropathological models such as hydrocephalus and ischemia, and leads to the decline of brain function in aging and aging-related neurodegenerative diseases such as AD. With aging, the protein content in cerebrospinal fluid will be increased, and this proportion is even higher in AD patients (Skillbäck T, et al. 2017).

In AD, the situation is further worsened due to amyloid vascular disease in the brain (Montagne A, et al. 2015; Zhao Z, et al. 2015). Several genetic risk factors for late-onset AD, such as apolipoprotein E4 (ApoE4) gene mutation (Silva I, et al. 2021), gene encoding protein

cluster protein and PICALM (Harold D, et al. 2009), single nucleotide polymorphisms, and blood brain Barrier dysfunction is related to impaired A β clearance through blood vessels (Zhao Z, et al. 2015). In AD transgenic mice, Evans blue injected into the brain was detected in deep cervical lymphnode (dCLN), suggests that the cerebral lymphatic system is another way to transport A β from the brain to the periphery (Louveau A, et al. 2017). The mechanism of action of meningeal functional lymphatic vessels on subarachnoid particles and cerebrospinal fluid inflow/intercellular fluid efflux is still unclear. This may be a new mechanism that helps the brain to resist neurodegenerative diseases and needs to be studied. Starting from the protection and repair of the damaged meningeal lymphatic system and enhancing the clearing ability of the A β lymphatic circulation pathway, it may be a potential therapeutic target for AD.

1.3. Microglia in AD pathogenesis

Microglia are the first immune sentinels in the central nervous system (CNS), and human genetic data have shown that microglia play a key role in the pathogenesis of AD. Although microglia are thought to be macrophages in the brain, in contrast to other tissue-resident macrophages, they are not generated by bone marrow precursors but originate from erythromyeloid progenitor cells in the embryonic yolk sac which then migrate and colonize the brain parenchyma before the cerebrovascular system and the blood-brain barrier are fully formed (Ginhoux, Greter et al. 2010, Ginhoux, Lim et al. 2013). The capability of microglia to divide and self-renew in situ throughout life is essential for microglia to maintain their normal function (Ajami, Bennett et al. 2007). In AD mouse models, which over-express Alzheimer's amyloid precursor protein (APP) in neurons, microglia are activated and recruited to A β deposits and are strongly associated with impaired cognitive performance (Bolmont, Haiss et al. 2008). Positron emission tomography (PET) scans have shown that a longitudinal increase of microglial activation in patients with AD, and the persistent neuroinflammation following microglial activation is associated with synaptic dysfunction and reduced glucose metabolism (Fan, Okello et al. 2015). Recent data suggest that microglia may even contribute to A β plaque dispersion as the elimination of microglia at a later stage of the disease prevents synaptic and neuronal loss in APP transgenic mice (Spangenberg, Lee et al. 2016).

A key event in the pathophysiology of AD is neuroinflammation, making the inflammatory process of microglia one of its most investigated functions in AD. Microglia, the primary immune cells in the brain, has played a vital role in coordinating inflammation in the brain. As we all know, a distinguishing feature of inflammation is cytokine release. Studies have shown that high expression of proinflammatory cytokines, including tumor necrosis factor (TNF), interleukin (IL)-1 β , and IL-6, is observed in the brain, cerebrospinal fluid, and serum of AD patients (Heneka, Kummer et al. 2014, Labzin, Heneka et al. 2018), these proinflammatory mediators are secreted mainly by microglia. There is a widely accepted hypothesis that these inflammatory cytokines can cause microglia dysfunction, particularly their phagocytic capacity. Proinflammatory cytokines produced in response to A β deposition have been shown to accelerate A β accumulation by down-regulating the expression of genes involved in A β clearance, thereby promoting neurodegeneration (Hickman, Allison et al. 2008). Moreover, in AD, microglia can rapidly enter a hyperactivation state and release reactive oxygen species and nitric oxide, which can be directly cytotoxic to neurons (Block, Zecca et al. 2007).

Microglia appear to play an integral role in amyloidosis. A recent study has shown a failure to form A β plaques in the brain parenchyma after pharmacological depletion of microglia in the 5xFAD mouse model of AD (Spangenberg, Severson et al. 2019), suggesting that microglia play a role in exacerbating amyloid pathology. Microglial-derived exosomes appear necessary for tau propagation, and microglia contributes to neuron death in models of tau-mediated neurodegeneration (Asai, Ikezu et al. 2015). There is further evidence that IL-1 β and IL-6 can promote tau hyperphosphorylation (Zilka, Kazmerova et al. 2012). There is no doubt that the accumulation of A β and phosphorylated Tau proteins can also induce microglial inflammatory activation. Collectively, microglia may exacerbate neurodegeneration by promoting progressive pathological responses of AD by interacting with A β and tau.

A majority of genetic variants associated with AD risk identified by genome-wide association studies are preferentially or exclusively expressed in microglia, which include triggering receptor expressed on myeloid cells 2 (TREM2) (Guerreiro, Wojtas et al. 2013), cluster of differentiation 33 (CD33), ATP-binding cassette sub-family A member 7 (ABCB7) (Apostolova, Risacher et al. 2018). TREM2 is another significant risk gene associated with AD in addition to APOE, which is the most commonly known genetic variant associated

with AD. TREM2 is a cell surface receptor exclusively expressed on cells within the myeloid lineage, its expression in the brain is dominant in microglia. Soluble Trem2 (sTrem2) levels in CSF were significantly higher in individuals with MCI or AD dementia compared to controls and were correlated with attenuated cognitive and clinical decline (Ewers, Franzmeier et al. 2019). TREM2 expression is elevated in plaque-associated microglia, and modulation of its expression alters microglia morphology interacting with A β and reprograms microglia responses (Lee, Daggett et al. 2018), implying that TREM2 is essential for the microglial response to the A β deposit. Besides, a recent study demonstrated that TREM2 is a receptor necessary for complete activation of disease-associated microglia (DAM), a subset of microglia that might play a protective role in neurodegeneration, pointing out the critical role of TREM2 in microglial activation (Keren-Shaul, Spinrad et al. 2017). CD33 is also a microglia receptor in which the genetic locus is strongly associated with the risk of AD. Its expression is increased in AD patients' brains and is associated with increased plaque burden and swifter disease progression (Jiang, Yu et al. 2014). ABCB7 is a membrane transporter protein highly expressed in neurons, microglia, oligodendrocytes, and endothelial cells. Still, it appears to affect AD pathology mainly by regulating the action of microglia on apoptotic cells and A β phagocytosis (De Roeck, Van Broeckhoven et al. 2019).

While the traditional view that microglia play a detrimental role in AD pathology, emerging studies on the effects of microglia on A β pathology and neuronal degeneration revealed activated microglia also exert protective effects in AD pathophysiology. A remarkable benefit on neurons in AD mice by microglia is the engulfment and clearance of A β peptides (Michaud, Bellavance et al. 2013). Many studies on AD have demonstrated that TREM2 is associated with the microglia-mediated phagocytosis of A β . A certain mutation in TREM2 (such as p.T66M) reduces the ability of microglia to phagocytose A β fibrils; in line with this, primary microglia from TREM2 knockout mice (TREM2 $^{-/-}$) showed a reduced phagocytic capacity to A β compared to wild-type controls (Kleinberger, Yamanishi et al. 2014). These observations support the concept that impaired microglia phagocytosis promotes the development of amyloidosis. Beyond clearance of A β , another important function of microglia in AD is to clean up debris from damaged or dying cells (Streit 2002). On the other hand, recent evidence suggests that microglia constitute a protective barrier around amyloid deposits, shielding them off from

neurons, and reducing neuritic tau hyperphosphorylation and axonal dystrophy in nearby neuropil, thereby exerting a neuroprotective effect (Condello, Yuan et al. 2015, Yuan, Condello et al. 2016). Moreover, microglia-mediated neuroinflammation promotes neuronal autophagy, facilitating the degradation of phosphorylated tau proteins in neurons(Qin, Liu et al. 2016).

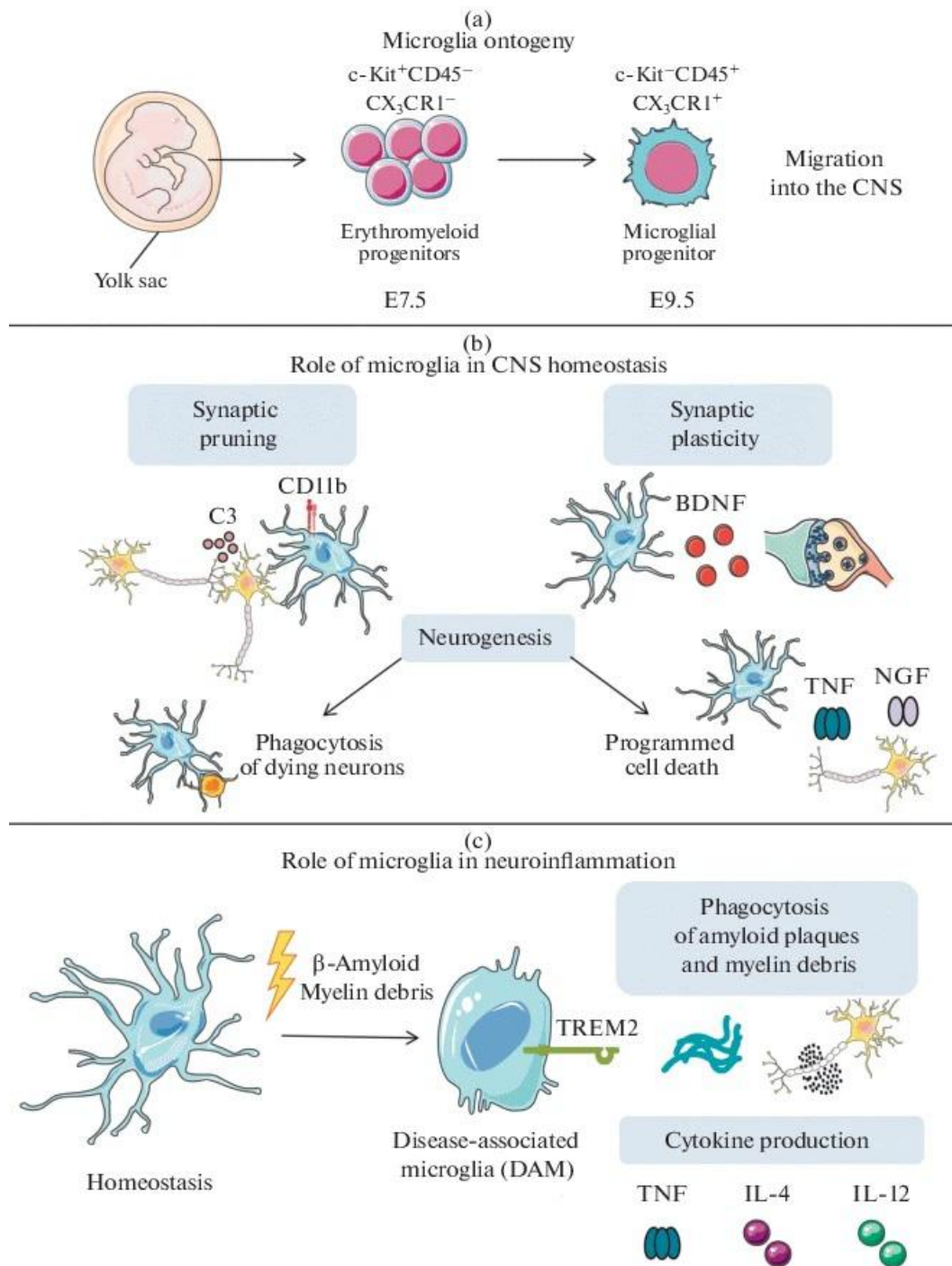


Figure 1.5 Microglia ontogeny and their physiological role in normal and pathological conditions. (a) Microglia derived from erythromyeloid progenitor cells in the yolk sac. (b) The role of microglia in maintaining CNS homeostasis, including synaptic pruning and plasticity as well as phagocytosis of dying neurons and activation of programmed cell death to regulate neurogenesis. (c) The aggregation of A β and myelin fragments triggers microglia activation, and activated microglia increase phagocytic activity and produce various cytokines. (Gogoleva, Drutskaya et al. 2019).

1.4. Innate immune signalling in AD

Microglia, the principal effector cells of the immune system in the brain, are armed with an extensive repertoire of pattern recognition receptors including Toll-like receptors 2 (TLR2), TLR2, TLR6, TLR9, and their co-receptors CD36, CD14, and CD47. These innate immune receptors mainly identify two types of molecular structures for activation, that are pathogen-associated molecular patterns produced by microbial pathogens, and damage-associated molecular patterns derived from damaged cells, such as misfolded or aggregated proteins (Akira, Takeda et al. 2001, Bsibsi, Ravid et al. 2002). Following ligands binding, CD14/TLR signaling is transduced through the common adaptor protein MyD88 and its downstream kinases, including inhibitor of NF- κ B kinase (IKK), p38 mitogen-activated protein kinase (p38-MAPK), and c-Jun N-terminal kinase (JNK), activating AP-1, CREB, and NF- κ B transcription factors, which regulate the expression of many crucial immune response genes (Akira, Takeda et al. 2001, O'Neill, Golenbock et al. 2013).

To date, multiple frequent variants associated with AD risk identified by GWAS are present in myeloid cells, including microglia, confirming the importance of the microglia response in AD progression (Mhatre, Tsai et al. 2015). An epigenomic analysis (Gjoneska, Pfenning et al. 2015) showed that AD-associated genetic variants were particularly enriched in enhancer sequences associated with innate immunity, implicating a crucial role for activation of the innate immune system as a disease-promoting factor in AD. As the primary immune cells in the brain, microglia use an ensemble of surface receptors composed of innate immune receptors to interact directly with A β and activate downstream signaling events that mediate innate immunity (Reed-Geaghan, Savage et al. 2009). Many studies through cross-breeding or bone marrow reconstruction have shown that the innate immune signaling regulates microglial activation in AD mice. As previously studied, chronic microglial neuroinflammation leads to neuronal

damage and death through various pathways, including the production of toxic substances that directly damage or kill neurons and activation of neuronal inflammasomes that can induce neuronal damage and death, or stressed neurons be phagocytosed by activated microglia (Brown and Vilalta 2015).

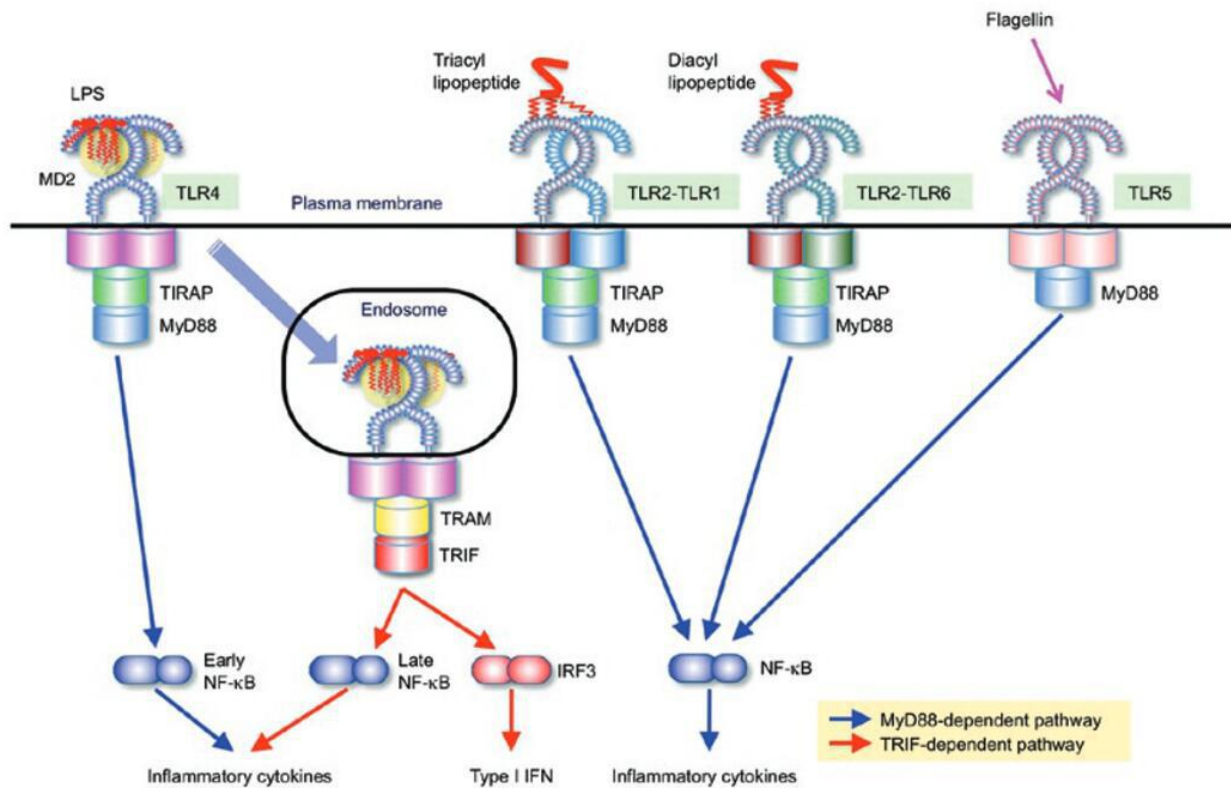


Figure 1.6 TLRs signaling pathway involved in innate immunity. TLR recognition of PAMP triggers activation of MyD88-dependent pathways: TLR4-MD2-LPS complex initially transmits signals for the early-phase activation of NF-κB by recruiting the TIR domain-containing adaptors TIRAP; TLR2-TLR1 and TLR2-TLR6 induce NF-κB activation through recruitment of TIRAP and MyD88; and TLR5 activates NF-κB through MyD88. Activation of NF-κB induces the secretion of inflammatory cytokines. (Kawai and Akira 2010).

However, results are often contradictory regarding the effects of innate immunity on Aβ pathology and neuronal degeneration in murine AD models. On the one hand, many studies indicated that deficiency of CD14 (Reed-Geaghan, Reed et al. 2010), TLR2 (Liu, Liu et al. 2012), TLR4 (Song, Jin et al. 2011), MyD88 (Hao, Liu et al. 2011), interleukin receptor-associated kinase 4 (IRAK4) (Cameron, Tse et al. 2012), IKKβ (Liu, Liu et al. 2014), or NLRP3 (Heneka,

Kummer et al. 2013) attenuates the degree of inflammation, shifts inflammatory activation from pro-inflammatory to anti-inflammatory profiles, or both in the brain of APP-transgenic mice. TLR4 mutations reduced microglial activation, increased A β deposition, and exacerbated cognitive dysfunction in a mouse model of AD(Song, Jin et al. 2011). Pharmacological inhibition of TLR4 activation reduced microglia activation associated with cortical amyloid plaque formation and prevented the pro-inflammatory effects of fibrillar A β on microglia(Capiralla, Vingtdoux et al. 2012). A recent study indicates that soluble A β aggregates lead to long term potentiation (LTP) deficits and neuronal death through an autocrine/paracrine mechanism of TLR4 signaling(Hughes, Choi et al. 2020). A common upregulation of TLR2 and CD14 have been found both in murine models of AD and human post-mortem brain tissues(Letiembre, Liu et al. 2009). Treatment with an anti-TLR2 antibody (α TLR2) in AD mouse models mitigated the A β -mediated impairment in LTP of hippocampal synaptic activity and attenuated the inflammatory response in microglia(Costello, Carney et al. 2015). Additionally, our group demonstrates that inhibition of TLR2 may be beneficial in AD, and that TLR2 deficiency leads to microglia conversion from the M1 to the M2 state in the brains of APP/PS1 transgenic mice, while improving BDNF expression and neuronal functions(Liu, Liu et al. 2012). IRAK4 is an essential intracellular signaling molecule for fibrillar A β to activate the TLR downstream signaling pathway, loss of IRAK4 function leads to reduced A β levels in a mouse model of AD, which is associated with a reduction in microglia and astrocytes in aged mice as well as promoting amyloid clearance mechanisms, including increased expression of insulin-degrading enzymes(Cameron, Tse et al. 2012).

1.4.1. MyD88-dependent pathways in AD

Myd88, an adaptor protein, bridges intracellular signals from most innate immune receptors to the nucleus. It has been reported that MyD88 deletion ameliorate β -amyloidosis by enhancing microglia phagocytosis through fractalkine (the ligand of CX3CR1) signaling and promoting apoE-mediated clearance of A β from the brain(Lim, Kou et al. 2011). Furthermore, microglia immunological receptors may act together and augment the response to A β exposure. For example, a study revealed that a fibrillar A β induced a complex of TLR4, TLR6, and CD36 as a hallmark of AD and that the scavenger receptor CD36 promotes inflammatory signaling through a heterodimer of Toll-like receptors 4 and 6 in microglia (Stewart, Stuart et al. 2010). Galia and

colleagues conducted an *in vitro* study that further showed interfering with TLR4-TLR6 dimer assemble with a TLR4-derived peptide reduced the secretion of pro-inflammatory mediators from microglia and ultimately rescued neuronal death(Shmuel-Galia, Klug et al. 2017). This hypothesis is further reinforced by the fact that disrupting the interaction between microglia immunological receptors can improve AD's pathology. TLR2 and MyD88 levels are elevated in the hippocampus and cortex of patients with AD and in a 5XFAD mouse model of AD, while selective disruption of TLR2-Myd88 interaction delays the disease process by inhibiting inflammation(Rangasamy, Jana et al. 2018).

All the data mentioned above strongly suggest that activation of the TLRs and its downstream signaling pathways may contribute to the deterioration of AD and that inhibition of its function may control disease progression. However, Toll-like receptors are also involved in the removal of A β by microglia. It was found that destructive mutations of TLR4 increased A β deposition compared to the TLR4 wild-type AD mouse model, and microglia (BV-2 cells) stimulate with innate immune ligands of TLR2, TLR4, and TLR9 speed up A β ingest *in vitro*(Tahara, Kim et al. 2006, Scholtzova, Kasczak et al. 2009). Also, peptidoglycan (PGN) activates TLR2 on microglia, promoting A β uptake via ERK1/2 and p38-MAPKs signaling pathways(Chen, Iribarren et al. 2006). A study further validates this concept that TLR2 deficiency in APP transgenic mice increased levels of A β 1-42 and accompanying cognitive decline compared with TLR2-wild-type mice; more importantly, using a lentiviral construct restore TLR2 gene expression in APP-TLR2-/- mouse had beneficial effects by rescuing the cognitive impairment(Richard, Filali et al. 2008). Rivest and colleagues demonstrated that MyD88 expression was reduced more than 50% in the AD mouse model, resulting in accelerated spatial learning and memory deficits, while impaired MyD88 signaling in APP^{swc}/PS1 mice resulted in increased levels of soluble A β oligomers and reduced brain IL-1 β gene expression (Michaud, Richard et al. 2011). Similarly, wild-type MyD88 was also reported to promote A β clearance and protect neurons(Michaud, Richard et al. 2012). There was a study even showing that complete deletion of the MyD88 in AD mice have no effect on neuroinflammation or A β deposition(Weitz, Gate et al. 2014).

It is difficult to explain the conflicting results delivered from different animal models and different experimental methods. However, these studies suggest that the innate immune system

and TLRs are involved in AD. MyD88 is essential for the activation of TLRs and its downstream signaling(Akira, Uematsu et al. 2006) and is also imperative to trigger microglial innate immune gene expression following exposure to exogenous and endogenous toxic stimuli(Kang and Rivest 2007, Naert, Laflamme et al. 2009). However, in the investigation of MyD88 and AD, it should be noted that MyD88 functions not only in microglia but also in other brain cells (e.g., neurons, astrocytes, and endothelial cells)(Gosselin and Rivest 2008, Shen, Qin et al. 2016, Hung, Chen et al. 2018) and that overall deletion of MyD88 in AD mice alters brain development and is potentially lethal(Michaud, Richard et al. 2011, Schnoder, Gasparoni et al. 2020). Therefore, to elucidate the pathogenic role of MyD88 in AD, MyD88 expression should be manipulated specifically in microglia or other brain cells within a designed time window in AD animals.

2. AIM OF THIS WORK

Increasing evidence suggests that the innate immune signaling pathways drive chronic inflammatory activation, control cerebral A β load, and subsequently affect neuronal degeneration in the AD brain. Recently, our group and others have observed that deficiency in certain innate immune molecules in microglia, such as CD14 (Reed-Geaghan et al., 2010), Toll-like receptor 2 (TLR2) (Liu et al., 2012), TLR4 (Song et al., 2011), interleukin receptor-associated kinase 4 (IRAK4) (Cameron et al., 2012), inhibitor of nuclear factor κ -B kinase subunit β (IKK β) (Liu et al., 2014), and NLRP3 (Heneka et al., 2013) attenuates the degree of neuroinflammation, shifts inflammatory activation from pro-inflammatory to anti-inflammatory profiles, or both. However, results on the effects of innate immunity on A β pathology and neuronal degeneration in AD mice are often contradictory. For example, other reports state that wild-type MyD88 is necessary for clearing A β from the brain and protecting cognitive function (Michaud et al., 2011; Michaud et al., 2012).

Therefore, this study is aimed to investigate the pathogenic effects of microglial MyD88 on neuroinflammatory activation, cerebral A β load and neuronal function. We also plan to investigate whether microglia play an important role in the interaction between parenchymal A β and vascular lesions.

The detailed purposes of this study are listed below:

- 1、 To investigate the role of microglial MyD88 in the neuroinflammatory activation, cerebral A β load and neuronal function in APP-transgenic mice.
- 2、 To investigate depletion of microglial MyD88 affect A β deposition in the cerebral blood vessels and the structure and function of BBB.

3. MATERIALS AND METHODS

3.1. Materials

3.1.1. Instruments

Instruments	Company
7500 Fast Real-Time PCR System	Applied Biosystems (Darmstadt, Germany)
Accu jet Pipettes Control	BrandTech Scientific (Essex, CT, USA)
Autoclave 3870 ELV	Systec (Wettenberg, Germany)
Autoclave V-150	Systec (Wettenberg, Germany)
Axiovert 25 inverted Microscope	Carl Zeiss Microscopy (Jena, Germany)
Axiovert 40 CFL Microscope	Carl Zeiss Microscopy (Jena, Germany)
Barnes Maze	Noldus Information Technology (Oberreifenberg, Germany)
Biofuge 13 Centrifuge	Heraeus (Hanau, Germany)
Biowizard KR-200 Bench	Kojair Tech Oy (Vilppula, Finland)
Coolbox KB 1001	Liebherr (Lindau, Germany)
Drying cabinet	Heraeus (Hanau, Germany)
Eclipse TS100 Invetiertes Microscop	Nikon Instruments (Melville, NY, USA)
Eclipse E600 Fluorescence Microscopy	Nikon Instruments (Melville, NY, USA)
FACSCanto II Flow Cytometer	BD Biosciences (Heidelberg, Germany)
Freezer Premium no frost	Liebherr (Lindau, Germany)
Freezer UF75-110 T	Colora (Frankfurt, Germany)
General Rotator STR4	Stuart Scientific (Staffordshire, UK)
HERAcell CO ₂ Incubators	Heraeus (Hanau, Germany)
HERAcell 150i CO ₂ Incubators	Thermo Scientific (Langenselbold, Germany)
HERAsafe HS 12 biological safety cabinet	Heraeus (Hanau, Germany)
Ice Machine	Eurfrigor Ice Makers Srl (Lainate, Italy)
Incubations hood TH-30	Edmund Bühler GmbH (Hechingen, Germany)
InoLab pH 720 pH-meter	WTW (Weilheim, Germany)
Jouan B4i Centrifuge	Thermo Scientific (Langenselbold, Germany)
Laboshaker	Gerhardt Analytical Systems (Königswinter, Germany)
Liquid Nitrogen Container	KGW-Isotherm (Karlsruhe, Germany)
Microwelle HF 26521	Siemens (München, Germany)
Mini-PROTEAN 3 Electrophoresis system	Bio-Rad Laboratories (München, Germany)
Mini Trans-Blot Cell	Bio-Rad Laboratories (München, Germany)
Multipette Plus	Eppendorf (Hamburg, Germany)
Nalgene Mr. Frosty Freezing Container	A. Hartenstein (Würzburg, Germany)

Nanodrop ND-1000 Spectrophotometer	PEQLAB Biotechnologie (Erlangen, Germany)
Optima Max Ultracentrifuge	Beckman Coulter (Krefeld, Germany)
Perfection V700 Photoscanner	Epson (Meerbusch, Germany)
Pipette PIPETMAN	Gilson (Middleton, WI, USA)
Pipette Single-Channel	Eppendorf (Hamburg, Germany)
Pipette Pipetus	Hirschmann (Eberstadt, Germany)
PowerPac 200 Power Supply	Bio-Rad Laboratories (München, Germany)
Precision Balance scale 770	Kern & Sohn (Balingen, Germany)
Precision Balance scale CP 42023	Sartorius (Göttingen, Germany)
PS250 Power Supply	Hybaid (Heidelberg, Germany)
PTC 200 DNA Engine Thermal Cycler	MJ Research (St. Bruno, Canada)
PURELAB Ultra Water Purification system	Elga (Celle, Germany)
QuadroMACS™ Separator	Miltenyi Biotec (Bergisch Gladbach, Germany)
Refrigerated Laboratory Centrifuge	Eppendorf (Hamburg, Germany)
Refrigerator KG39VVI30	Siemens (München, Germany)
Refrigerator Premium	Liebherr (Lindau, Germany)
Refrigerator V.I.P. Series -86 °C Freezer	Sanyo (Wood Dale, IL, USA)
Rocky 3D	Labortechnik Frübel (Lindau, Germany)
Savant SpeedVac DNA 110	Thermo Scientific (Langenselbold, Germany)
Shakers SM-30	Edmund Bühler (Hechingen, Germany)
SmartSpec 3000 Spectralphotometer	Bio-Rad Laboratories (München, Germany)
Sunrise Microtiter plate reader	Tecan (Männedorf, Schweiz)
Tabletop Centrifuge 4K10	Sigma Laborzentrifugen (Osterode am Harz, Germany)
Tabletop Centrifuge 4K15C	Sigma Laborzentrifugen (Osterode am Harz, Germany)
Thermoblock TDB-120	BioSan (Riga, Latvia)
Thermomixer comfort	Eppendorf (Hamburg, Germany)
TLA-55 Rotor Package, Fixed Angle	Beckman Coulter (Krefeld, Germany)
Transsonic Ultrasonic Cleaning Units	Elma (Singen, Germany)
Ultrospec 3100 pro Spectralphotometer	Amersham Biosciences (München, Germany)
Vortex Genie 2	Scientific Industries (Bohemia, NY, USA)
Vortex Shaker REAX 2000	Heidolph (Schwabach, Germany)
Water bath	Köttermann (Hänigsen, Germany)
XCell SureLock Mini-Cell Electrophoresis system	Invitrogen (Darmstadt, Germany)

3.1.2. Experimental material

Experimental materials	Company
------------------------	---------

Amersham Hyperfilm ECL	GE Healthcare (Buckinghamshire, UK)
Beackers	VWR (Darmstadt, Germany)
Biosphere Filter Tips (10 µl, 200 µl, 1000 µl)	Sarstedt (Nümbrecht, Germany)
Blotting Paper Grade GB003	Whatman (Dassel, Germany)
Cell Scrapers	TPP (Trasadingen, Schweiz)
Centrifugentubes (15 ml, 50 ml)	Sarstedt (Nümbrecht, Germany)
Combitips Plus (5 ml, 10 ml)	Eppendorf (Hamburg, Germany)
CryoPure tubes 1.8 ml	Sarstedt (Nümbrecht, Germany)
Cuvettes	Sarstedt (Nümbrecht, Germany)
Erlenmeyer Flasks	Schott (Mainz, Germany)
Falcon Multiwell Cell Culture Plates	BD Biosciences (Heidelberg, Germany)
Falcon Round bottom test tubes 5 ml	BD Biosciences (Heidelberg, Germany)
Filtropur Cell Strainer	Sarstedt (Nümbrecht, Germany)
Filtropur Syringe Filter	Sarstedt (Nümbrecht, Germany)
Glass Bottles	Fisher Scientific (Schwerte, Germany)
Gloves, Latex	VWR (Darmstadt, Germany)
Gloves, Nitril	VWR (Darmstadt, Germany)
Hemocytometer	Brand (Wertheim, Germany)
LS Columns	Miltenyi Biotec (Bergisch Gladbach, Germany)
MicroAmp Optical 96-Well Reaction Plate	Applied Biosystems (Darmstadt, Germany)
MicroAmp Optical Adhesive Film	Applied Biosystems (Darmstadt, Germany)
Microlance™ needles	BD Biosciences (Heidelberg, Germany)
Microlon 600 96-Well Microplate	Greiner Bio-One (Frickenhausen, Germany)
Microscopic cover glasses 12x12 mm	R. Langenbrinck (Emmendingen, Germany)
Microtestplate 96-Well	Sarstedt (Nümbrecht, Germany)
Mini-PROTEAN 3 Short Plates	Bio-Rad Laboratories (München, Germany)
Mini-PROTEAN 3 Spacer Plates 1,5 mm	Bio-Rad Laboratories (München, Germany)
Mini-PROTEAN Comb (15 Wells, 1,5 mm)	Bio-Rad Laboratories (München, Germany)
Myelin Removal Beads II	Miltenyi Biotec (Bergisch Gladbach, Germany)
Nunc MaxiSorp 96-Well Plate, black	Thermo Scientific (Langenselbold, Germany)
Overhead Transparencies	R. Langenbrinck (Emmendingen, Germany)
Pasteur Pipettes	VWR (Darmstadt, Germany)
PCR Soft Tube 0.2 ml	Biozym Scientific (Oldendorf, Germany)
Pipette Tips (10 µl, 200 µl, 1000 µl)	Sarstedt (Nümbrecht, Germany)
Polyallomer Tube, 1.5 ml, Snap-On Cap	Beckman Coulter (Krefeld, Germany)
Precision Wipes Kimtech Science	Kimberly-Clark (Koblenz, Germany)
Pro-Gel 10-20% Tris-Tricin-Gel	Anamed Elektrophorese (Groß-Bieberau/Rodau, Germany)
Protran Nitrocellulose Transfermembranes	Whatman (Dassel, Germany)
PVDF Western Blotting Membranes	Roche (Mannheim, Germany)

Safe-Lock Tubes (0.5 ml, 1 ml, 2 ml)	Eppendorf (Hamburg, Germany)
Scalpel Blades	B. Braun (Melsungen, Germany)
Serological Pipettes (5 ml, 10 ml, 25 ml)	Sarstedt (Nümbrecht, Germany)
Slide Box	neoLab (Heidelberg, Germany)
Standing Cylinders	VWR (Darmstadt, Germany)
Syringes	B. Braun (Melsungen, Germany)
Tissue Culture Dish	Sarstedt (Nümbrecht, Germany)
Tissue Culture Flask	Sarstedt (Nümbrecht, Germany)
UV Quartz cuvette 10 mm	Hellma (Müllheim, Germany)

3.1.3. Chemicals

Chemicals	Company
0.05% Trypsin/EDTA (1x)	Invitrogen (Darmstadt, Germany)
AKT Inhibitor VIII	Sigma Aldrich (Taufkirchen, Germany)
(3-Aminopropyl) triethoxysilane	Sigma Aldrich (Taufkirchen, Germany)
β -Mercaptoethanol	Sigma Aldrich (Taufkirchen, Germany)
β -Secretase Substrate IV, Fluorogenic	Merck (Darmstadt, Germany)
γ -Secretase Substrate , Fluorogenic	Merck (Darmstadt, Germany)
Agarose	Biozym (Oldendorf, Germany)
Ammoniumpersulfat (APS)	Sigma Aldrich (Taufkirchen, Germany)
Antibiotic-Antimycotic 100x	Invitrogen (Darmstadt, Germany)
Bovine Serum Albumin (BSA)	Sigma Aldrich (Taufkirchen, Germany)
Borat	VWR (Darmstadt, Germany)
Bromphenol blue	Sigma Aldrich (Taufkirchen, Germany)
Casein	Fluka (Buchs, Switzerland)
Chloroform	Applichem (Darmstadt, Germany)
Citrate acid	Serva (Heidelberg, Germany)
Congo red	Sigma Aldrich (Taufkirchen, Germany)
Collagen Coating Solution	Sigma-Aldrich (Taufkirchen, Germany)
Dimethylsulfoxid (DMSO)	Sigma Aldrich (Taufkirchen, Germany)
Diaminobenzidin-Hydrochlorid (DAB)	Sigma Aldrich (Taufkirchen, Germany)
DNA Ladder (100 bp, 1 kb)	New England Biolabs (Frankfurt am Main, Germany)
dNTP Mix	Roche (Mannheim, Germany)
Dithiothreitol (DTT)	Sigma Aldrich (Taufkirchen, Germany)
Digest-All 3 (Pepsin)	Thermo Fisher Scientific (Mannheim, Germany)
Dulbecco's Modified Eagle Medium (DMEM)	Invitrogen (Darmstadt, Germany)
Entellan®mounting media	VWR (Darmstadt, Germany)
Ethidiumbromid	Carl Roth (Karlsruhe, Germany)

Ethanol	Sigma Aldrich (Taufkirchen, Germany)
Ethylendiaminetetraacetat acid (EDTA)	Sigma Aldrich (Taufkirchen, Germany)
Ethylene glycol tetraacetic acid (EGTA)	Sigma Aldrich (Taufkirchen, Germany)
Fetal Bovine Serum (FBS)	Invitrogen (Darmstadt, Germany)
Glycine	Carl Roth (Karlsruhe, Germany)
Glycerol	Sigma Aldrich (Taufkirchen, Germany)
Guanidine Hydrochloride	Sigma Aldrich (Taufkirchen, Germany)
H ₂ O ₂	Otto Fishar (Saarbrueken, Germany)
H ₂ SO ₄	Fluka (Buchs, Switzerland)
HCl	Sigma Aldrich (Taufkirchen, Germany)
Ham's F-12 Medium	Invitrogen (Darmstadt, Germany)
Hank's Buffered Salt Solution (HBSS)	Sigma Aldrich (Taufkirchen, Germany)
Hexamer Random Primer	Invitrogen (Darmstadt, Germany)
HiLyte Fluor™ 488-conjugated Aβ42	AnaSpec(Fremont, USA)
Isoflurane	Baxter (Unterschleißheim, Germany)
Isopropanol	Carl Roth (Karlsruhe, Germany)
KHCO ₃	Merck (Darmstadt, Germany)
KCl	Merck (Darmstadt, Germany)
Lipopolysaccharide (LPS)	Axxora (Lörrach, Germany)
MgCl ₂	Fluka (Buchs, Switzerland)
MgSO ₄	Fluka (Buchs, Switzerland)
Methoxy-XO4	Bio-Techne GmbH
Methanol	Sigma Aldrich (Taufkirchen, Germany)
MCC950	Sigma Aldrich (Taufkirchen, Germany)
Milk powder	Carl Roth (Karlsruhe, Germany)
NaCl	Merck (Darmstadt, Germany)
NaF	Merck (Darmstadt, Germany)
Na ₂ HPO ₄	Carl Roth (Karlsruhe, Germany)
NaH ₂ PO ₄ x H ₂ O	Merck (Darmstadt, Germany)
Na ₄ P ₂ O ₇	Sigma Aldrich (Taufkirchen, Germany)
Na ₃ VO ₄	Sigma Aldrich (Taufkirchen, Germany)
NH ₄ Cl	Sigma Aldrich (Taufkirchen, Germany)
Okadic acid	Sigma Aldrich (Taufkirchen, Germany)
Orange G	Merck (Darmstadt, Germany)
PageRuler Prestained Protein Ladder	Invitrogen (Darmstadt, Germany)
Pam3CSK4	Invivogen (San Diego, CA, USA)
Paraformaldehyd (PFA)	Merck (Darmstadt, Germany)
Protease inhibitor Cocktail	Roche (Mannheim, Germany)
Pericyte medium(PM)	Sciencell Research Laboratories(Carlsbad, CA, USA)

Pericyte growth factors	Sciencell Research Laboratories(Carlsbad, CA, USA)
Penicillin-streptomycin	Sciencell Research Laboratories(Carlsbad, CA, USA)
Rotiphorese Gel 30	Carl Roth (Karlsruhe, Germany)
RPMI 1640	Invitrogen (Darmstadt, Germany)
Recombinant human IL-1 β	R&D Systems(Wiesbaden, Germany)
Sodium acetate	Merck (Darmstadt, Germany)
Sodium dodecylsulfat (SDS)	Carl Roth (Karlsruhe, Germany)
Sucrose	VWR (Darmstadt, Germany)
Tetramethylethylendiamin (TEMED)	Serva (Heidelberg, Germany)
Tricine	Carl Roth (Karlsruhe, Germany)
Trizma®base	Sigma Aldrich (Taufkirchen, Germany)
Triton X-100	Sigma Aldrich (Taufkirchen, Germany)
TRizol	Sigma Aldrich (Taufkirchen, Germany)
Tween 20	Sigma Aldrich (Taufkirchen, Germany)
Western Lightning ECL Substrate	Perkin Elmer (Rodgau, Germany)
Xylene	Otto Fischar (Saarbrücken, Germany)
Xylene cyanol	Molekula (München, Germany)

3.1.4. Kits

Title	Company
Bio-Rad Protein Assay	Bio-Rad Laboratories (München, Germany)
DyNAmo™ Flash probe qPCR Kit	Thermo Scientific (Bonn, Germany)
DyNAmo™ Flash SYBR Green qPCR Kit	Thermo Scientific (Bonn, Germany)
Mouse TNF alpha ELISA Ready-SET-Go!	eBioscience (San Diego, CA, USA)
MTT-based Cell Proliferation Kit I	Roche (Mannheim, Germany)
Neural Tissue Dissociation Kit (papain-based)	Miltenyi Biotec (B.V. & Co. KG, Bergisch Gladbach, Germany)
OptEIA™ TMB Substrate Reagent Set	BD Bioscience (Heidelberg, Germany)
RNeasy® Plus Mini Kit	Qiagen (Hilden, Germany)
RQ1 RNase-free DNase	Promega (Mannheim, Germany)
SuperScript® II Reverse Transcriptase	Invitrogen (Darmstadt, Germany)
VECTOR Blue Alkaline Phosphatase Substrate kit	Vector Laboratorie (Burlingame, USA)
VectaStain Elite ABC kit	Vector Laboratorie (Burlingame, USA)

VectaStain Elite ABC-AP kit	Vector Laboratorie (Burlingame, USA)
-----------------------------	--------------------------------------

3.1.5. Oligonucleotides

Table 3.1 Primers for the Real-Time-quantitative-PCR (SYBR® Green method)

Gen	Primer forward 5' - 3'	Primer reverse 5' - 3'
<i>mouse osteopontin (opn)</i>	CAGCCATGAGTCAAGTCAGC	TGTGGCTGTGAACTTGTGG
<i>mouse vegf</i>	CCCTTCGTCCTCTCCTTACC	AGGAAGGGTAAGCCACTCAC
<i>mouse ppia</i>	AGCATAACAGGTCCTGGCATCTTGT	CAAAGACCACATGCTTGCCATCCA
<i>mouse ccl-2</i>	AAGAGATCAGGGAGTTTGCT	CTGCCTCCATCAACCACTTT
<i>mouse gapdh</i>	ACAACTTTGGCATTGTGGAA	GATGCACGGATGATGTTCTG
<i>mouse il-1β</i>	GAAGAAGAGCCCATCCTCTG	TCATCTCGGAGCCTGTAGTG
<i>mouse il-10</i>	AGGCGCTGTCATCGATTTCTC	TGCTCCACTGCCTTGCTCTTA
<i>mouse inos</i>	ACCTTGTTTCAGCTACGCCTT	CATTCCCAAATGTGCTTGTC
<i>mouse tnf-α</i>	ATGAGAAGTTCCCAAATGGC	CTCCACTGGTGGTTTGCTA

3.1.6. Antibody

Table 3.2 Antibodies used in this work

Antibody	Company
<i>mouse monoclonal anti α-tubulin</i> Clone:DM1A	Abcam (Cambridge, UK)
<i>rabbit polyclonal anti β-actin,clone: 13E5</i>	Cell Signaling (Cell Signaling Technology Europe)
<i>mouse monoclonal anti Amyloid β</i> Clone:WO2	Millipore (Schwalbach, Germany)
<i>mouse monoclonal anti Amyloid β</i> Clone:6F/3D	Dako (Hamburg, Germany)
<i>rat monoclonal anti CD16/CD32</i> Clone:2.4G2	BD Pharmingen (NJ, USA)
<i>rabbit monoclonal anti PDGFRβ,clone: 28E1</i>	Cell Signaling (Cell Signaling Technology)

	Europe)
<i>rabbit monoclonal anti CD13/APN,clone: D6V1W</i>	Cell Signaling (Cell Signaling Technology Europe)
<i>rabbit monoclonal anti cleaved caspase-3 ,clone: 5A1E</i>	Cell Signaling (Cell Signaling Technology Europe)
<i>mouse monoclonal anti proliferating cell nuclear antigen (PCNA) clone: PC10</i>	Cell Signaling (Cell Signaling Technology Europe)
<i>rabbit polyclonal anti Collagen type IV</i>	Abcam (Cambridge, UK)
<i>Mouse anti-NLRP3/NALP3, mAb (Cryo-2) (AG-20B-0014)</i>	AdipoGen (San Diego, USA)
<i>Griffonia Simplicifolia Lectin I isolectin B4 (Catalog: B-1205;</i>	Vector Laboratories(Burlingame, CA, USA)
<i>chicken polyclonal anti GFP</i>	Abcam (Cambridge, UK)
<i>mouse monoclonal anti Iba1 Clone:20A12.1</i>	Millipore (Schwalbach, Germany)
<i>rabbit polyclonal anti Iba1</i>	Wako (Neuss, Germany)
<i>rabbit polyclonal anti phosphorylated AKT (Ser473)</i>	Cell Signaling (Cell Signaling Technology Europe)
<i>rabbit polyclonal anti AKT</i>	Cell Signaling (Cell Signaling Technology Europe)
<i>rabbit monoclonal anti phosphorylated ERK1/2 (Thr202/Tyr204)clone: D9E</i>	Cell Signaling (Cell Signaling Technology Europe)
<i>mouse monoclonal anti ERK1/2 ,clone: L34F12</i>	Cell Signaling (Cell Signaling Technology Europe)
<i>rabbit monoclonal anti phosphorylated NFκB p65 (S536), clone: D13.14.4E</i>	Cell Signaling (Cell Signaling Technology Europe)
<i>rabbit monoclonal anti NFκB p65,clone:D14E12</i>	Cell Signaling (Cell Signaling Technology Europe)
<i>rabbit monoclonal anti Ki67 Clone, SP6</i>	Abcam (Cambridge, UK)
<i>rabbit polyclonal anti Munc18-1</i>	Cell Signaling (Cell Signaling Technology Europe)

<i>mouse monoclonal anti NeuN</i> <i>Clone, A60</i>	Millipore (Schwalbach, Germany)
<i>rabbit monoclonal anti phosho-p65</i> <i>Clone, 93H1</i>	Cell Signaling (Cell Signaling Technology Europe)
<i>rabbit monoclonal anti p65</i> <i>Clone, D14E12</i>	Cell Signaling (Cell Signaling Technology Europe)
<i>mouse monoclonal anti PSD95</i> <i>Clone, 6G6-1C9</i>	Abcam (Cambridge, UK)
<i>rabbit polyclonal anti RFP</i>	Rockland (Gilbertsville, USA)
<i>mouse monoclonal anti S100</i> <i>Clone: 4C4.9</i>	Abcam (Cambridge, UK)
<i>rabbit polyclonal anti phosho-GSK-3β</i> <i>(Ser9)</i>	Cell Signaling (Cell Signaling Technology Europe)
<i>rabbit monoclonal anti GSK-3β</i> <i>Clone: 3D10</i>	Cell Signaling (Cell Signaling Technology Europe)
<i>rabbit monoclonal anti ABCB1</i> <i>Clone: E1Y7S</i>	Cell Signaling (Cell Signaling Technology Europe)
<i>rabbit polyclonal anti LRP-1</i>	Cell Signaling (Cell Signaling Technology Europe)
<i>rabbit monoclonal anti vinculin</i> <i>Clone: E1E9V</i>	Cell Signaling (Cell Signaling Technology Europe)
<i>rabbit polyclonal anti tight junction protein 1 (TJP1); NBP1-85047</i>	Novus Biologicals(Wiesbaden-Nordenstadt, Germany)
<i>rabbit monoclonal anti Claudin-5</i>	Thermo Fisher Scientific(Bonn, Germany)
<i>mouse monoclonal anti aquaporin 4 (AQP4)</i>	Proteintech Europe (Manchester, United Kingdom)
<i>goat anti chicken Alexa 488 Conjugate</i>	Invitrogen (Darmstadt, Germany)
<i>goat anti rabbit Alexa 488 Conjugate</i>	Invitrogen (Darmstadt, Germany)
<i>goat anti rabbit cy3 Conjugate</i>	Cell Signaling (Cell Signaling Technology Europe)
<i>goat anti mouse Alexa 546 Conjugate</i>	Invitrogen (Darmstadt, Germany)
<i>goat anti mouse Alexa 594 Conjugate</i>	Invitrogen (Darmstadt, Germany)
<i>goat anti rabbit biotin Conjugate</i>	Vector Laboratorie (Burlingame, USA)

<i>goat anti rat biotin Conjugate</i>	Vector Laboratorie (Burlingame, USA)
<i>goat anti mouse HRP Conjugate</i>	Dako (Hamburg, Germany)
<i>goat anti rabbit HRP Conjugate</i>	Promega (Mannheim, Germany)

3.1.7. Buffer

Table 3.3 Recipe of solution

Recipe	Chemicals	Amount	Concentration
10x Citric buffer	Citric acid	2.014g Up to 1 Liter	10mM
10x PBS	NaCl KCl Na ₂ HPO ₄ NaH ₂ PO ₄ x H ₂ O dest. H ₂ O Adjust to pH 7.4	400 g 10 g 71 g 69 g Up to 5 Liter	1.37 M 27 mM 100 mM 100 mM
10x TBS	Tris NaCl dest. H ₂ O Adjust to pH 7.4	302.5 g 425 g Up to 5 Liter	500 mM 1.45 M
5x DNA-Loading buffer	Bromphenol blue Xylene cyanol Orange G Sucrose 0.5 M EDTA [pH 8.0] dest. H ₂ O	1 mg 2 mg 2 mg 500 mg 2 µl Up to 1 ml	0.1% 0.2% 0.2% 50% 1 mM
5x TBE	Tris	270 g	446 mM

MATERIALS AND METHODS

	Borat	137.5 g	446 mM
	0.5 M EDTA [pH 8.0]	100 ml	10 mM
	dest. H ₂ O	Up to 5 Liter	
3x SDS-PAGE Loading buffer	1 M Tris/HCl [pH 6.8]	187.5 µl	187.5 mM
	20% SDS	300 µl	6%
	Glycerol	300 µl	30%
	β-Mercaptoethanol	150 µl	15%
	3% Bromphenol blue (w/v)	10 µl	0.03%
	dest. H ₂ O	Up to 1 ml	
10x SDS-Tris-Glycine Running buffer	Tris	151.5 g	250 mM
	Glycine	720.5 g	1.92 M
	SDS	50 g	1% (w/v)
	dest. H ₂ O	Up to 5 Liter	
10x SDS-Tris-Tricine running buffer	Tris	121 g	1 M
	Tricine	171 g	1 M
	SDS	10 g	1% (w/v)
	dest. H ₂ O	Up to 1 Liter	
10x Transfer buffer	Tris	30 g	248 mM
	Glycine	138 g	1.84 M
	dest. H ₂ O	Up to 1 Liter	
* for use mix 100 mL 10X Transfer buffer with 200 mL methanol and 700 mL dest. H ₂ O			
Blocking buffer	Nonfatty milk	5g	10%
	1x PBS	Up to 50 ml	
DMEM media	Dulbecco's Modified Eagle Medium (DMEM)(High Glucose)	445 ml	89%
	Fetal bovine serum	50 ml	10%

	Antibiotic-antimycotic(100x)	5 m	1%
* Fetal bovine serum should be inactivated in 56°C water bath for 30 min.			
RPMI media	RPMI 1640 Medium	445 ml	89%
	Fetal bovine serum	50 ml	10%
	Antibiotic-antimycotic(100x)	5 ml	1%
* Fetal bovine serum should be inactivated in 56°C water bath for 30 min.			
SDS-Cell lysis buffer	1 M Tris/HCl [pH 7.5]	2.5 ml	50 mM
	0.5 M EDTA [pH 8.0]	200 µl	2 mM
	0.5 M EGTA [pH 8.0]	200 µl	2 mM
	Protease inhibitor Cocktail	1 Tablet	1x
	20 µM Okadic acid	125 µl	50 mM
	0.25 M Na ₄ P ₂ O ₇	1 ml	5 mM
	1 M Na ₃ VO ₄	100 µl	100 µM
	1 M DTT	50 µl	1 mM
	1 M NaF	2.5 ml	50 mM
	20% SDS	5 ml	2%
	dest. H ₂ O	Up to 50 ml	

3.1.8. Mice and Cross-breeding

APP/PS1-double transgenic mice over-expressing human mutated APP (KM670/671NL) and PS1 (L166P) under Thy-1 promoters (Radde et al., 2006) were kindly provided by M. Jucker, Hertie Institute for Clinical Brain Research, Tübingen, Germany; myd88-floxed mice (B6.129P2[SJL]-Myd88tm1Defr/J; MyD88fl/fl; Stock number: 008888) (Hou, Reizis, & DeFranco, 2008) were imported from the Jackson Laboratory, Bar Harbor, ME, USA; and Cx3Cr1-CreERT2 mice that express a fusion protein of Cre recombinase and an estrogen receptor ligand binding domain under the control of endogenous cx3cr1 promoter/enhancer elements (Goldmann et al., 2013) were kindly provided by M. Prinz, University of Freiburg, Germany. APP/PS1-transgenic mice were cross-bred with MyD88fl/fl and Cx3Cr1-Cre mice to

obtain mice with the following genotypes: APPtg or wt MyD88fl/wtCre^{+/-} and APPtg or wt MyD88fl/wtCre^{-/-}. In order to minimize potential toxic effects of MyD88 deficiency, we used heterogenous myd88-floxed mice (MyD88fl/wt) in the whole study. To induce the recombination of myd88 gene, 6-month-old mice were injected (i.p.) with tamoxifen (Sigma-Aldrich Chemie GmbH, Munich, Germany; 100 mg/kg) in corn oil once a day over 5 days. The phenotype of APP/PS1-transgenic mice with or without MyD88 deletion was compared between siblings. All animal experiments were performed in accordance with relevant national rules and authorized by Landesamt für Verbraucherschutz, Saarland, Germany (permission numbers: 29/2016).

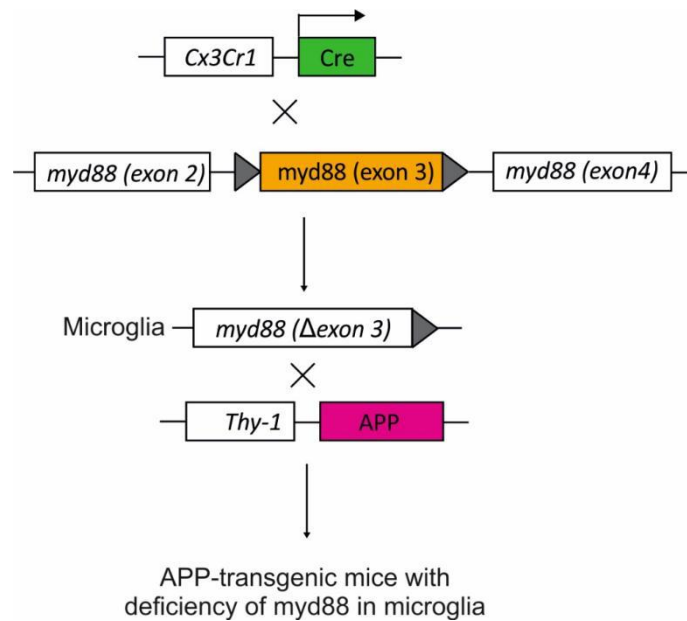


Fig 3.1 APP/PS1-transgenic mice with deficiency of myd88 in microglia. APP/PS1-transgenic mice were cross-bred with MyD88fl/fl and Cx3Cr1-Cre mice to obtain mice with the following genotypes: APPtg or wt MyD88^{fl/wt}Cre^{+/-} and APPtg or wt MyD88^{fl/wt}Cre^{-/-}. (Fig from Alex Liu)

All animal experiments were approved by the regional ethical committee of the regional council in Saarland, Germany.

3.2. Methods

3.2.1. Culture of pericytes

Human primary brain vascular pericytes (HBPC) were immortalized by infecting cells with tsSV40T lentiviral particles (Umehara et al., 2018). The selected immortalized HBPC clone 37

(hereafter referred to as HBPC/ci37) was used for our study. HBPC/ci37 cells were cultured at 33 °C with 5% CO₂/ 95% air in pericyte medium (Catalog: # 1201; Sciencell Research Laboratories, Carlsbad, CA, USA) containing 2% (v/v) fetal bovine serum, 1% (w/v) pericyte growth factors, and penicillin-streptomycin. Culture flasks and plates were treated with Collagen Coating Solution (Catalog: # 125-50; Sigma-Aldrich). HBPC/ci37 cells were used at 40 ~ 60 passages in this study.

3.2.2. Pericyte treatments

To investigate the effects of inflammatory activation on expression of LRP1, PDGFR β and CD13, pericytes were cultured in 12-well plate at 5.0×10^5 cells/well. Before experiments, we replaced culture medium with serum-free pericyte medium and cultured cells at 37°C for 3 days to facilitate cell differentiation (Umehara et al., 2018). Thereafter, pericytes were treated for 24 hours with recombinant human IL-1 β (Catalog: # 201-LB; R&D Systems, Wiesbaden, Germany) at 0, 5, 10 and 50 ng/ml, at 0, 5, 10 and 50 ng/ml for 24 hours, or for 8 days with and without withdrawal of IL-1 β for the last 3 days. At the end of experiments, cultured cells were lysed in RIPA buffer supplemented with protease inhibitor cocktail. Protein levels of LRP1, PDGFR β and CD13 were detected with quantitative Western blot as described in section 3.2.13. For Quantitative Western blot, the following antibodies were used: rabbit monoclonal antibodies against PDGFR β , CD13/APN, β -actin, GAPDH (clone: 28E1, D6V1W, 13E5, and 14C10, respectively; Cell Signaling Technology Europe), α -tubulin (clone: DM1A; Abcam).

3.2.3. Positive selection of CD11b-positive microglia in the adult mouse brain

To determine the gene expression in microglia, CD11b-positive cells were isolated from the entire cerebrum of 9-month-old APP/PS1-transgenic mice with our established protocol (Y. Liu et al., 2014). A single-cell suspension was prepared with Neural Tissue Dissociation Kit (papain-based) (Miltenyi Biotec B.V. & Co. KG, Bergisch Gladbach, Germany) and selected with MicroBeads-conjugated CD11b antibody (Miltenyi Biotec). Lysis buffer was immediately added to CD11b-positive cells for isolation of total RNA with RNeasy Plus Mini Kit (Qiagen, Hilden, Germany).

Procedure is as follows:

1. Prepare 1950 μ l enzyme mix 1 for up to 400 mg tissue and vortex. Pre-heat the mixture at 37 °C for 10 minutes before use.
2. Remove the mouse brain. Determine the weight of tissue in 1 ml of cold HBSS to make sure the 400 mg limit per digestion is not exceeded.
3. Place the brain on the lid of a 100 mm diameter petri dish, remove the meninges, and cut brain into small pieces using a scalpel.
4. Using a 5 ml pipette, add 5 ml of HBSS (w/o) and pipette pieces back into an appropriate-sized tube. Rinse with HBSS (w/o).
5. Centrifuge at 300 g for 7 minutes at room temperature and aspirate the supernatant carefully.
6. Add 1950 μ l of pre-heated enzyme mix 1 (Solutions 1 and 2) per up to 400 mg tissue.
7. Incubate in closed tubes for 15 minutes at 37 °C under slow, continuous rotation.
8. Prepare 30 μ l enzyme mix 2 per tissue sample by adding 20 μ l of Solution 3 to 10 μ l of Solution 4. Then add to samples.
9. Invert gently to mix. Do not vortex.
10. Dissociate tissue mechanically using the 17G needles by pipetting up and down 8 times slowly. Avoid forming air bubbles.
11. Incubate at 37 °C for 10 minutes.
12. Dissociate tissue mechanically using the 22G needles. Pipette slowly up and down 5 times with each pipette, or as long as tissue pieces are still observable. Be careful to avoid the formation of air bubbles.
13. Incubate at 37 °C for 10 minutes.
14. Apply the cell suspension to a 70 μ m cell strainer, placed on a 50 ml tube.
15. Discard cell strainer and centrifuge cell suspension at 300 g for 10 minutes at room temperature. Aspirate supernatant completely.
16. Suspend cells with buffer to the required volume for further applications.

After pelleting cells by centrifugation, 80 μ l of blocking buffer containing 25 μ g/ml rat anti-mouse CD16/CD32 antibody (2.4G2, BD), 10% FBS was added to prevent non-specific binding. Thirty minutes after blocking at 4 °C, 20 μ l MicroBeads-conjugated CD11b antibody (Miltenyi Biotec GmbH) was directly added to the cells. After 1 more hour of incubation at 4°C, cells were washed with buffer and loaded onto MACS LS Column (Miltenyi Biotec GmbH) to separate

CD11b-positive and negative cells. Lysis buffer was immediately added to both the CD11b-positive and the CD11b-negative cells for isolation of total RNA using RNeasy Plus Mini Kit (Qiagen GmbH).

3.2.4. Morris water maze test

The Morris water maze test, consisting of a 6-day training phase and a 1-day probe trial, was used to assess the cognitive function of APP/PS1-transgenic mice and their wild-type littermates, as previously described (Qin et al., 2016; Schnöder et al., 2020). During training phase, water was made opaque with nontoxic white paint to prevent animals from seeing the platform. The circular platform was hidden 1 cm beneath water surface at a fixed position. Mice were trained to find the hidden escape platform. There were four trials per training day, with a trial interval of 15 min. Mice were placed into the pool facing the sides at one of four starting locations. Latency time, path length, and velocity were recorded with Ethovision video tracking equipment and software (Noldus Information Technology, Wageningen, the Netherlands). After 6 training days, there was 1 day of rest, followed by a probe trial on the 8th day. During the probe trial, the platform was removed and the swimming path was recorded during 5 min. Time spent in each quadrant as well as path length, velocity, latency of first entrance and frequency of entries in the target quadrant, and the location of original platform were measured.

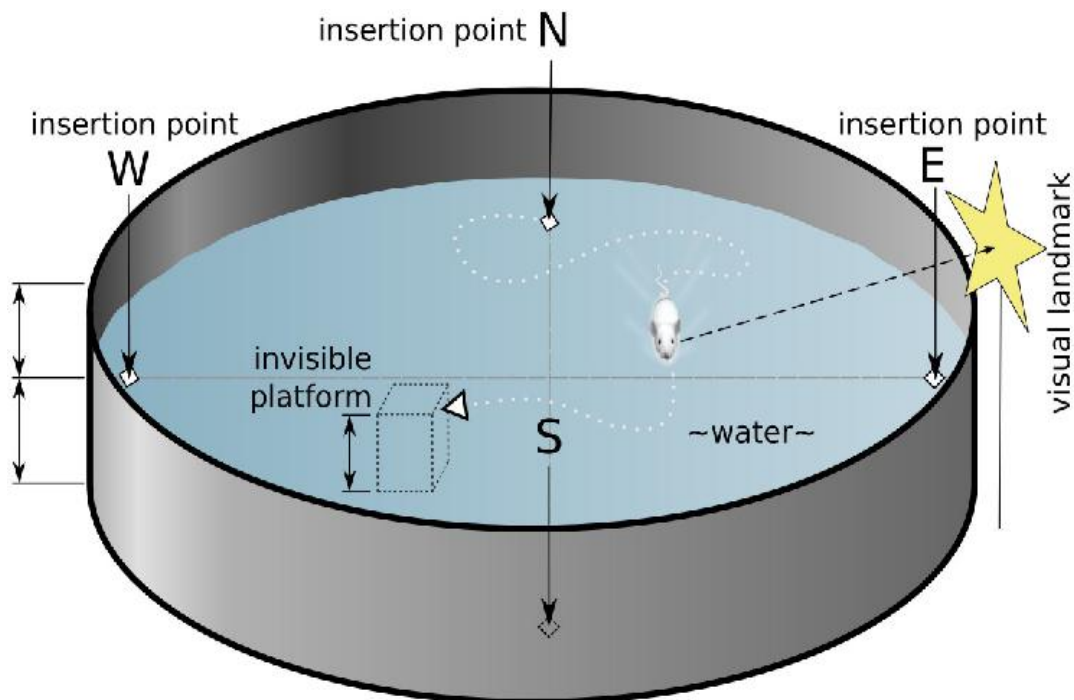


Fig 3.2 Morris water maze test. For Morris water maze test, a hidden platform (10cm diameter) was located 1cm below water level in a water bath (150cm diameter, 60cm depth). Four visual landmarks were placed on the walls of the water bath so that the mice can position themselves during the testing days (insertion points N S W E, example of landmark: yellow star). These cues allow the experimenter to virtually divide the water bath into four quadrants for further analysis of the results. The quadrant containing the platform was named q1, while the three other quadrants were named oq (other quadrants). (De Castell, S., Jenson, J., & Larios, H. (2015). Gaming Experience and Spatial Learning in a Virtual Morris Water Maze. *Journal For Virtual Worlds Research*, 8(1)).

3.2.5. Tissue collection

Animals were euthanized at 6 or 9 months of age by inhalation of isoflurane (Abbott, Wiesbaden, Germany). Whole blood was collected via intracardial puncture and kept in EDTA-containing Eppendorf tubes. Mice were then rapidly perfused transcardially with ice-cold PBS and the brain removed and divided. The left hemi-brain was immediately fixed in 4% paraformaldehyde (PFA, Sigma) for immunohistochemistry. A 0.5mm thick piece of tissue was sagittally cut from the right hemi-brain. The cortex and hippocampus were carefully separated and homogenized in Trizol (Life Technologies) for RNA isolation. The remainder of the right hemi-brain was snap frozen in liquid nitrogen for biochemical analysis (Fig 3.3) (Hao et al., 2011; Liu et al., 2012; Xie et al., 2013).

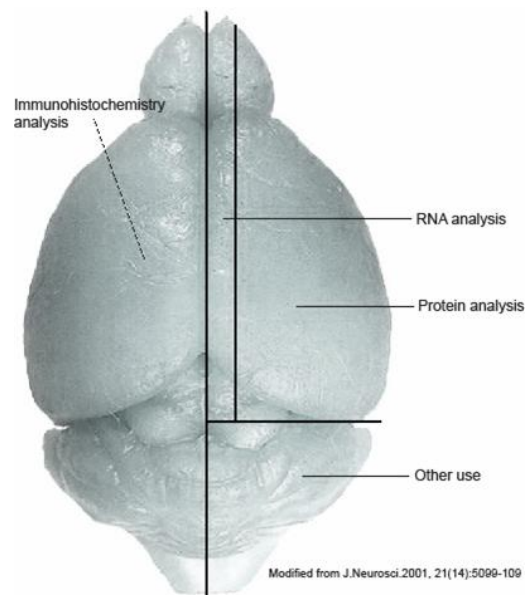


Fig 3.3 Schematic figure of brain sample sections preparation. The brain was divided into 4 parts. The left hemi-brain was immediately fixed in 4% PFA and stored at 4 °C for immunohistochemistry process. A 0.5

mm-thick piece of cerebral tissue was sagittally cut from the right hemi-brain, homogenized in TRIzol for RNA isolation. The rest of right hemi-cerebral was snap frozen in liquid nitrogen for biochemical analysis. The remained part was frozen in liquid nitrogen as well([Picture from: Shirong Liu](#)).

3.2.6. Isolation blood vessels of mice brain

Animals were euthanized at 9 months of age by inhalation of isofluorane. Mice were then perfused with ice-cold PBS, and the brain was removed and divided. The left hemisphere was immediately fixed in 4% paraformaldehyde (Sigma-Aldrich Chemie GmbH) in PBS and embedded in paraffin for immunohistochemistry. For one part of mice, A 0.5- μ m-thick sagittal piece of tissue was cut from the right hemisphere. The cortex and hippocampus were carefully separated and homogenized in TRIzol (Thermo Fisher Scientific, Darmstadt, Germany) for RNA isolation. The remainder of the right hemisphere was snap-frozen in liquid nitrogen and stored at -80°C until biochemical analysis.

For the other part of mice, the cortex and hippocampus from right hemisphere were carefully dissected and brain vessel fragments were isolated according to the published protocol (Boulay, Saubamea, Decleves, & Cohen-Salmon, 2015). Briefly, brain tissues were homogenized in HEPES-contained Hanks' balanced salt solution (HBSS) and centrifuged at 4,400 g in HEPES-HBSS buffer supplemented with dextran from *Leuconostoc* spp. (molecular weight 70,000; Sigma-Aldrich Chemie GmbH) to delete myelin. The vessel pellet was re-suspended in HEPES-HBSS buffer supplemented with 1% bovine serum albumin (Sigma- Aldrich Chemie GmbH) and filtered with 20 μ m-mesh. The blood vessel fragments were collected on the top of filter and stored at -80°C for biochemical analysis.

Procedure is as follows:

1. Prepare isolation vessel solutions: B1, add 1.5 ml of HEPES 1M to 150 ml of HBSS; B2, add 3.6 g of Dextran 7000 to 20 ml of B1; B3, add 1 g of BSA to 100 ml of B1.
2. Modify the filter holder by cutting the bottom off the upper screwing part.
3. Prepare immunostaining solutions: Fixation solution, 4% Paraformaldehyde in PBS (pH 7.4) ; Permeabilization/blocking solution, dilute goat serum to 5% and Triton X100 to 0.25% in PBS (pH 7.4).

4. Prepare a 50 ml beaker with 20 ml of B1 solution. Keep on ice and cover with parafilm to avoid air contamination.
5. Deeply anesthetize the mouse under a hood with a small paper towel soaked in 1 ml of pure Isoflurane that is added into the cage. Anesthesia is verified by a lack of reaction to a toe pinch. Kill the mouse by cervical dislocation.
6. Section the skin with a scalpel from the neck to the nose and pull it away. Remove all contaminating hairs with 1x PBS buffer.
7. To open the skull, first insert scissors anteriorly to the olfactory bulb, and open the scissors to rupture the skull in two parts.
8. Carefully remove the brain using a brain spatula. Dissect out the choroid plexus from the lateral ventricles as they would contaminate the blood vessel preparation.
9. Transfer the brain into the beaker containing B1 solution on ice. Up to 8 brains can be treated together.
10. Using two scalpels, manually and vigorously beat the brain in the B1 solution subsequently obtaining small pieces of about 2 mm.
11. Homogenize the preparation with an automatized Dounce homogenizer, performing 20 strokes at 400 rpm. Ensure that the glass tube is maintained in ice and that the upper part of the douncer is in solution when moving up and down, so as to prevent the formation of air pockets. If several samples are prepared, wash the douncer with ionized water between each homogenization.
12. Transfer the homogenate into a 50 ml plastic tube and proceed to the centrifugation at 2,000 g for 10 min at 4 °C. A large white interface (mostly myelin) will form on the top of the vessel pellet (red if no perfusion was performed) .
13. Discard the supernatant. The vessel pellet and the white interface will remain attached together. Add 20 ml of ice-cold B2 solution and shake the tube manually and vigorously for 1 min.

14. Proceed to the second centrifugation at 4,400 g for 15 min at 4 °C. The myelin will now form a dense white layer at the surface of the supernatant.
15. Carefully detach the myelin layer from the tube walls by holding the tube and slowly rotating it to allow the supernatant to pass along the walls. Discard myelin with the supernatant. The pellet containing the vessels remains attached at the bottom of the tube.
16. Blot the inside wall of the tube with an absorbent paper wrapped around a 5 ml plastic pipette and remove all residual fluids, avoid touching the vessel pellet. Keep the tube upside-down on an absorbent paper to drain any remaining liquid.
17. Suspend the pellet in 1 ml of ice-cold B3 solution by pipetting up and down with low-binding tips , keeping the tube on ice, then add another 5 ml of B3 solution. Make sure that vessels are dispersed as much as possible and do not form aggregates.
18. Prepare a beaker on ice with 30 ml of ice-cold B3 solution. Cover with parafilm to avoid air contamination.
19. Place a 20 µm-mesh filter on a modified filter holder on the top of a becker flask and equilibrate by applying 10 ml of ice-cold B3 solution.
20. Pour the vessel preparation on the filter and rinse the vessels with 40 ml of ice-cold B3 solution.
21. Recover the filter using clean forceps and immediately immerse it in the beaker containing the B3 solution. Detach the vessels from the filter by shaking it gently.
22. Pour the beaker content in a 50 ml plastic tube and centrifuge at 2,000 g for 10 min at 4 °C.
23. Add 1 ml B3 solution into the 50 ml plastic tube and transfer to a 1.5ml tube, 2,000 g for 5 min at 4 °C.

24. Add 50ul RIPA solution into the blood vessel sediment, Use the Ultrasonic cracker treat for 1 min. Protein levels of ABCB1,LRP1, PDGFR β , CD13 and others antibody were detected with quantitative Western blot as described in section 3.2.13.

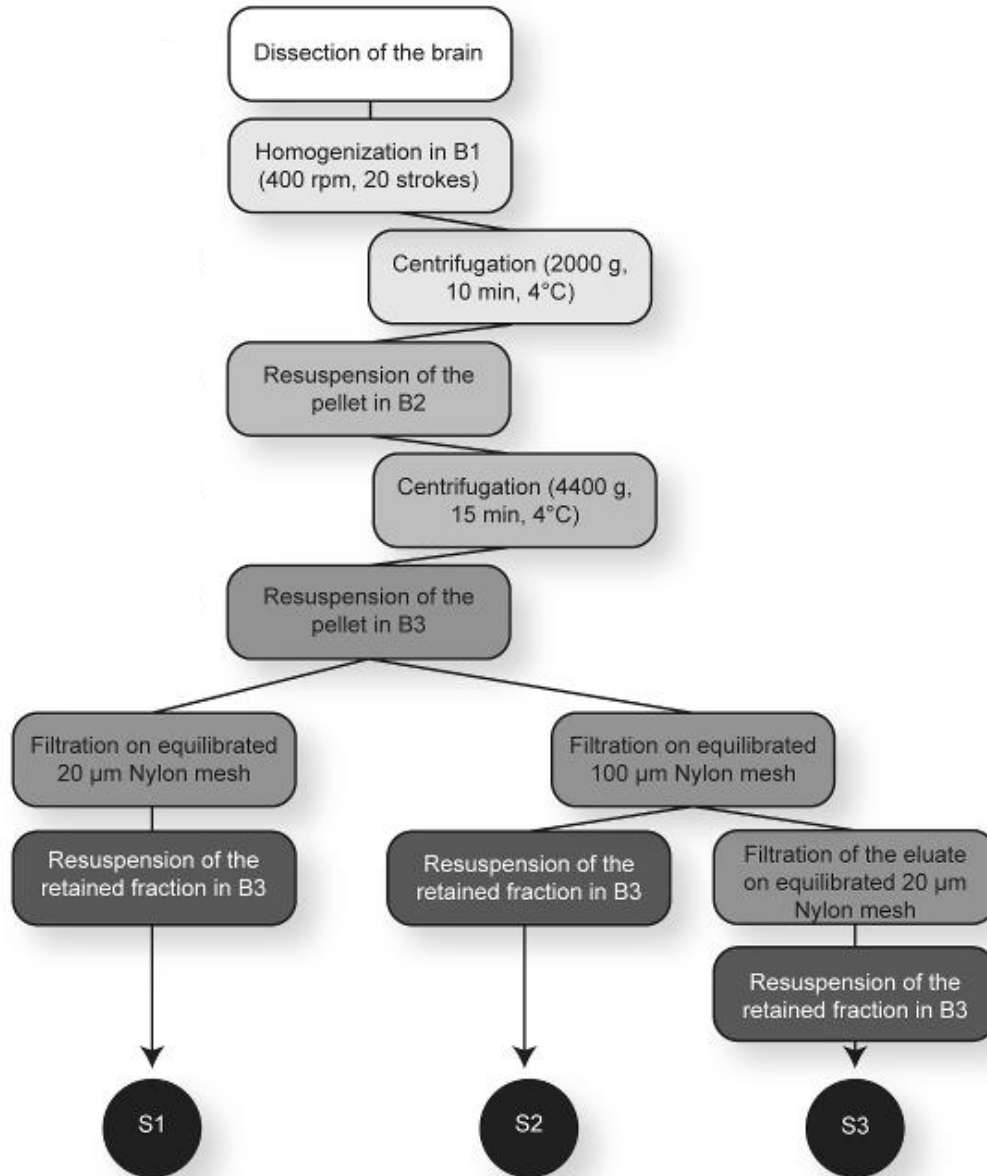


Fig3.4 Summary Scheme of the Brain Vessel Purification Protocol. The principal steps are presented. This sketch indicates the three possible vessel fractions that can be obtained depending on the filters used (20 or 100 μ m-mesh). S1: microvessels and large vessels, S2: large vessels and S3: microvessels.(*Boulay, A.C., Saubaméa, B., Declèves, X., Cohen-Salmon, M. Purification of Mouse Brain Vessels. J. Vis. Exp. (105), e53208,doi:10.3791/53208 (2015).*)

3.2.7. Quantify vasculature of mice brain

To quantify vasculature in the brain, our established protocol was used (Decker et al., 2018). Four serial paraffin-embedded sections per mouse with 300 μ m of distance in between were deparaffinized, heated at 80°C in citrate buffer (10mM, pH = 6) for 1 hour and digested with Digest-All 3 (Pepsin) (Thermo Fisher Scientific) for 20 minutes. Thereafter, brain sections were stained with rabbit anti-collagen IV polyclonal antibody (Catalog: # ab6586; Abcam, Cambridge, UK) and Alexa488-conjugated goat anti-rabbit IgG (Thermo Fisher Scientific). After being mounted, the whole hippocampus was imaged with Microlucida (MBF Bioscience). The length, branching points and density of collagen type IV staining-positive blood vessels were analyzed with a free software, AngioTool (<http://angiotool.nci.nih.gov>) (Zudaire, Gambardella, Kurcz, & Vermeren, 2011). The mean diameter of blood vessels was calculated by dividing total area of blood vessels with the total length of vessels. The parameters of analysis for all compared samples were kept constant. The length and branching points were adjusted with area of interest.

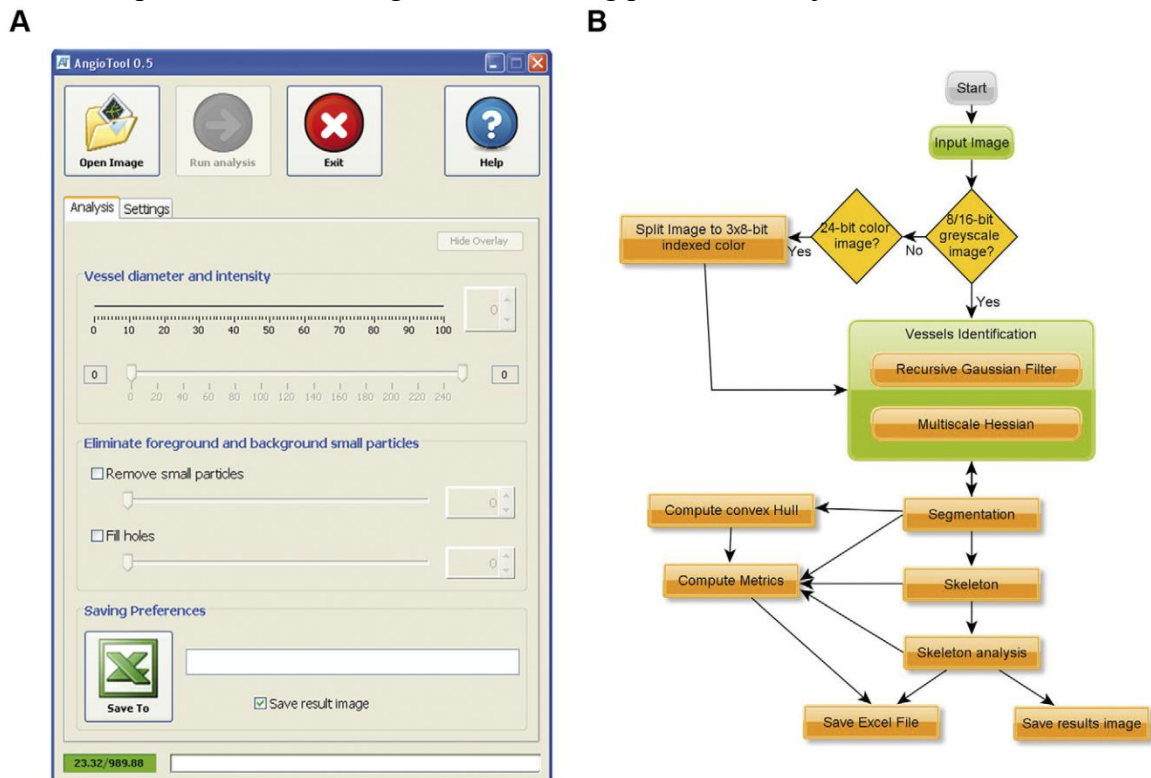


Fig 3.5 AngioTool's GUI and analysis flow. (A) AngioTool GUI for analysis of angiogenesis networks. A detailed quick analysis guide can be accessed through the help button. (B) Representation of the logical analysis flow performed by AngioTool which is based on identification of vessels using multiscale Hessian analysis and skeletonization. The analysis process is mostly automated (yellow boxes) with minimal user

intervention required to select the test image and during the visual identification of vessels (green squares). (Zudaire E, Gambardella L, Kurcz C, Vermeren S. A computational tool for quantitative analysis of vascular networks. *PLoS One*. 2011;6(11):e27385. doi: 10.1371/journal.pone.0027385.)

3.2.8. Immunohistochemistry for A β staining

In order to evaluate A β load, the sections throughout the entire hippocampus were randomly selected according to the random sampling method described in the last section. Volumes of A β , congo red staining and brain tissues (hippocampus and cortex) were estimated with the *Cavalieri* probe (Gundersen and Jensen, 1987) with 20 μ m of a grid size, which provided CE estimates <0.04. The A β load was demonstrated as the ratio of A β volume to relevant brain tissue volume. Detailed procedures are as follows:

1. The slides were serially deparaffinized in the solutions (2 \times 5 min Xylene, 2 \times 5 min 100% ethanol, 5 min 96% ethanol, 5 min 70% ethanol, and 5 min 50% ethanol).
2. Antigen retrieval by cooking the sections in HCl solution (2 mM) in a microwave oven, 560 watts, 3 min \times 5 times. Refill with solution between each cooking. Cool down with distill water after cook and incubate in formic acid for 1 min.
3. Wash slides with TBS, 5 min \times 2 times and then with TBS-T, 5 min, once.
4. Block with blocking buffer (0.2% casein + 0.1% Tween 20 +0.01% Triton X-100 in PBS), RT, 1h.
5. 1st Antibody reaction: with 1:50 dilution of the mouse monoclonal anti-human A β antibody (clone 6F/3D, Dako, Hamburg, Germany) in dilution buffer (0.02% casein + 0.01% Tween 20 +0.01% Triton X-100 in PBS), incubate at 4 °C, overnight.
6. Wash as step 3.
7. 2nd Antibody reaction: with the 1:200 diluted HRP-conjugated goat anti-mouse IgG (Dako) in dilution buffer, RT, 1h.
8. Wash as step 3.
9. Develop with DAB, 120 sec, and then wash with dH₂O, 3 times.
10. Dehydration: serially treat the slides in the following solutions: water, 3 min, 50% ethanol, 3 min 70% ethanol, 3 min 96% ethanol, 2 \times 3 min 100% ethanol, 2 \times 5 min Xylene.

11. Mount the slides with Entellan® Neu (Merck), and then cover the tissue with cover glass.

All images were acquired by Zeiss AxioImager.Z2 microscope (Carl Zeiss, Göttingen, Germany) equipped with a Stereo Investigator system (MicroBrightField, Williston, USA). The stereological technique was used to count the number of microglia. Briefly, after systematic random sampling of every 10th section throughout the entire hippocampus and cortex dorsal to the hippocampus, the Optical Fractionator as the stereological probe was used to quantify Iba-1-labelled cells with 120 × 120 × 18 μm of a disector and 400 × 400 μm of a sampling grid. The estimated coefficient of error (CE) was less than 0.08. Tissue thickness was measured at each disector location, using a focus drive with ±0.1 μm accuracy. In each disector, only Iba-1 positive cells with clear haematoxylin nucleus staining were counted.

The proliferating microglia, which appeared with typical brown microglial processes and dark blue nuclei, were counted in the total hippocampus area in the randomly selected sections as described above. Data were reported as the number of antibody-labeling cells divided by the full area (mm²) of interest. All immunohistochemical analyses were performed by an experimenter blinded to the genotype of mice.

To demonstrate the Aβ deposits in the blood vessel, we cooked Congo red-stained sections in citrate buffer and then treated them with pepsin (Life Technologies) for the antigen retrieval. After being blocked in goat serum, the sections were incubated with a rabbit polyclonal against collagen type IV (Cat. ab6586, Abcam) as the first antibody and Alexa488-conjugated goat anti-rabbit IgG as the second antibody.

To analyze the distribution of Aβ plaque size, we acquired images of hippocampus after Congo red staining with a 10 × objective (Carl Zeiss) using the Virtual Tissue Module (MicroBrightField). The hippocampus was delineated and the area of individual plaques was determined after performing histogram-based segmentation with Image-Pro Plus 6.0 software (Media Cybernetics, Silver Spring, MD, USA).

3.2.9. Immunofluorescent staining

3.2.9.1. Methoxy-X04 Staining for A β deposition

To evaluate the cerebral A β deposition, four serial brain sections from each animal were labeled with methoxy-X04 (Tocris Bioscience, Wiesbaden-Nordenstadt, Germany) after deparaffinization.

Detailed procedures are as follows:

1. The slides were serially deparaffinized in the solutions (2 \times 5 min Xylene, 2 \times 5 min 100% ethanol, 5 min 96% ethanol, 5 min 70% ethanol, and 5 min 50% ethanol).
2. Rehydrate the sections by incubating for 30 s in distilled water .
3. Antigen retrieval by cooking the sections in 1 \times citrate buffer (10 mM, pH 6.0) in a microwave oven, 560 watts, 3 min \times 5 times. Refill with buffer between each cooking. Cool down slowly by leaving on the bench for >30 min after cook.
4. Diluted methoxy-X04 to 1:1000 with DMSO, Incubated the slides for 20 min in the methoxy-X04 solution .
5. Washed 3 \times 5 times by PBST buffer .
6. Mount with Mowiol.

The whole cortex and hippocampus were imaged with Microlucida (MBF Bioscience) and merged. Fluorescence-labeled areas were measured using Image J software (<https://imagej.nih.gov/ij/>) with fixed thresholds for all compared animals. The percentage of A β coverage in the brain was calculated.

3.2.9.2. Iba-1 Staining

In order to evaluate neuroinflammatory activation, 4% PFA-fixed left hemispheres were embedded in paraffin and serial 40 μ m thick sagittal sections were cut and mounted on glass slides. Immunohistochemical staining with the primary antibody, rabbit anti-Iba-1 (1:500, Wako Chemicals, Neuss, Germany), was performed on these sections (Liu et al., 2013). Detailed procedures are as follows:

1. The slides were serially deparaffinized in the solutions (2 x 5 min Xylene, 2 x 5 min 100% ethanol, 5 min 96% ethanol, 5 min 70% ethanol, and 5 min 50% ethanol).

2. Antigen retrieval by cooking the sections in 1× citrate buffer (10 mM, pH 6.0) in a microwave oven, 560 watts, 3 min × 5 times. Refill with buffer between each cooking. Cool down slowly by leaving on the bench for >30 min after cook.
3. The endogenous peroxidase of the tissue was inactivated via incubating the slides in the mixture of H₂O₂/Methanol/dH₂O buffer, RT, 30min.
4. Wash slides with TBS, 5 min × 2 times and then with TBS-T, 5 min, once.
5. Block with blocking buffer (0.2% Casein (w/v) + 0.1% Tween 20 + 0.1% Triton X-100 in PBS), RT, 1h.
6. 1st Antibody reaction: with 1:500 dilution of the polyclonal rabbit-anti mouse-Iba-1 (Wako) in dilution buffer (0.02% Casein (w/v) + 0.01% Tween 20 + 0.01% Triton X-100 in PBS), incubate at 4 °C, overnight.
7. Wash as step 4.
8. 2nd Antibody reaction: with the 1:500 diluted HRP labeled Alexa488-conjugated anti-rabbit IgG (Thermo Fisher Scientific) in dilution buffer, RT, 1h.
9. Wash as step 4.
10. Mount with Mowiol.

To detect the deposition of A β at blood vessels, brain sections were co-stained with human A β antibody (clone D12B2) and biotin-labeled Griffonia Simplicifolia Lectin I isolectin B4 (Catalog: B-1205; Vector Laboratories, Burlingame, CA, USA), and Alexa488-conjugated anti-rabbit IgG and Cy3-conjugated streptavidin, respectively (Thermo Fisher Scientific).

The relationship between microglia and A β deposits was investigated as we did in a previous study (Hao et al., 2011). Serial brain sections were stained with Iba-1 antibody (Wako Chemicals) and Alexa546-conjugated anti-rabbit IgG (Thermo Fisher Scientific), and then co-stained with methoxy-X04 (Bio-Techne GmbH). Under Zeiss microscopy with 40× objective, A β deposits were imaged with green fluorescence filter. Thereafter, Z-stack serial scanning from -10 to +10 μ m was performed under both green and orange fluorescence filters. From each section, more than 10 randomly chosen areas were analyzed. The total number (> 200) of Iba-1-positive cells co-localizing with A β deposits were counted. The area of A β was measured with Image J and used for the adjudgment of microglial cell number.

3.2.10. Brain homogenates

The brain was homogenized as previously described (Liu et al., 2012). Briefly, frozen hemispheres were bounce-homogenized in the TBS containing protease inhibitor cocktail (Roche Applied Science, Mannheim, Germany) and centrifuged at 16,000×g for 30 minutes at 4°C. The supernatant (TBS-soluble fraction) was collected and stored at -80°C. The pellets were re-suspended in the TBS plus 1% Triton-X (TBS-T), sonicated for 5 minutes in 4°C water bath and centrifuged at 16,000×g for another 30 minutes at 4°C. The supernatant was collected and stored at -80°C as the TBS-T-soluble fraction. The pellets were extracted for a third time using an ice-cold guanidine buffer (5M guanidine-HCl/50mM Tris, pH 8.0, herein referred to as guanidine-soluble fraction). The protein concentration of all samples was measured using Bio-Rad Protein Assay (Bio-Rad Laboratories GmbH, Munich, Germany), with results normalized based on the sample's protein concentration.

3.2.11. Bio-Rad Protein Assay

Protein concentration Bio-Rad Assay was completed with Protein Assay Reagent (Bio-Rad), based on the Bradford dye-binding procedure (Bradford, 1976), a simple colorimetric assay for measuring total protein concentration. Protein concentrations between 200 µg/ml and 1,400 µg/ml (20-140 µg totals) can be assayed in a microplate format. Briefly, in high-concentration assay, 10 µl sample or serial diluted standards were loaded on a 96-well format microplate, and then 200 µl 1× assay reagent was added to each well. Absorption at 595 nm was read with a Micro-plate reader and protein concentration was determined according to a standard curve.

3.2.12. Western blot analysis

Frozen mouse brains were homogenized on ice in 5× radioimmunoprecipitation assay buffer (RIPA buffer; 50mM Tris [pH 8.0], 150mM NaCl, 0.1% SDS, 0.5% sodiumdeoxy- cholate, 1% NP-40, and 5mM EDTA) supplemented with protease inhibitor cocktail (Sigma- Aldrich Chemie GmbH), followed by centrifugation at 16,000 × g for 30 minutes at 4 °C to collect the supernatants. Isolated blood vessels were directly lysed in 2 × SDS-PAGE sample loading buffer containing 4% SDS and sonicated before loading. The protein levels of synaptic proteins: Munc18-1 protein mammalian homolog (Munc18-1), synaptosome-associated protein 25

(SNAP-25), postsynaptic density protein 95 (PSD-95) and synaptophysin were detected with rabbit polyclonal antibodies (Catalog numbers: 13414, 3926 and 2507, respectively; Cell Signaling Technology) and mouse monoclonal antibody (clone SY38; Abcam). In the same sample, β -actin was detected as a loading control using rabbit monoclonal antibody (clone: 13E5; Cell Signaling Technology). For the detection of proteins in cerebral capillaries, rabbit Sodium dodecyl sulfate-polyacrylamide gel electrophoresis monoclonal antibodies against platelet-derived growth factor receptor β (PDGFR β), CD13/APN, ABCB1 and vinculin (clone: 28E1, D6V1W, E1Y7S and E1E9V respectively; Cell Signaling Technology) and rabbit polyclonal antibodies against LRP1 and α -tubulin (Catalog numbers: 64099 and 2144, respectively; Cell Signaling Technology), tight junction protein 1 (TJP1; Catalog numbers: NBP1-85047; Novus Biologicals, Wiesbaden-Nordenstadt, Germany), Claudin-5 (Thermo Fisher Scientific) and aquaporin 4 (AQP4; Proteintech Europe, Manchester, United Kingdom) were used. Western blots were visualized via the ECL method (PerkinElmer LAS GmbH, Rodgau, Germany). Densitometric analysis of bands was performed with Image J software. For each sample, the protein level was calculated as a ratio of target protein/ β -actin, α -tubulin or vinculin.

For detection of A β oligomers, the proteins in the brain homogenate or in the isolated blood vessels were separated by 10 - 20% pre-casted Tris-Tricine gels (Anamed Elektrophorese GmbH, Groß-Bieberau/Rodau, Germany). For Western blot, anti-human A β mouse monoclonal antibody (clone W0-2; Merck Chemicals GmbH, Darmstadt, Germany), anti- β -actin or anti- α - tubulin antibodies (Cell Signaling Technology) were used.

For detection of PDGFR β and CD13 in cerebral blood vessels, isolated blood vessels were lysed in RIPA buffer (50mM Tris [pH 8.0], 150mM NaCl, 0.1% SDS, 0.5% sodiumdeoxycholate, 1% NP-40, and 5mM EDTA) supplemented with protease inhibitor cocktail (Roche Applied Science, Mannheim, Germany) on ice. The tissue lysate was sonicated before being loaded onto 10% SDS-PAGE. For Western blot detection, rabbit monoclonal antibodies against PDGFR β and CD13/APN (clone: 28E1 and D6V1W, respectively; Cell Signaling Technology Europe) were used. In the same sample, β -actin was detected as a loading control using rabbit monoclonal antibody (clone: 13E5; Cell Signaling Technology Europe). Western blots were visualized via the ECL method (PerkinElmer LAS GmbH, Rodgau, Germany). Densitometric

analysis of band densities was performed with ImageJ software (<https://imagej.nih.gov/ij/>). For each sample, the protein level was calculated as a ratio of target protein/ β -actin.

The sodium dodecyl sulfate-polyacrylamide gel electrophoresis (SDS-PAGE) technique separates proteins according to their mobility difference in an electric field. Protein samples treated with SDS show an identical charge per unit mass and migrate in SDS gels only according to their molecular masses. The SDS-PAGE system used in this study is the Mini-PROTEAN® 3 Cell electrophoresis system (Bio-Rad). One gel is composed of a lower separating gel and an upper stacking gel. The stacking gel is 5%, while the percentage of the separating gel varies from 8% to 15%. Low percentage gels are used for large proteins, while small proteins are separated in high percentage gels. In this study, 10% separating gel was used. The gel and the electrodes were assembled in the SDS-PAGE chamber. The samples were diluted 1:2 in 3 × SDS-PAGE Sample loading buffer and heated at 95°C for 5min. Then, 20 μ l sample per well was loaded to 10% Acrylamide gel for electrophoresis running at 120 V until the Bromophenol blue front runs out of the gel. Proteins on the gel were transferred to membranes of nitrocellulose (NC) or polyvinylidene fluoride (PVDF) and detected by immunoblotting.

3.2.13. Protein detection using immunoblotting

Proteins separated by SDS-PAGE were further transferred to NC or PVDF membranes. PVDF membranes must be activated prior to the transfer by short incubation in 100 % methanol.

In this work, the membrane and sponges were immersed in transfer buffer before the transfer and the transfer buffer was cooled at 4 °C. In the transfer, the gel and membrane were sandwiched between sponge and paper (sponge/paper/gel/membrane/paper/sponge) and all are clamped tightly together after ensuring no air bubbles have formed between the gel and membrane. The transfer chamber was completely filled with transfer buffer and completed the transfer at 250 mA for 65 min. Subsequently, the sandwich was unpacked and the SDS gel discarded. The membrane with the immobilized protein was 10% skim milk powder (w/v) in PBS for 1 h at RT or 4 ° C overnight in order to saturate unspecific binding sites. Then, the membrane was washed twice for 5 minutes each with PBS. The primary antibody was diluted in PBS with 1% skimmed milk powder (w/v) at the concentration indicated below, and incubated with the membrane at 4 °C overnight. The membrane was washed 3x10 min in TBS + 0.05% Tween 20 to remove

residual primary antibody. The membrane was then incubated with the appropriate secondary antibody at the concentration indicated below. The secondary antibody was diluted in PBS +1% skim milk powder (w/v) and the incubation period was 1 hours. Therefore, the membrane was washed 3×10 min with TBS + 0.05% Tween 20. Lightning ECL substrate (Perkin Elmer) was developed. According to the manufacturer charges substrate solution A and B substrate solution were mixed in a 1:1 ratio and evenly distributed on the membrane. After 2 minutes, the substrate mixture was removed and the chemiluminescence detected using Amersham Hyperfilm ECL (GE Healthcare) in a darkroom. Kodak GBX developer and fixer were used to make signals visible.

The western blot films were scanned with the Epson Perfection V700 Photo Scanner. Densitometric analyzes were performed with the image processing program Image J (NIH, Version 1.43).

3.2.14. Purification of membrane components and β - and γ -secretase activity assays

Membrane components were purified from 6-month-old APP-transgenic and non-transgenic littermate mouse brains with established methods (Burg et al., 2013; Hao et al., 2011; Xie et al., 2013). Briefly, brain tissue was homogenized in sucrose buffer (10mM Tris/HCl, pH=7.4, 1mM EDTA, 200mM sucrose). Cell nuclei were removed by centrifugation at 1,000×g and 4°C for 10 minutes. The supernatant was transferred to a new tube and centrifuged again at 10,000×g and 4°C for 10 minutes. The resulting supernatant was centrifuged at 187,000×g and 4°C for 75 minutes in an Optima MAX Ultracentrifuge (Beckman Coulter, Krefeld, Germany). The supernatant was discarded and the pellet containing the crude membrane fraction was stored at -80°C until use. β - and γ -secretase activities were measured by incubating the crude membrane fraction at 0.1mg/ml for β -secretase and 1mg/ml for γ -secretase with 8 μ M secretase-specific FRET substrates. At 37°C, in the β -secretase buffer (0.1M sodium acetate, pH=4.5) and γ -secretase buffer (50mM Tris/HCl, pH=6.8, 2mM EDTA), both secretases cleaved the fluorogenic substrates resulting in continuous accumulation of fluorescence signals which were measured by Synergy Mx Monochromator-Based Multi-Mode Microplate Reader (BioTek, Winooski, USA). For both secretase assays, dynamic reading of fluorescence intensity in each well was performed

for 73 cycles with intervals of 5 minutes. Fluorescence intensity of the first cycle was considered to be background and subtracted for each well. Data were presented as an activity-time curve.

3.2.15. Reverse transcription and quantitative PCR for analysis of gene transcripts

Real-time PCR is a quantitative PCR method for the determination of cope number of PCR templates such as DNA or complementary DNA (cDNA) in a PCR reaction. There are two types of real-time PCR: intercalator-based and probe-based. Both methods require a special thermocycler equipped with a sensitive camera that monitors the fluorescence in each well of the 96-well plate at frequent intervals during the PCR Reaction. Intercalator-based method (also known as SYBR Green method) requires a double-stranded DNA dye in the PCR reaction which binds to newly synthesized double-stranded DNA and gives fluorescence. Probe-based real-time PCR (also known as TaqMan PCR) requires a pair of PCR primers (as regular PCR does) an additional fluorogenic probe which is an oligonucleotide of 20-26 nucleotides with both a reporter fluorescent dye and a quencher dye attached. The probe is designed to bind only the DNA sequence between the two specific PCR primers. Only a specific PCR product can generate a fluorescent signal in TaqMan PCR. Therefore, the TaqMan method is more accurate and more reliable than SYBR green method.

In our study, real-time PCR was performed using SYBR green (Roche Applied Science) or Taqman® probes (Life Technologies) with the 7500 Fast Real-Time PCR System (Life Technologies). Taqman® gene expression assays from Life Technologies were used to measure transcripts of the following genes: Taqman gene expression assays of mouse tumor necrosis factor (*tnf-α*), interleukin-1β (*il-1β*), inducible nitric oxide synthase (*inos*), chemokine (C–C motif) ligand 2 (*ccl-2*), *il-10*, chitinase-like 3 (*chi3l3*), mannose receptor C type 1 (*mrc1*), insulin growth factor (*igf*)-1 , triggering receptor expressed on myeloid cells 2 (*trem2*), *apoe*, CX3C chemokine receptor 1 (*cx3cr1*), purinergic receptor P2Y12 (*p2ry12*), C-type lectin domain family 7 member A (*clec7a*), lipoproteinlipase (*lpl*), transforming growth factor β receptor 1 (*tgfbr1*), integrin α X (*itgax*) and glyceraldehyde 3-phosphate dehydrogenase (*gapdh*) (Thermo Fisher Scientific). The transcription of osteopontin (*opn*), vascular endothelial growth factor (*vegf*) and peptidyl-prolyl cis-trans isomerase A (*ppia*) genes in CD11b-positive cells. The primer sequences for detecting transcripts of those genes were the same as used in our earlier study (Liu et al., 2006; Liu et al., 2014).

3.2.15.1. Brain total RNA isolation with Trizol

Homogenization: The 0.5 mm-thick piece of tissue sagittally cut from the right hemi-brain (see above tissue preparation section 3.2.6) was homogenized in 1 ml Trizol (Invitrogen).

1. Phase separation: Incubate the homogenized samples for 5 min at room temperature to permit complete dissociation of nucleoprotein complexes. Then add 0.2 ml of chloroform and shake vigorously by hand for 15 sec, and then incubate at room temperature for 3 min. Centrifuge the samples at $12,000 \times g$ for 15 min at 4°C . The sample mixture was separated into a lower red, phenol-chloroform phase, an interphase and a colorless upper aqueous phase. RNA remains in the aqueous phase.
2. RNA precipitation: Transfer the colourless aqueous phase to a fresh tube; precipitate the RNA from the aqueous phase by mixing with 0.5 ml isopropyl alcohol. Incubate at room temperature for 10 min and then centrifuge at $12,000 \times g$ for 10 min at 4°C . The precipitated RNA is the gel-like pellet on the bottom side of the tube.
3. RNA wash: remove the supernatant and wash the RNA once with 1 ml 75% ethanol. Mix by vortexing and centrifuge at $7,600 \times g$ for 5 min at 4°C .
4. Redissolve the RNA: briefly dry the RNA pellet, incubating for 10 min at RT and then dissolve it in appropriate volume of RNase-free water.

3.2.15.2. Genome DNA degradation prior to RT-PCR

Components	Volume/10μl reaction
RNA sample in water	8 μ l
RQ1 RNase-Free DNase 10 \times Reaction buffer	1 μ l
RQ1 RNase-Free DNase	1 U/ μ g RNA
Nuclease-free water	To a final volume of 10 μ l

3.2.15.4. Real-time quantitative PCR

For quantification of *tnf- α* , *il-1 β* , *mrc1*, *arg1*, *chi3l3*, (*igf*)-1, *trem2*, *apoe*, *cx3cr1*, *p2ry12*, *clec7a*, *lpl*, *tgfbr1*, *itgax*, *gapdh*, *opn*, vascular endothelial growth factor (*vegf*) and peptidyl-prolyl cis-trans isomerase A (*ppia*) transcription level, real-time quantitative PCR with the Taqman® gene expression assays was performed using the 7500 Fast real-time PCR system (Applied Biosystems) with a DyNAmo™ Flash Probe qPCR kit (Roche Applied Science).

Reaction setup for Taqman probe:

Components	Volume	Concentration
2× DyNAmo™ Flash Probe Master Mix	10 μ l	1×
Primer Mix (10 μ M)	1 μ l	0.5 μ M
50× ROX reference dye	0.06 μ l	0.3×
cDNA	1 μ l	max. 150 ng
ddH ₂ O	Up to 20 μ l	

Select FAM-labeled detectors and set up reaction system cycling to run:

step	purpose	temp	time	cycles
1	Initial denaturation	95 °C	10 min	1
2	Denaturation	95 °C	10 s	45
	Annealing+extension	60 °C	30 s	

The amount of double-stranded PCR product synthesized in each cycle was measured by detecting the free FAM dye cleaved from the Taqman® probes. Threshold cycle (Ct) values for each test gene from the replicate PCRs was normalized to the Ct values for the 18s RNA control from the same cDNA preparations. The ratio of transcription of each gene was calculated as $2^{(\Delta Ct)}$, where ΔCt is the difference Ct (*gapdh*) – Ct (test gene).

3.2.16. Statistical analysis

Data shown in the Figures are presented as mean \pm SD (for in vitro data) or mean \pm SEM (for in vivo data). For multiple comparisons, one-way or two-way ANOVA followed by Bonferroni's, Tukey's Honestly Significant Difference or Tamhane's T2 post hoc test (dependent on the result of Levene's test to determine the equality of variances) was applied. Two-independent-samples t-test was used to compare means for two groups of cases. All statistical analysis was performed on GraphPad Prism 8 version 8.0.2. for Windows (GraphPad Software, San Diego, CA, USA). Statistical significance was set at $p < 0.05$.

4. RESULTS

4.1. Establishment of APP/PS1-transgenic mice with haploinsufficiency of MyD88 in microglia

To investigate effects of microglial MyD88 on AD pathogenesis, we mated APP/PS1-transgenic mice with MyD88^{fl/fl} mice and Cx3Cr1-CreERT2 mice. Littermate mice with APP^{tg}Myd88^{fl/wt}Cre^{+/-} and APP^{tg}Myd88^{fl/wt}Cre^{-/-} of genotypes were injected with tamoxifen at 6 months of age. Tamoxifen induced gene recombination should delete one allele of *myd88* gene in >93% microglia but not in other brain cells (Goldmann et al., 2013). Tamoxifen injection also knocks out loxP site-flanked *myd88* gene in peripheral Cx3Cr1-positive myeloid cells; however, normal MyD88-expressing myeloid cells produced from the bone marrow should replace these MyD88-deficient cells within 1 month (Goldmann et al., 2013). By detecting *myd88* gene transcripts in CD11b-positive brain cells from 9-month-old APP^{tg}Myd88^{lox/wt}Cre^{+/-} (Myd88^{het}) and APP^{tg}Myd88^{lox/wt}Cre^{-/-} (Myd88^{wt}) mice, we observed that the transcriptional level of *myd88* in microglia of Myd88^{het} mice was only 11.4 % of that in Myd88^{wt} mice (Fig 4.1, A; *myd88/gapdh*: 0.178 ± 0.054 [wt] and 0.020 ± 0.004 [het]; *t* test, *p* = 0.044; *n* = 3 per group), which was in accordance with a previous observation that heterozygous knockout of *myd88* gene reduced *myd88* transcripts by 66% in the whole brain of APP-transgenic mice (Michaud et al., 2011). As a control, transcriptional levels of *myd88* (*myd88/gapdh*) in CD11b-positive blood cells were 0.100 ± 0.023 and 0.123 ± 0.025, in Myd88^{het} and Myd88^{wt} mice, respectively (Fig 4.1, B; *t* test, *p* = 0.518; *n* = 4 per group).

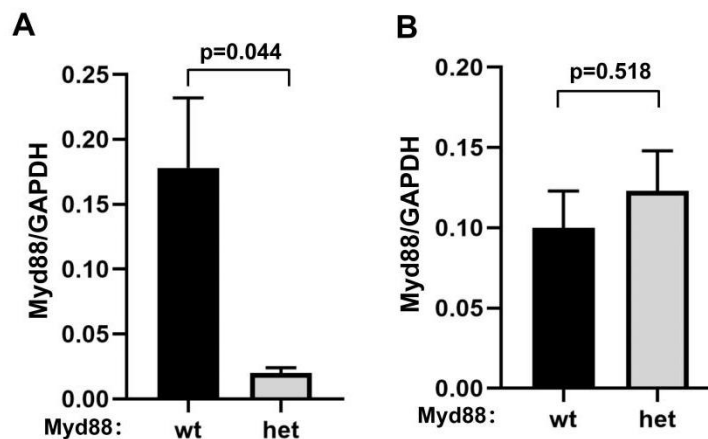


Fig 4.1 Establishment of APP/PS1-transgenic mice with haploinsufficiency of MyD88 in microglia.

We detected *myd88* gene transcripts in CD11b-positive brain cells from 9-month-old APP^{tg}Myd88^{lox/wt}Cre^{+/-} (Myd88^{het}) and APP^{tg}Myd88^{lox/wt}Cre^{-/-} (Myd88^{wt}) mice, transcriptional level of *myd88* in microglia of Myd88^{het} mice was only 11.4 % of that in Myd88^{wt} mice (A; *t* test, $p = 0.044$; $n = 3$ per group), transcriptional levels of *myd88* (*myd88/gapdh*) in CD11b-positive blood cells were no difference in Myd88^{het} and Myd88^{wt} mice, respectively (B; *t* test, $p = 0.518$; $n = 4$ per group).

4.2. Haploinsufficiency of microglial MyD88 improves cognitive function of APP/PS1-transgenic mice

We used the Morris water maze test to examine cognitive function of mice. During the acquisition phase, 9-month-old non-APP-transgenic (APP^{wt}) littermate mice with or without deletion of MyD88 in microglia (APP^{tg}Myd88^{lox/wt}Cre^{+/-} and APP^{tg}Myd88^{lox/wt}Cre^{-/-}) showed no significant differences in either swimming time or swimming distance before climbing onto the escape platform (Fig 4.2, A and B; two-way ANOVA, $p > 0.05$). Compared to APP^{tg}Myd88^{lox/wt}Cre^{+/-} littermates, 9-month-old APP^{tg}Myd88^{lox/wt}Cre^{-/-} mice with normal MyD88 expression spent significantly more time (Fig 4.2, A; two-way ANOVA, $p < 0.05$) and traveled longer distances (Fig 4.2, B; two-way ANOVA, $p < 0.05$) to reach the escape platform. Interestingly, APP^{tg}Myd88^{lox/wt}Cre^{+/-} mice with the heterozygous deletion of microglial MyD88 performed significantly better than their APP^{tg}Myd88^{lox/wt}Cre^{-/-} littermates in searching and finding the platform after 3 days of training (Fig 4.2, A and B; two-way ANOVA, $p < 0.05$). The swimming velocity did not differ between MyD88-deficient and wild-type APP-transgenic mice or for the same mice on different training dates (data not shown).

Twenty-four hours after the end of training phase, the escape platform was removed and a 5-minute probe trial was performed to test the memory of mice. Compared to APP^{wt}Myd88^{lox/wt}Cre^{-/-} littermates, APP^{tg}Myd88^{lox/wt}Cre^{+/-} mice crossed the region where the platform had been located with significantly less frequency, and remained for a significantly longer time in their first visit to the original platform region during the total 5-minute probe trial (Fig 4.2, C and D; one-way ANOVA followed by *post-hoc* test, $p < 0.05$). Interestingly, when compared to APP^{tg}Myd88^{lox/wt}Cre^{-/-} mice, APP^{tg}Myd88^{lox/wt}Cre^{+/-} mice were able to cross the region more frequently and reach the original platform region in significantly less time (Fig 4.2, C and D; one-way ANOVA followed by *post-hoc* test, $p < 0.05$). We observed differences in

neither parameter analyzed in the probe trial between $APP^{wt}Myd88^{lox/wt}Cre^{+/-}$ and $APP^{wt}Myd88^{lox/wt}Cre^{-/-}$ littermate mice (Fig 4.2, C and D; one-way ANOVA, $p > 0.05$).

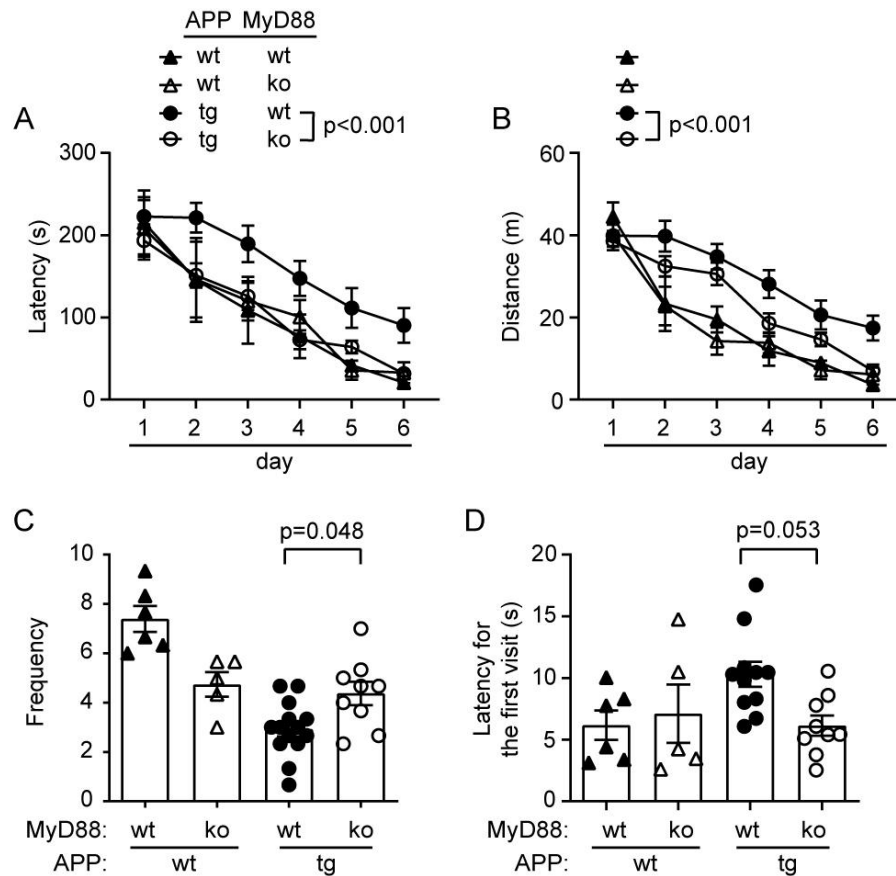


Fig 4.2 Haploinsufficiency of microglial MyD88 improves cognitive function in APP/PS1-transgenic mice. During the training phase of the water maze test, 9-month-old APP-transgenic mice (APPtg) spent more time and traveled longer distances to reach the escape platform than did their non-APP-transgenic littermates (APPwt). Compared to mice with normal expression of MyD88 (wt), heterozygous deletion of MyD88 in microglia (het) significantly reduced the traveling time and distance of APPtg mice but not of APPwt mice (A, B; two-way ANOVA followed by Bonferroni *post hoc* test; $n \geq 5$ per group). In the probe trial, APPtg mice crossed the region where the platform was previously located with significantly less frequency during the total 5-minute experiment, and spent significantly longer time in the first visit to the platform region; deletion of MyD88 in microglia recovered these APP expression-induced cognitive impairments (C, D; one-way ANOVA followed by Bonferroni *post hoc* test).

4.3. Haploinsufficiency of microglial MyD88 preserves synaptic proteins in APP/PS1-transgenic mice

In our previous study, we have observed that over expression of APP/PS1 decreases protein levels of synaptic proteins (Schnöder et al., 2020). We further used Western blot analysis to quantify the levels of four synaptic structure proteins: Munc18-1, synaptophysin, SNAP-25, and PSD-95 in the brain homogenate of 9-month-old APP^{Tg} littermate mice with different expression of MyD88. As shown in Fig 4.3, A-E, protein levels of synaptophysin, and SNAP-25 in APP^{Tg}MyD88^{lox/wt}Cre^{+/-} mice were significantly higher than levels of these proteins derived from APP^{Tg}MyD88^{lox/wt}Cre^{-/-} littermate mice (*t* test, *p* < 0.05). Deficiency of microglial MyD88 tended to increase the protein level of PSD-95 in the brain as compared with MyD88-wild type AD mice (Fig 4.3, E; *t* test, *p* = 0.096).

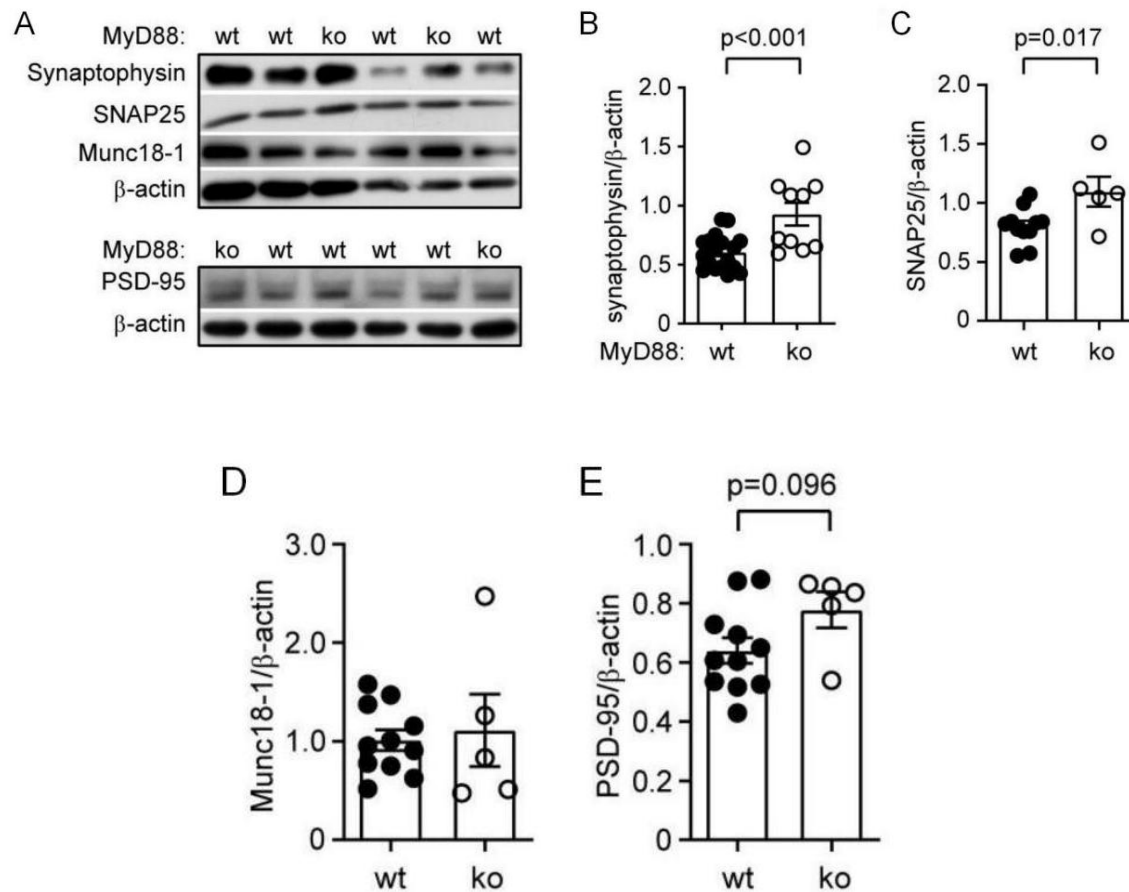


Fig 4.3 Haploinsufficiency of microglial MyD88 attenuates AD-associated loss of synaptic proteins in APP/PS1-transgenic mice. Western blotting was used to detect the amount of synaptic structure proteins,

Munc18-1, SNAP25, synaptophysin, and PSD-95 in the brain homogenate of 9-month-old APPtg mice (A-E). Deficiency in microglial MyD88 was associated with higher protein levels of synaptophysin and SNAP25 (*t* test; $n \geq 5$ per group).

4.4.Haploinsufficiency of microglial MyD88 reduces A β load in the brain parenchyma of APP/PS1-transgenic mice

After observing that heterozygous deletion of MyD88 in microglia attenuated cognitive deficits of APPtg mice but not of APP wt littermates, we analyzed the effects of microglial MyD88 on A β load in the APP tg mice, as A β is the key molecule leading to neurodegeneration in AD (Mucke & Selkoe, 2012). We stained brain sections from APP^{tg}Myd88^{lox/wt}Cre^{+/-} and APP^{tg}Myd88^{lox/wt}Cre^{-/-} mice with methoxy-X04, which specifically recognizes β -sheet secondary structure of A β . We observed that Haploinsufficiency of microglial MyD88 significantly reduced the area of methoxy-X04 staining-positive A β plaques in both hippocampus and cortex of APP/PS1-transgenic mice (Fig 4.4, A and B; *t* test, $p < 0.05$). We then used standard immunohistological and stereological Cavalieri methods to evaluate A β volume, adjusted relative to the volume of analyzed tissues, in the hippocampus of 9-month-old APP^{tg}Myd88^{lox/wt}Cre^{+/-} and APP^{tg}Myd88^{lox/wt}Cre^{-/-} mice. The volume of 7.67 % \pm 0.71 % of APP^{tg}MyD88^{fl/wt}Cre^{+/-} mice was significantly lower than that of APP^{tg}MyD88^{fl/wt}Cre^{-/-} mice (10.83 % \pm 0.56 %; Fig 4.4, C and D; *t* test, $p < 0.05$).

To measure the amount of oligomeric A β in brain tissues, quantitative Western blot was performed as we did in previous studies (Schnöder et al., 2020; Schnöder et al., 2016). We observed that the protein level of dimeric but not monomeric A β in 9-month-old APP^{tg}MyD88^{fl/wt}Cre^{+/-} mice was significantly lower than that in APP^{tg}MyD88^{fl/wt}Cre^{-/-} littermates (Fig 4.4, E, F and G; *t* test, $p < 0.05$). Dimer has been considered as a toxic species of A β aggregates (Shankar et al., 2008).

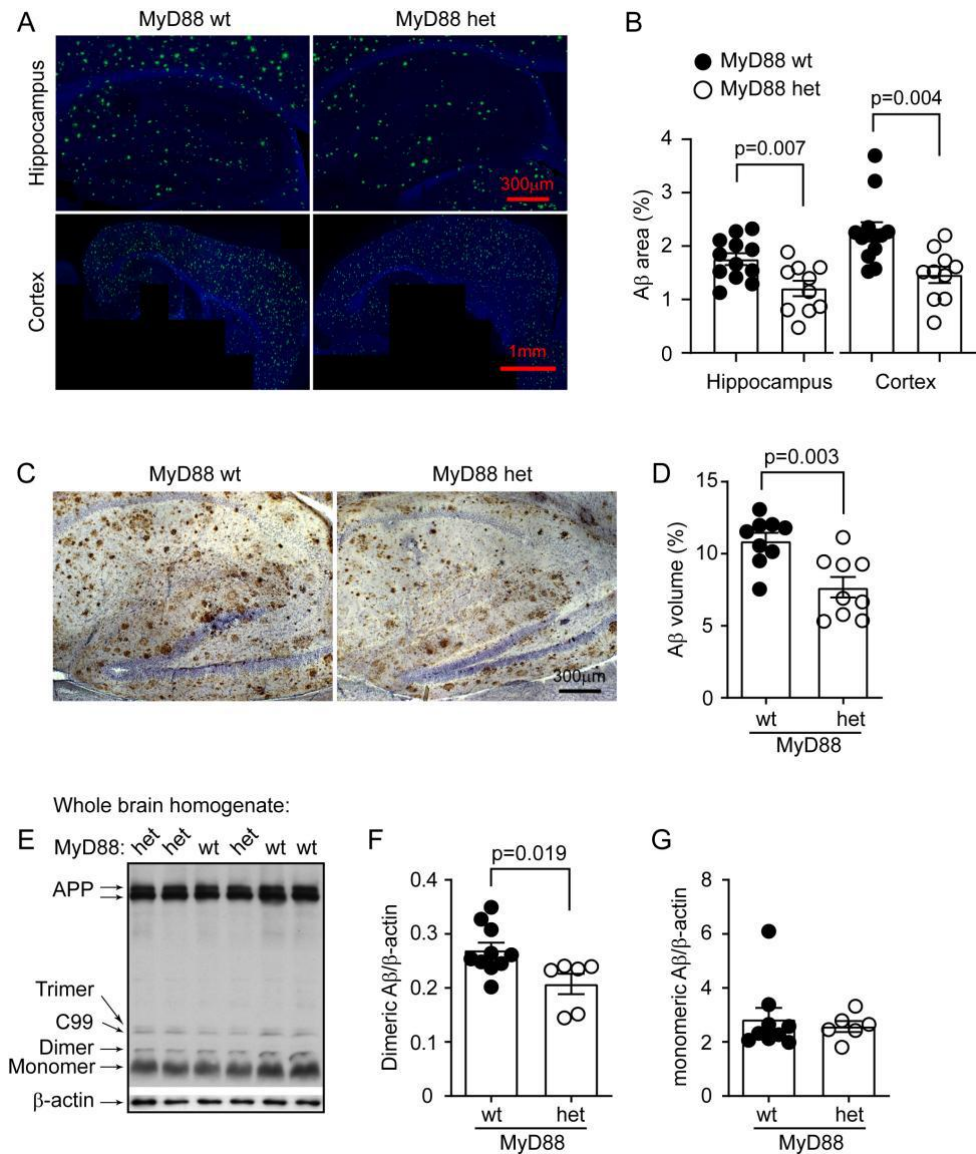


Fig4.4 Haploinsufficiency of microglial MyD88 reduces cerebral A β load in APP/PS1-transgenic mice. Six-month-old APP^{tg}MyD88^{fl/wt}Cre^{+/-} (MyD88 het) and APP^{tg}MyD88^{fl/wt}Cre^{-/-} (MyD88 wt) were injected with tamoxifen and analyzed by 9 months of age for A β load in the brain. Brain sections were first stained with methoxy-X04 and imaged with Microlucida (A). The area of A β plaques were quantified and adjusted by the area of analyzed brain tissue (B). Brain sections were further stained with human A β -specific antibodies (C) and the volume of immune reactive A β deposits in hippocampus were estimated with stereological Cavalieri method and adjusted by the volume of analyzed tissues (D). Deletion of microglial MyD88 significantly decreases A β deposits in the brain (B and D; t test; n \geq 9 per each group). The brains derived from 9-month-old microglial MyD88-het and wt APP-transgenic mice were also homogenized in RIPA buffer for Western blot analysis of soluble A β (monomeric and dimeric) (E). Deletion of microglial MyD88 significantly decreases the protein level of dimeric but not monomeric A β in the brain (F and G; t test; n \geq 9 per each group).

4.5. Haploinsufficient expression of MyD88 in microglia reduces A β load in the brain blood vessels of APP/PS1-transgenic mice

A β is deposited not only in the brain parenchyma, but also at blood vessels (Stakos et al., 2020). Blood circulation contributes to A β clearance (Roberts et al., 2014). APP/PS1-transgenic mice used in our study was not a typical animal model for amyloid angiopathy; however, we observed an impairment of vasculature in their brain (Decker et al., 2018). Thus, we examined the potential localization of A β at blood vessels. We did observe that A β deposited in and around cerebral blood vessels of APP/PS1-transgenic mice (Fig 4.5, A). To quantify the blood vessels-associated A β , we isolated capillaries from the brain homogenate and detected A β in the tissue lysate. Interestingly, the protein level of dimeric A β in APP^{tg}MyD88^{fl/wt}Cre^{+/-} mice was also significantly lower than that in APP^{tg}MyD88^{fl/wt}Cre^{-/-} littermate mice (Fig 4.5, B and C; *t* test, *p* < 0.05). As a negative experimental control, oligomeric A β species could not be detected in capillaries isolated from non-APP transgenic mice (Fig 4.5, D).

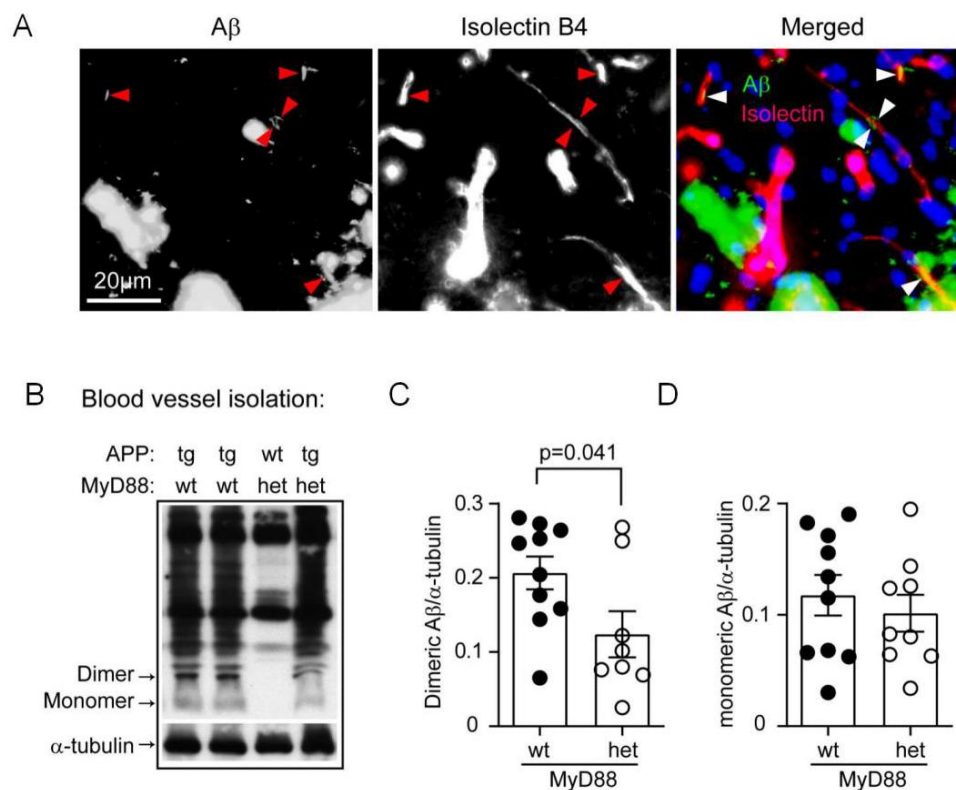


Fig4.5 Haploinsufficient expression of MyD88 in microglia reduces A β load in the brain blood vessels of APP/PS1-transgenic mice. To demonstrate the relationship between blood vessels and A β , brain sections

were co-stained A β antibodies and isolectin B4. Some A β deposits are located in and around the vessels (A; marked with arrow heads). Thereafter, micro blood vessels were isolated from 9-month-old MyD88-het and wt APP-transgenic mice and homogenized in RIPA buffer for Western blot analysis of monomeric and dimeric A β . Deficiency of MyD88 significantly reduces dimeric A β in the whole brain homogenate and isolated cerebral blood vessels of APP-transgenic mice (B, C and D; *t* test; $n \geq 6$ per each group).

4.6.Haploinsufficient expression of MyD88 in microglia inhibits pro-inflammatory activation in APP/PS1- transgenic mouse brain

Microglial inflammatory activation contributes to neuronal degeneration (Heneka et al., 2015). We observed that the number of Iba-1-immunoreactive cells (representing microglia) in the hippocampus was significantly fewer in 9-month-old microglial MyD88-deficient APP-transgenic mice than in MyD88-wild-type APP-transgenic littermates (APP^{tg}Myd88^{lox/wt}Cre^{+/-} mice, $1.64 \pm 0.16 \times 10^4$ cells/mm³ vs. APP^{tg}Myd88^{lox/wt}Cre^{-/-} mice, $2.60 \pm 0.29 \times 10^4$ cells/mm³; *t* test, $p < 0.05$; Fig 4.6, A and B). Deficiency of MyD88 in microglia did not change the number of Iba-1-positive cells in 9-month-old non-APP transgenic mice (Fig 4.6, B; *t* test, $p > 0.05$).

We further measured transcripts of M1-inflammatory genes (*tnf- α* , *il-1 β* , *inos*, and *ccl-2*) and M2-inflammatory genes (*il-10*, *chi3l3*, and *mrc1*) in brains of 9-month-old APP^{tg}Myd88^{lox/wt}Cre^{+/-} and APP^{tg}Myd88^{lox/wt}Cre^{-/-} mice. As shown in Fig 4.6, C and D, deficiency of microglial MyD88 significantly reduced cerebral *tnf- α* and *il-1 β* transcripts in APP-transgenic mice compared to MyD88-wildtype AD littermate mice (*t* test, $p < 0.05$). However, the transcription of other genes tested was not changed by MyD88 deficiency in microglia (Fig 4.6, E - I).

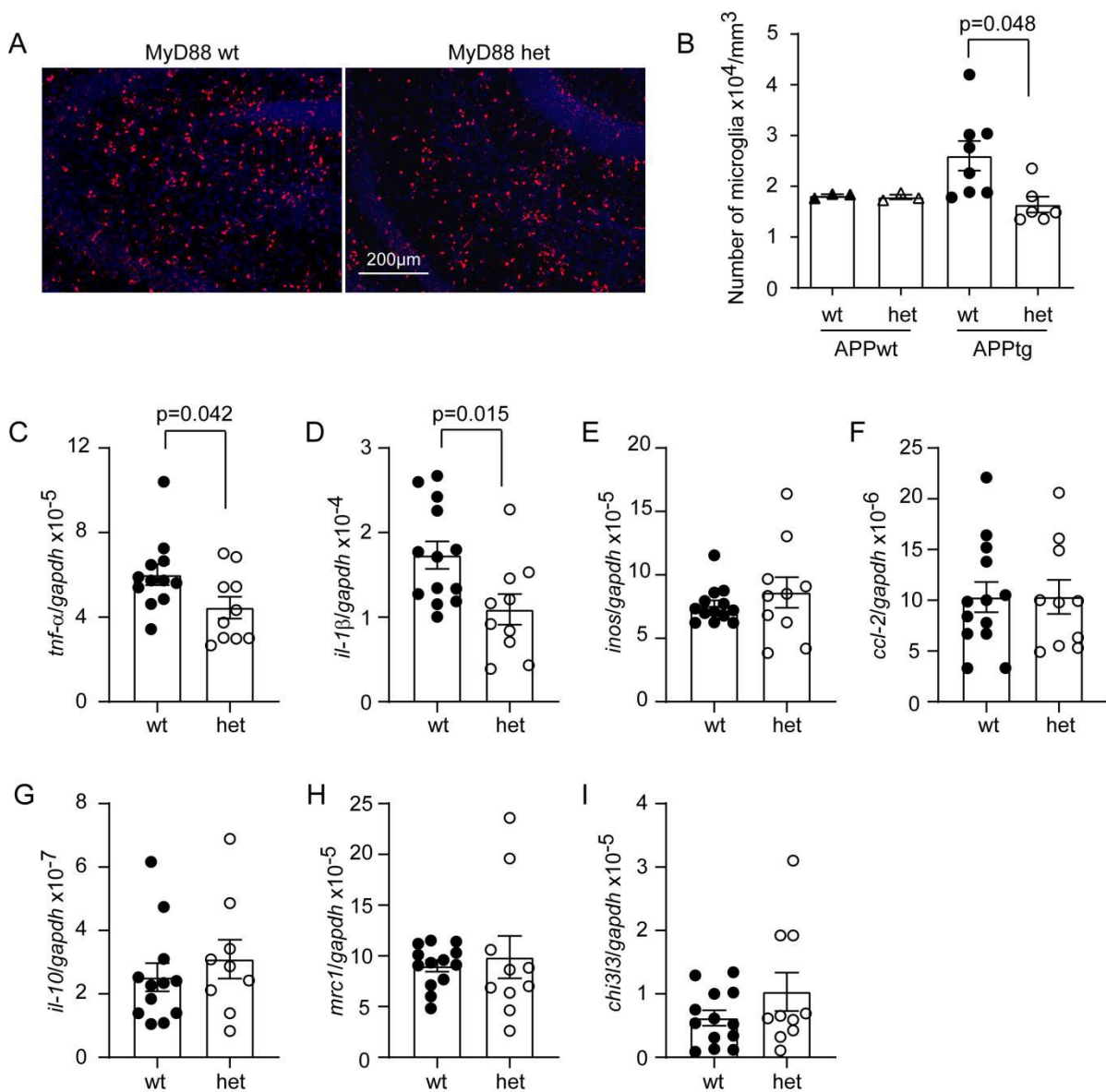


Fig 4.6 Haploinsufficient expression of MyD88 in microglia inhibits inflammatory activation in the brain of APP-transgenic mice. Six-month-old $\text{APP}^{\text{tg}}\text{MyD88}^{\text{fl}/\text{wt}}\text{Cre}^{+/-}$ (MyD88 het) and $\text{APP}^{\text{tg}}\text{MyD88}^{\text{fl}/\text{wt}}\text{Cre}^{-/-}$ (MyD88 wt) mice were injected with tamoxifen and analyzed at 9 months of age for neuroinflammation. Microglia were stained with fluorescence-conjugated Iba-1 antibodies (A) and counted with the stereological probe, Optical Fractionator. Deficiency of MyD88 reduced Iba-1-positive cells in 9-month-old APP-transgenic (APP tg) mice, but not in 9-month-old APP-wild-type (APP wt) mice (B; one-way ANOVA followed by Bonferroni *post hoc* test; $n \geq 6$ per group for APP tg mice and $n = 3$ per group for APP wt mice). The inflammatory activation in brain was further analyzed with real-time PCR to detect transcripts of both pro- and anti-inflammatory genes (C- I). Transcription of pro-inflammatory genes, *tnf- α* and *il-1 β* , was reduced by deletion of MyD88 in 9-old APP tg mice (C and D; *t* test; $n \geq 9$ per group).

4.7. Haploinsufficient expression of MyD88 suppressed pro-inflammatory activation in microglia but enhanced microglial responses to A β in APP/PS1-transgenic mouse brain

Recently, disease-associated microglia (DAM) phenotype was defined after comparing microglial transcriptome between APP/PS1-transgenic and wild-type mice. This signature is characterized by an induction of pro-inflammatory genes (including *il-1 β* , *ccl2*, and *itgax*), and a suppression of homeostatic genes (e.g. *cx3cr1*, *p2ry12*, *tmem119*, *tgfbr1*, *sall1*, and *csf1r*). APOE and TREM2 are two signaling proteins essential for DAM development (Keren-Shaul et al., 2017; Krasemann et al., 2017). We quantified the transcription of several DAM signature genes to characterize the effects of MyD88 on microglial activation. We observed that haploinsufficiency of MyD88 significantly decreased transcripts of pro-inflammatory genes, *tnf- α* and *il-1 β* (Fig 4.7, A and B; *t* test, $p < 0.05$), and also reduced the transcription of anti-inflammatory gene *chi3l3* (Fig 4.7, E; *t* test, $p < 0.05$) and homeostatic gene *cx3cr1* (Fig 4.7, I; *t* test, $p < 0.05$), as compared with MyD88-wildtype microglia.

Deficiency of Cx3Cr1 has been shown to increase the migration of microglia toward A β deposits and enhance microglial phagocytosis of A β (Hickman, Allison, Coleman, Kingery-Gallagher, & El Khoury, 2019; Lee et al., 2010; Z. Liu, Condello, Schain, Harb, & Grutzendler, 2010). We co-stained brain sections of 9-month-old AD mice with Iba-1-specific antibodies and methoxy-X04. There were significantly more microglia surrounding A β deposits in APP^{tg}Myd88^{lox/wt}Cre^{+/-} mice ($6.21 \pm 0.47 \times 10^2$ cells/mm²) than in APP^{tg}Myd88^{lox/wt}Cre^{-/-} mice ($2.68 \pm 0.24 \times 10^2$ cells/mm²; Fig4.7, O and P; *t* test, $p < 0.001$), which agrees with our previous observation that MyD88 deficiency increases the recruitment of microglia/brain macrophages toward A β deposits in APP-transgenic mice (Hao et al., 2011).

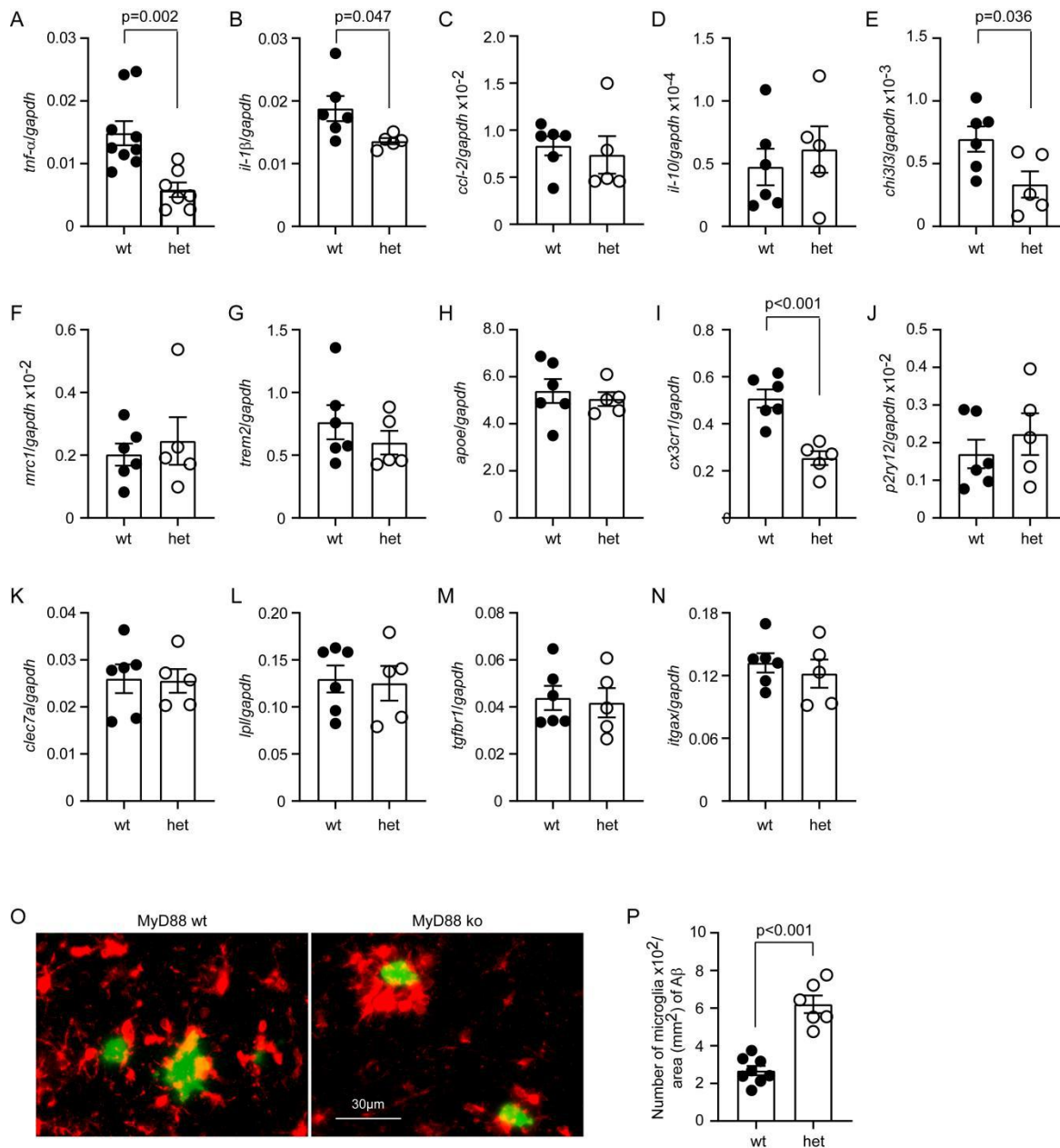


Fig 4.7 Haploinsufficient expression of MyD88 inhibits pro-inflammatory activation in microglia and enhances microglial responses to Aβ deposits in the brain of APP-transgenic mice. Microglia were selected with magnetic beads-conjugated CD11b antibodies from 9-month-old tamoxifen-injected APP^{tg}MyD88^{fl/wt}Cre^{+/-} (MyD88het) and APP^{tg}MyD88^{fl/wt}Cre^{-/-} (MyD88wt) mice. Transcription of signature genes associated with neurodegenerative diseases were detected with real-time PCR. MyD88 deficiency significantly decreases transcripts of *tnf-α*, *il-1β*, *chi3l3* and *cx3cr1* genes (A, B, E and I; *t* test; *n* ≥ 5 per

group). Iba-1 was also co-stained with methoxy-X04, which recognizes aggregated A β (O). Deficiency of MyD88 significantly increases recruitment of microglia toward A β deposits (P; *t* test; $n \geq 6$ per each group).

4.8. Haploinsufficiency of microglial MyD88 in microglia increases cerebral vasculature of APP/PS1-transgenic mice

We observed that cerebral microvasculature is reduced in APP/PS1-transgenic mice (Decker et al., 2018). In this study, we asked whether haploinsufficiency of microglial MyD88 changed the vasculature in AD mouse brain. We stained brains of 9-month-old APP^{tg}Myd88^{lox/wt}Cre^{+/-} and APP^{tg}Myd88^{lox/wt}Cre^{-/-} mice with collagen type IV-specific antibodies, skeletonized and quantified the immunoreactive blood vessels (Fig 4.8, A). As shown in Fig 4.8, B-D, MyD88 deficiency in microglia significantly increased the total length, vessel density and branching points of micro-blood vessels (*t* test, $p < 0.05$), but did not change the mean diameter of blood vessels (Fig 4.8, E; *t* test, $p > 0.05$).

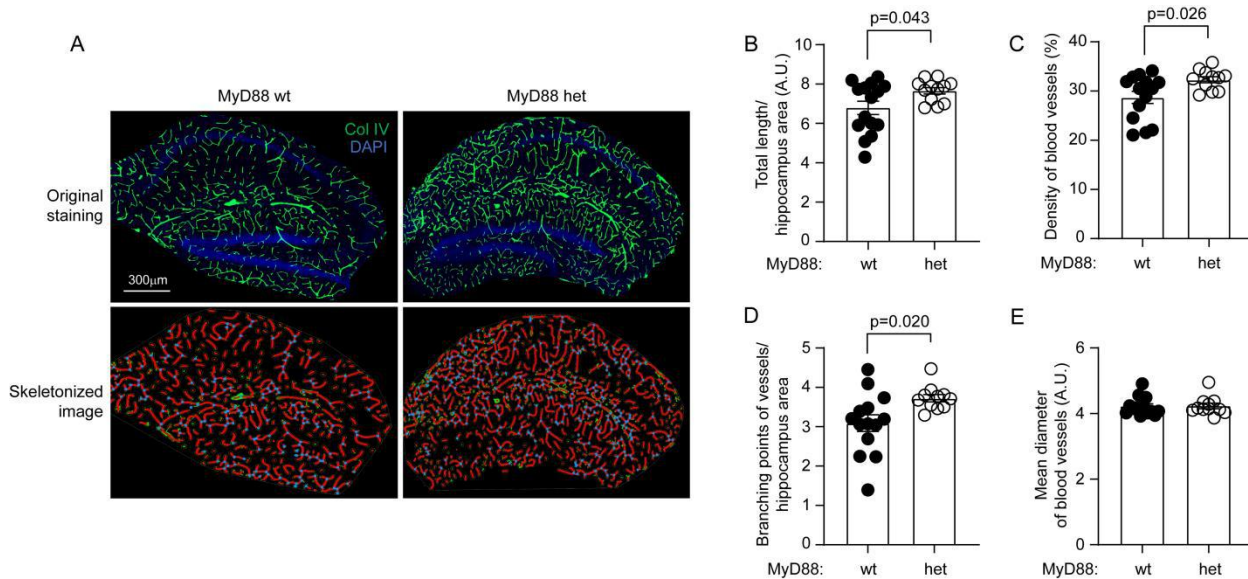


Fig4.8 Haploinsufficiency of microglial MyD88 in microglia increases cerebral vasculature of APP/PS1-transgenic mice. The brains of 9-month-old tamoxifen-injected APP^{tg}MyD88^{fl/wt}Cre^{+/-} (MyD88het) and APP^{tg}MyD88^{fl/wt}Cre^{-/-} (MyD88wt) mice were stained for collagen type IV (Col IV). The blood vessels in the hippocampus were thresholded and skeletonized. The skeleton representation of vasculature is shown in red and branching points of blood vessels are in blue (A) The total length, density and branching points of blood vessels were calculated and adjusted by area of analysis (B - D; *t* test, $n = 11$ per group). The mean diameter of blood vessels was calculated by dividing area of total blood vessels with total length of vessels (E).

4.9. Haploinsufficiency of microglial MyD88 increases cerebral vasculature of APP/PS1-transgenic mice

As resident microglia serve pro-angiogenic effects in the brain (Brandenburg et al., 2016; Jiang et al., 2020; Mastorakos et al., 2021), we co-stained Iba-1 and isolectin B4 on brain sections of 9-month-old $APP^{tg}Myd88^{lox/wt}Cre^{+/-}$ and $APP^{tg}Myd88^{lox/wt}Cre^{-/-}$ mice and counted microglia with and without contact with blood vessels in CA1 area of the hippocampus (Fig4.9a, A). We observed that deletion of MyD88 significantly increased the distribution of microglia to blood vessels (Fig4.9a, B; one-way ANOVA followed by *post-hoc* test, $p < 0.05$). Furthermore, we quantified gene transcription of pro-angiogenic genes in CD11b-positive brain cells. As shown in Fig4.9a, C-E, MyD88 deficiency significantly up-regulated the transcription of *opn* and *igf-1* genes (*t* test, $p < 0.05$).

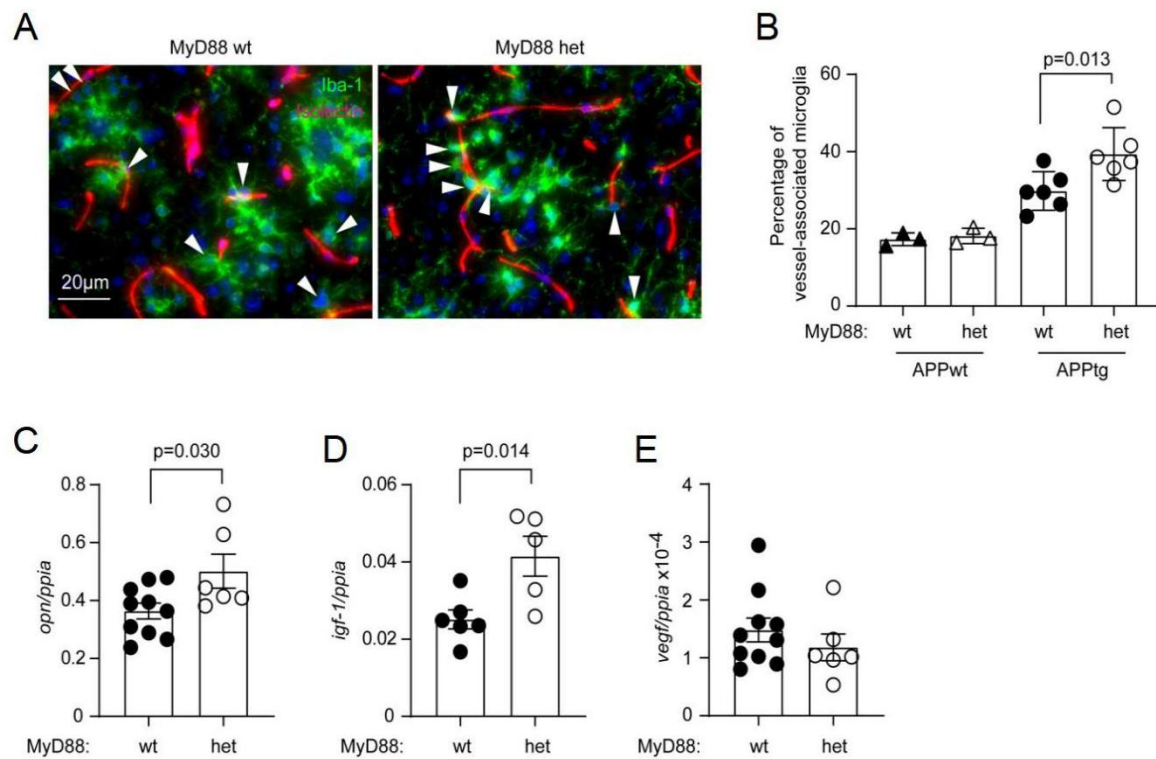


Fig 4.9a Haploinsufficiency of microglial MyD88 significantly increased the distribution of microglia around blood vessels of APP/PS1-transgenic mice. In order to analyze the relationship between vasculature and microglia, brain sections were co-stained with isolectin B4 (in red) and Iba-1 antibodies (in green)(A). Deficiency of MyD88 in microglia significantly increased the distribution of microglia around blood vessels (B; one-way ANOVA followed

by Bonferroni *post hoc* test; $n = 6$ per group for APP-transgenic [tg] mice and $= 3$ per group for APP-wildtype [wt] mice). Moreover, CD11b-positive brain cells were quantified for the transcription of pro-angiogenic genes. The transcription of *opn* and *igf-1* genes, but not of *vegf* gene was significantly up-regulated by MyD88 deficiency (C, D and E; *t* test, $n = 5$ per group).

To evaluate the integrity of BBB in AD mice, we quantified TJP1, Claudin-5 and AQP4 in blood vessels isolated from 9-month-old APP^{tg}Myd88^{lox/wt}Cre^{+/-} and APP^{tg}Myd88^{lox/wt}Cre^{-/-} mice. As shown in Fig4.9b, A-D, Haploinsufficiency of MyD88 in microglia did not significantly alter the protein levels of all proteins tested (*t* test, $p > 0.05$).

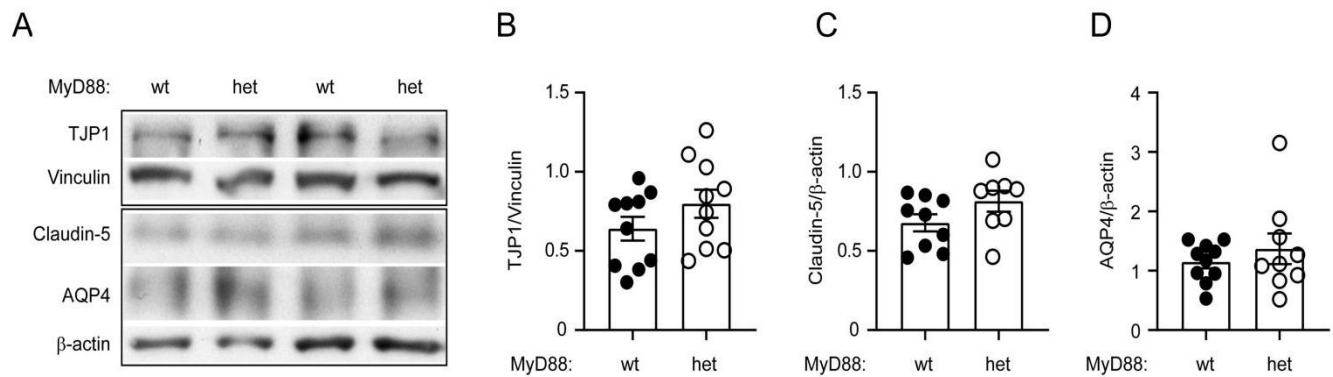


Fig 4.9b Haploinsufficiency of MyD88 in microglia did not change the integrity of BBB in APP/PS1-transgenic mice. In order to evaluate the integrity of BBB, isolated brain capillaries were detected for TJP1, Claudin-5 and AQP4 with quantitative Western blot (A). Deficiency of MyD88 in microglia did not significantly change the expression levels of all proteins tested (B- D; *t* test, $p > 0.05$, $n = 8$ per group).

4.10. Haploinsufficiency of MyD88 in microglia increases LRP1 at BBB of APP/PS1-transgenic mice

LRP1 mediates A β efflux and local clearance by pericytes at BBB (Kuhnke et al., 2007; Shinohara et al., 2017). We isolated micro-vessels from brains of 9-month-old APP^{tg}Myd88^{lox/wt}Cre^{+/-} and APP^{tg}Myd88^{lox/wt}Cre^{-/-} mice and observed that Haploinsufficiency of MyD88 in microglia significantly increased protein levels of LRP1, but not ABCB1 in APP-transgenic mice, as compared with MyD88-wildtype AD mice (Fig 4.10, A-C; *t* test, $p < 0.05$). The protein levels of pericyte markers, PDGFR β and CD13, were not changed by microglial deficiency of MyD88 (Fig4.10, D and E; *t* test, $p > 0.05$). In isolated blood vessels from non-

APP-transgenic control mice ($APP^{wt}Myd88^{lox/wt}Cre^{+/-}$ and $APP^{wt}Myd88^{lox/wt}Cre^{-/-}$), deletion of MyD88 in microglia did not alter the protein levels of all molecules examined (data not shown).

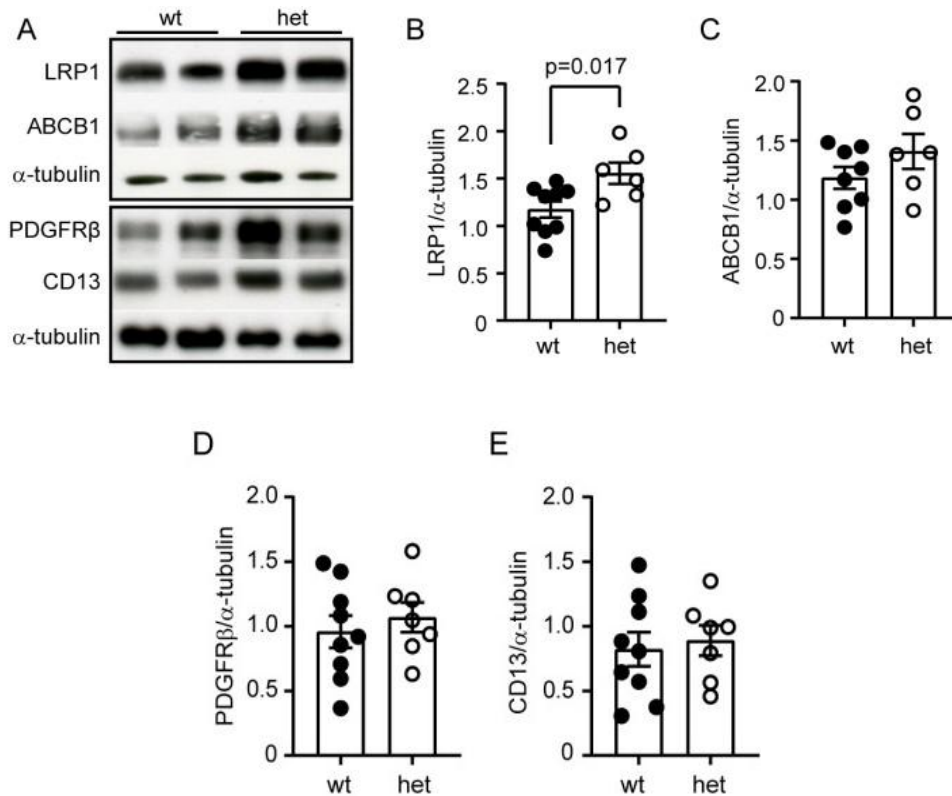


Fig 4.10 Haploinsufficiency of microglial MyD88 increases LRP1 in cerebral micro-vessels of APP/PS1-transgenic mice. Micro blood vessels were isolated from the brains of 9-month-old $APP^{tg}MyD88^{fl/wt}Cre^{+/-}$ (MyD88het) and $APP^{tg}MyD88^{fl/wt}Cre^{-/-}$ (MyD88wt) mice, which were injected with tamoxifen 3 months ago. Protein levels of LRP1, ABCB1, PDGFRβ and CD13 were determined with quantitative Western blot (A-E). Deletion of MyD88 in microglia significantly elevates LRP1 protein level but not for other proteins tested, compared with MyD88-wildtype APP/PS1- transgenic mice (B; t test, $n \geq 6$ per group).

4.11. IL-1β treatment decreases LRP1 in cultured pericytes

To examine the effects of inflammatory activation on LRP1 expression, we treated cultured pericytes with recombinant IL-1β either for 24 hours or for 8 days. As shown in Fig 4.11, A and E, both short-term and long-term treatments of IL-1β significantly decreased the protein levels of LRP1 in a dose-dependent manner (one-way ANOVA, $p < 0.05$). In the 8-day treatment experiment, withdrawal of IL-1β for the last 3 days restored expression of LRP1 in cultured pericytes (Fig4.11, E and F; two-way ANOVA, $p < 0.05$). The short-term treatment of IL-1β

markedly increased expression of PDGFR β and CD13, which corroborates our recent finding (Quan et al., 2020) (Fig4.11, A, C and D; one-way ANOVA, $p < 0.05$).

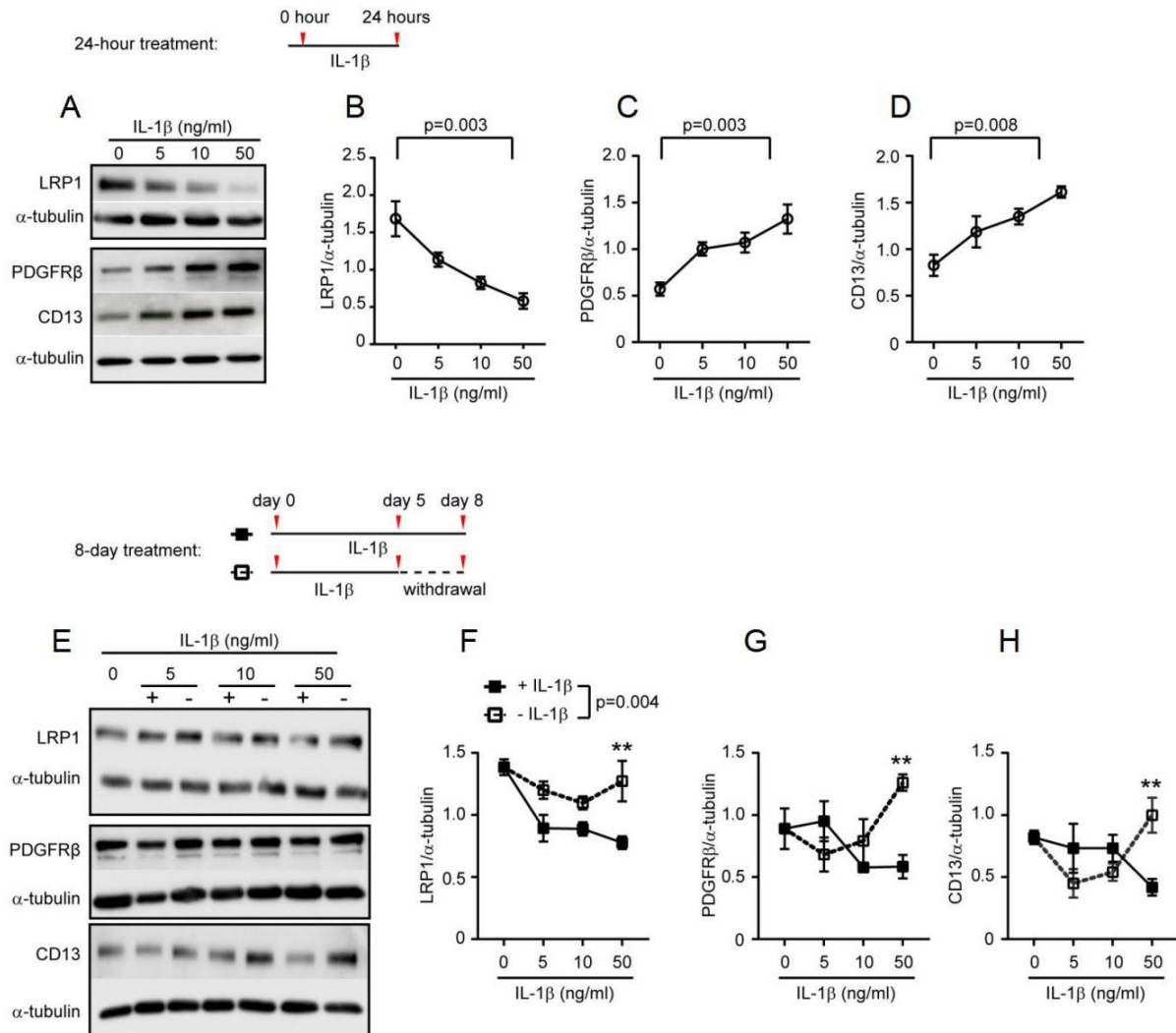


Fig 4.11 IL-1 β treatment decreases LRP1 in cultured pericytes. Immortalized pericytes from human cerebral capillaries were cultured and treated with IL-1 β at various concentrations for 24 hours (A-D) or for 8 days with and without withdrawal of IL-1 β during the last 3 days (E-H). At the end of experiments, cell lysates were prepared from IL-1 β -treated pericytes and detected for LRP1, PDGFR β and CD13 with quantitative Western blot. One-way ANOVA comparing levels of each tested protein at different concentrations of IL-1 β shows that: 1) IL-1 β treatments significantly decreases LRP1, but increases PDGFR β and CD13 in a concentration-dependent manner after a 24-hour treatment (A-D; p values are shown in the figure); 2) IL-1 β treatments significantly decreases LRP1 in a concentration-dependent manner after a 8-day treatment ($p < 0.01$); and 3) IL-1 β treatments does not significantly changes protein levels of PDGFR β and CD13 after a 8-

day treatment (G and H). Two-way ANOVA comparing protein levels of LRP1, PDGFR β or CD13 with and without withdrawal of IL-1 β in the last 3 days of experiments shows that withdraw of IL-1 β recovers expression of LRP1 (F; $p = 0.004$), but not for PDGFR β and CD13 (G and H). t test was used to analyze the difference of protein levels in cells treated with IL-1 β at 50ng/ml shows that withdrawal of IL-1 β significantly recovers expression of LRP1, PDGFR β and CD13 (E - H; $p < 0.01$, $n = 3$ or 4 per group).

The long-term treatment of IL-1 β only at a high concentration (e.g. 50ng/ml) tended to decrease the expression of PDGFR β and CD13; however, it was not statistically significant (shown in Fig4.11, G and H with solid lines; one-way ANOVA, $p > 0.05$). The withdrawal of IL-1 β recovered the expression of PDGFR β and CD13 in cultured pericytes after treatment of IL-1 β at 50ng/ml (Fig4.11, G and H; t test comparing cells with and without treatment of IL-1 β at 50ng/ml, $p < 0.05$).

4.12.Haploinsufficient expression of MyD88 in microglia decreases β - and γ -secretase activity but does not affect neprilysin and *ide* gene transcription in the brain of APP/PS1-transgenic mice

Cerebral A β level is determined by A β generation and clearance. We continued to ask whether MyD88-deficient microglia regulated A β production. Using our established protocols (Hao et al., 2011; Xie et al., 2013), we detected the activity of β - and γ -secretases in brains of 9-month-old APP^{tg}Myd88^{fl/wt}Cre^{+/-} and APP^{tg}Myd88^{fl/wt}Cre^{-/-} mice. Interestingly, the activity of both enzymes was significantly lower in the brain of APP^{tg}Myd88^{fl/wt}Cre^{+/-} mice than in MyD88-wildtype APP^{tg}Myd88^{fl/wt}Cre^{-/-} littermates (Fig4.12A-B; two-way ANOVA, $p < 0.05$). To further investigate the clearance of A β , we quantified gene transcripts of A β -degrading enzymes, *neprilysin*, and *ide* (Leissring et al., 2003). There were no changes in the transcription of *neprilysin* and *ide* genes in both brain tissues and microglia from 9-month-old APP^{tg}Myd88^{fl/wt}Cre^{+/-} mice compared with APP^{tg}Myd88^{fl/wt}Cre^{-/-} mice (Fig4.12 C - F; t test, $p > 0.05$), suggesting that haploinsufficiency of MyD88 in microglia does not affect A β catabolism.

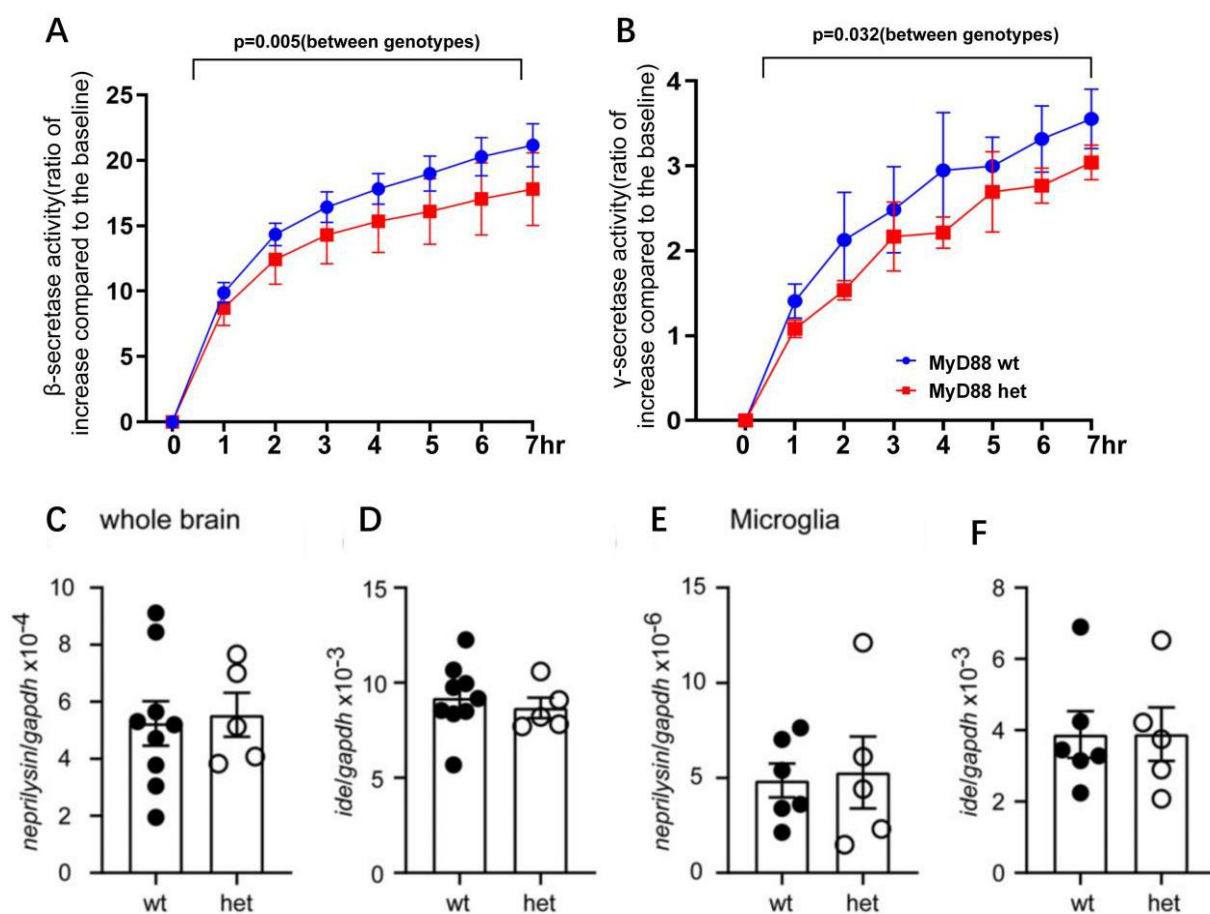


Fig4.12 Haploinsufficiency of MyD88 in microglia decreases β - and γ -secretase activity, but does not affect the transcription of neprilysin and ide genes in the brain of APP/PS1-transgenic mice. The brains of 9-month-old tamoxifen-injected $APP^{tg}MyD88^{fl/wt}Cre^{+/-}$ (MyD88 het) and $APP^{tg}MyD88^{fl/wt}Cre^{-/-}$ (MyD88 wt) mice were used to prepare membrane components and RNA isolation. β - and γ -secretase activity was measured by incubating membrane components with fluorogenic β - and γ -secretase substrates, respectively (A, B, two-way ANOVA comparing MyD88 wt and het mice; $n = 4$ per group). The transcripts of neprilysin and ide genes in the brain tissue (C, E) and isolated microglia (D, F) were measured with real-time PCR, which showed that transcription of neprilysin and ide genes was not changed by the haploinsufficiency of MyD88 in microglia (t test; $n \geq 5$ per group).

5. DISCUSSION

AD is a progressive neurodegenerative disorder and the most common form of dementia, which is characterized by A β deposits, hyperphosphorylated tau-composed neurofibrillary tangle and microglia activation. Emerging evidences have suggested that microglia act as a double-edged sword in AD pathogenesis: on one side, they contribute to neuronal death by secreting inflammatory mediators; and on the other side, they clear neurotoxic A β to prevent AD progression. Innate immune signaling cascade, *e.g.* TLRs-MyD88-NF- κ B, regulate the inflammatory mediators, and modify AD pathogenesis (Tahara et al., 2006; Reed-Geaghan et al., 2010; Hao et al., 2011; Lim et al., 2011; Michaud et al., 2011 and 2012; Song et al., 2011; Cameron et al., 2012; Liu et al., 2012). However, the net effect of microglial activation in AD is still unclear. The mechanism switching between detrimental and beneficial effects need to be understood. In this study, we demonstrated that a deficiency in IKK β in myeloid cells, especially in endogenous microglia, simultaneously reduces inflammatory activation and A β load in the brain and improves cognitive function in AD mice. These findings corroborate the results of our earlier studies of the deficiency of myeloid TLR2 or MyD88 in APP-transgenic mice (Hao et al., 2011; Liu et al., 2012).

Microglial activation has been extensively investigated in AD brain (Heneka et al., 2015), but microglial effects on A β pathology and neuronal degeneration remain inconclusive. In this study, we haploinsufficiency MyD88 specifically in microglia in APP/PS1-transgenic mice by 6 months. Notably, by 9 months of age these animals showed attenuation both in the total number of microglia and in the transcription levels of pro-inflammatory genes (*e.g.*, *tnf- α* and *il-1 β*) within the whole brain and individual microglia, correlating with decreased A β load and improved cognitive function. Interestingly, MyD88-deficient microglia might prevent APP/PS1 overexpression-induced changes of cerebral vasculature and LRP1 expression at BBB.

The regulating effects of innate immune signaling on the role of microglia in AD pathogenesis are highly heterogenous. For example, TREM2 is essential for microglial response to A β in the brain (Ulland et al., 2017). One group reported that TREM2 deficiency in APP-transgenic mice increases hippocampal A β burden and accelerates neuron loss (Wang et al., 2015), while another group showed that TREM2 deletion reduces cerebral A β accumulation (Jay

et al., 2015). Subsequent work suggested that TREM2 may have a protective effect at the early disease stage through phagocytic clearance of A β , but display a pathogenic effect at the later disease stage by triggering neurotoxic inflammatory responses (Jay et al., 2017; Parhizkar et al., 2019). In our studies, we reduced MyD88 expression in microglia or in bone marrow cells of APP- transgenic mice after noticeable A β has already developed in the brain, which decreases cerebral A β load and protects neurons (Hao et al., 2011). In the experiments by other groups, MyD88 expression was manipulated in APP-transgenic mice before the birth (by cross- breeding) or at 2 months of age (by bone marrow reconstruction) before A β deposits appear in the brain. With such an experimental setting, MyD88-deficient microglia promote A β accumulation in the brain and accelerate spatial memory deficits (Michaud et al., 2011, 2012). Thus, the pathogenic role of innate immune molecules in microglia is shaped by the evolving cellular environment and should be analyzed dynamically during AD progression.

MyD88, as a common signaling adaptor for most TLRs and IL-1 receptor, plays an essential role in the innate immune response (O'Neill, Golenbock, & Bowie, 2013). It is not surprising that the heterozygous deletion of *myd88* gene inhibits the inflammatory activation of microglia in APP/PS1-transgenic mice. MyD88 deficiency might reduce the generation of new microglia, as we previously observed that deletion of IKK β , a signaling molecule downstream to MyD88, decreases proliferating microglia in APP-transgenic mice (Y. Liu et al., 2014). MyD88 deficiency likely prevents microglial cell death, as blocking MyD88 signaling inhibits TLR4 activation-induced microglial apoptosis (Jung et al., 2005), while TLR4 is a receptor mediating microglial response to A β challenge (Walter et al., 2007). Interestingly, we observed that MyD88 deficiency promotes clustering of microglia around A β deposits as we observed in MyD88-deficient bone marrow chimeric AD mice (Hao et al., 2011). As deficiency of MyD88, IKK2, or TLR2 increases A β internalization by cultured microglia or macrophages (Hao et al., 2011; S. Liu et al., 2012; Y. Liu et al., 2014), the haploinsufficiency of MyD88 perhaps enhances microglial clearance of A β in AD brain. The relationship between microglial clustering and A β reduction in APP-transgenic mice has been described in many studies. For example, deficiency of TREM2 blocks microglial recruitment to A β , which is correlated with cerebral A β accumulation (Y. Wang et al., 2015). Administration of TREM2 agonist antibodies increases A β -associated microglia, which decreases A β in the brain (Fassler, Rappaport, Cuno, & George,

2021; Price et al., 2020; S. Wang et al., 2020). However, the molecular mechanisms, which mediate the migration of microglia toward A β and the following A β internalization, remain unclear.

Haploinsufficiency of MyD88 in microglia reduces inflammation and A β in the brain of APP/PS1- transgenic mice, which corroborates our previous observation in MyD88-deficient bone marrow chimeric AD mice (Hao et al., 2011). In both animal models, MyD88 deficiency promotes clustering of microglia or brain macrophages around A β deposits (Hao et al., 2011). As potential mechanisms, MyD88 deficiency strongly decreases the transcription of *cx3cr1*, *chi3l3*, *tnf- α* and *il-1 β* genes in microglia. Cx3Cr1 expression is up-regulated in the brain of AD patients or animal models (Gonzalez-Prieto et al., 2021). Cx3Cr1 deficiency constantly enhances A β phagocytosis by microglia and decreases cerebral A β load in various APP- transgenic mice (Hickman et al., 2019; Lee et al., 2010; Z. Liu et al., 2010). Cx3Cr1 deficiency even pushes microglial migration toward A β deposits (Z. Liu et al., 2010). Chi3l3 is a known marker for alternative activation of microglia and macrophages. Its transcription is also elevated in APP-transgenic mouse brain (Colton et al., 2006). However, the pathogenic function of microglial Chi3l3 in AD is indeed unknown. Our previous studies on myeloid TLR2, MyD88 or IKK β -deficient APP-transgenic mice revealed that the attenuation of TNF- α and IL-1 β expression is correlated with decreased A β level in the brain (Hao et al., 2011; S. Liu et al., 2012; Y. Liu et al., 2014). In cultured microglia, pro-inflammatory activation inhibits A β phagocytosis (Koenigsknecht-Talboo & Landreth, 2005), which suggests that inhibition of TNF- α and/or IL-1 β signaling might promote A β clearance by microglia. However, systemic injection of TLR4 or TLR9 agonist induces both pro- and anti-inflammatory activation and decreases A β in the brain of AD mice (Michaud et al., 2013; Scholtzova et al., 2014). Thus, how inflammatory activation regulates cerebral A β clearance needs to be further investigated.

There is growing evidence showing that microvascular circulation is damaged in AD brain; for example, capillary density and cerebral blood flow decrease, while BBB permeability increases (Watanabe et al., 2020). Our previous study showed that the blood flow goes down in correlation with a reduced vasculature in the hippocampus of APP-transgenic mice (Decker et al., 2018). A β -activated perivascular macrophages injure the neurovascular coupling through producing reactive oxygen species (Park et al., 2017). However, microglia were observed to

serve pro-angiogenic effects in brains with glioma, ischemia or direct vascular injury (Brandenburg et al., 2016; Jiang et al., 2020; Mastorakos et al., 2021). Transcription of *opn*, *vegf* and *igf1* genes in microglia was associated with angiogenesis (Jiang et al., 2020). Our study showed that haploinsufficiency of *MyD88* in microglia increases cerebral vasculature, and distribution of microglia around blood vessels. Moreover, *MyD88* deficiency up-regulates the transcription of *opn* and *igf-1* genes in microglia. As *OPN* enhances *VEGF* expression in endothelial cells (Dai et al., 2009) and *IGF-1* drives the tissue repairment, including angiogenesis, in the brain (Vannella & Wynn, 2017), *MyD88*-deficient microglia might prevent vascular impairment in AD brain. However, a postmortem tissue study showed a higher density of capillaries in the brain of AD patients (Fernandez-Klett et al., 2020). *Tg4510* tau-transgenic mice display increased capillaries, but with atypical and spiraling morphologies, and reduced luminal diameter of blood vessels (Bennett et al., 2018). Thus, more studies, especially functional analysis of the effects of microglia on the microvascular circulation in AD are needed.

BBB breakdown is an early biomarker of AD (Nation et al., 2019). *APOE4* variant was recently linked to the loss of BBB integrity before the cognition decline (Montagne et al., 2020). The cerebrovascular leakage of ~ 100 nm nanoparticles was also observed in *APP*-transgenic mice (Tanifum, Starosolski, Fowler, Jankowsky, & Annapragada, 2014). However, the effects of microglia on BBB integrity in AD brain remain unclear. In a mouse model of systemic lupus erythematosus, microglial activation around blood vessels protects BBB at the initial phase by expressing tight-junction protein *Claudin-5*, and impairs BBB by phagocytosing astrocytic end-foot after the inflammation is sustained (Haruwaka et al., 2019). In our study, we did not observe altered protein levels of *TJP1*, *Claudin-5* and *AQP-4* in microglial *MyD88*-deficient AD mice. However, we were not able to exclude small damages of BBB integrity, which need advanced techniques for the detection.

LRP1 contributes to $A\beta$ clearance at BBB through mediating $A\beta$ efflux and pericyte internalization of $A\beta$ (Ma et al., 2018; Shinohara et al., 2017). Deletion of *LRP1* in endothelial cells accumulate $A\beta$ in *APP*-transgenic mouse brain (Storck et al., 2016). *LRP1* expression decreases in brain capillaries with aging and in AD (Shibata et al., 2000). Pro-inflammatory cytokines, such as *IL-1 β* , *IL-6* and *TNF- α* , down-regulate *LRP1* in cultured microvascular endothelial cells (Hsu, Rodriguez-Ortiz, Zumkehr, & Kitazawa, 2021). Our experiments further

indicated that IL-1 β treatments decrease LRP1 expression in cultured brain pericytes. In APP/PS1-transgenic mice, MyD88-deficient microglia elevates LRP1 protein level in cerebral capillaries, which might be due to the inflammatory inhibition. It was supported by another observation that inflammatory activation in the brain by systemic administration of lipopolysaccharide decreases A β efflux at BBB (Erickson, Hansen, & Banks, 2012).

PDGFR β and CD13 are essential for the survival and integration of pericytes in blood vessels (Lindahl, Johansson, Leveen, & Betsholtz, 1997; Rangel et al., 2007). In our experiments, IL-1 β did not decrease PDGFR β and CD13 expression in cultured pericytes, except that the cells were treated by IL-1 β at a high concentration (50 ng/ml) and for a long time-duration (8 days). Although the coverage of PDGFR β -positive pericytes on cerebral micro-vessels was reported to decrease in AD brains (Sengillo et al., 2013), a recent study demonstrated that the density of PDGFR β -immunoreactive pericytes is reserved during AD pathogenesis (Fernandez-Klett et al., 2020).

A β is produced after serial digestions of APP by β -(BACE1) and γ -secretases (Haass, Kaether, Thinakaran, & Sisodia, 2012). The expression of BACE1 in neurons is up-regulated by inflammatory activation (He et al., 2007; Sastre et al., 2006). Our studies showed that p38 α -MAPK deficiency promotes BACE1 degradation in neurons (Schnöder et al., 2016). Recently, inflammatory cytokines, such as interferon- γ and α , were shown to induce the expression of interferon-induced transmembrane protein 3 in neurons and astrocytes, which binds to γ -secretase and increases its activity (Hur et al., 2020). Thus, haploinsufficient expression of MyD88 in microglia in our APP/PS1-transgenic mice decreases neuroinflammation, and inhibits β - and γ -secretase activity in the brain, which might serve as another mechanism decreasing A β level in AD mice.

In summary, haploinsufficiency of MyD88 in microglia at a late disease stage slows down the cognitive decline of APP/PS1-transgenic mice. MyD88 deficiency inhibits pro-inflammatory activation of microglia, but enhances microglial response to A β , which subsequently attenuates A β load in the brain. Haploinsufficiency of MyD88 might enhance pro-angiogenic effects of microglia, and prevent the loss of LRP1-mediated A β clearance at BBB in AD. However, the

effects of microglia on the structure and function of micro-vessels in AD are far from being understood.

To answer these questions will be the focus of our following studies.

PART II NLRP3 deficiency differently regulates cerebral vasculature under physiological and pathological conditions

1. INTRODUCTION

1.1 The vascular pathogenesis of Alzheimer's disease

Growing evidence suggests that vascular dysfunction might be a third contributor to AD pathogenesis. Several cardiovascular risk genes including APOE4 gene variant, and variants within MBLAC, DDB2 and MINK1 genes are associated with AD development (Broce et al., 2019). Postmortem brain tissues from up to 80% diagnosed AD patients display vascular pathologies, such as cerebral amyloid angiopathy (CAA), microbleeding, microinfarction, and atherosclerosis at Willis's circle (Power et al., 2018; Toledo et al., 2013). Breaking down of blood-brain-barrier (BBB) was observed in the hippocampus of AD patients at a very early disease stage (Montagne et al., 2015; van de Haar et al., 2016).

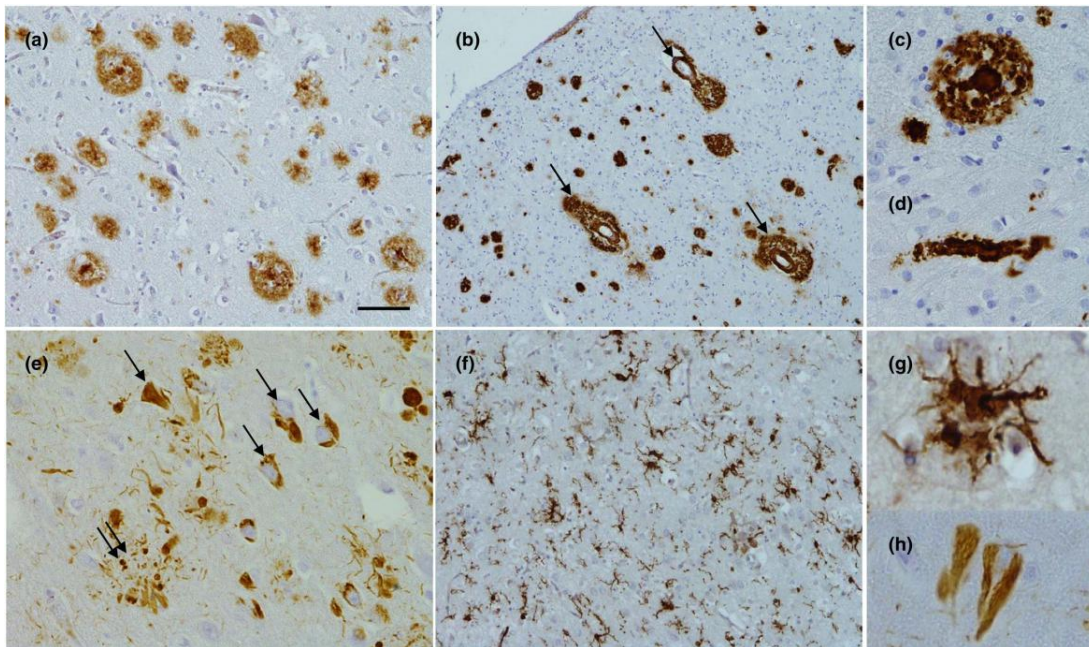


Fig1.1 Pathology of Alzheimer's disease. A β immunohistochemistry highlights the plaques in the frontal cortex (a) and cerebral amyloid angiopathy (CAA) where A β accumulates within blood vessel (b, arrows). An A β cored plaque is shown at higher magnification in (c) showing a central core. In severe CAA A β accumulates within capillaries (d). Tau immunohistochemistry demonstrates both neurofibrillary tangles (e, arrows; h at higher magnification) and neuritic plaques (e, double arrow). Neuroinflammation is a prominent feature in Alzheimer's disease and this is evident by the number of reactive microglia (f; g at higher magnification). (Lane CA, Hardy J, Schott JM. Alzheimer's disease. *Eur J Neurol.* 2018;25(1):59-70. doi:10.1111/ene.13439)

Prospective studies showed that cerebral hypoperfusion starts in pre-symptomatic AD patients and predicts the future development of AD (Wolters et al., 2017). Individuals, who have one or more vascular risk factors, including body mass index ≥ 30 , current smoking, hypertension, diabetes, and total cholesterol ≥ 200 mg/dL, in their mid-life are prospected to have more A β deposition in the brain in their late-life (20 years later) (Gottesman et al., 2017). A cohort study has identified blood-brain barrier failure as a major mechanism in cerebral small vessel disease and dementia (Wardlaw, Makin et al. 2017). We have observed that cerebral vasculature and blood flow are reduced in the hippocampus of AD mice, which over express Alzheimer's precursor protein (APP) or Tau protein in neurons (Decker et al., 2018). However, how cerebral vascular circulation is damaged in AD and how vascular dysfunction contributes to AD pathogenesis remains unclear.

1.2 The function of cerebrovascular pericytes in the pathogenesis of AD

Pericytes are contractile cells wrapping around endothelial cells of cerebral capillaries. They regulate BBB permeability, angiogenesis, hemodynamic responses, neuroinflammation and other brain functions (Sweeney et al., 2016). Pericytes express platelet-derived growth factor receptor β (PDGFR β), CD13, neural/glial antigen-2 (NG2), and CD146, which are often used as protein markers of pericytes in the brain (Smyth et al., 2018).

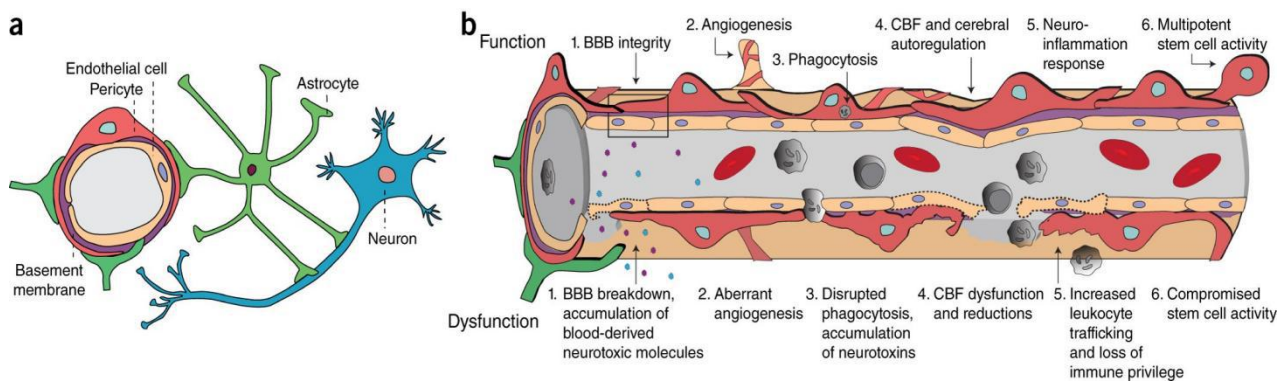


Figure 1.2 The multifunctional role of pericytes in the CNS. a) Pericytes at the neurovascular unit. b) Under physiological conditions (top row), pericytes play an important role in BBB integrity, angiogenesis, phagocytosis, CBF and capillary diameter, neuroinflammation, multipotent stem cell activity. Pericyte dysfunction (bottom row) causes a variety of alterations including BBB breakdown, aberrant angiogenesis, impaired phagocytosis, CBF dysfunction and reduction, increased leukocyte trafficking promoting neuroinflammation, and impaired stem cell-like capacity that can contribute to AD pathogenesis. (Sweeney, Ayyadurai et al. 2016)

The number of PDGFR β or CD13-positive pericytes decreases in AD brain in correlation with increased BBB leakage (Sengillo et al., 2013). Pericytes and PDGFR β proteins are lost in association with A β accumulation in the retinas of mild cognitive impairment (MCI) and AD patients (Shi et al., 2020). PDGFR β is shed from injured pericytes. In old adults with cognitive dysfunction at very early stage, soluble PDGFR β has already increased in the cerebral spinal fluid (Nation et al., 2019). The binding of endothelial cells-released PDGF-B to PDGFR β on pericytes is essential for the proliferation and integration of pericytes in cerebral vasculature (Lindhahl et al., 1997). In PDGFR β -deficient mice, loss of pericytes leads to accumulation of blood derived fibrin or fibrinogen, decreased vasculature and reduced blood flow in the brain parenchyma, and finally results in demyelination, axonal degeneration and oligodendrocyte loss in the white matter, which are characteristic pathological changes in microcirculationimpaired brain (Montagne et al., 2018). In APP-transgenic mice, deficiency of PDGFR β causes pericyte loss and increases A β deposition in the brain parenchyma and blood vessels, perhaps due to the decrease of A β internalization by pericytes (Ma et al., 2018; Sagare et al., 2013). Recently, it was demonstrated that oligomeric A β triggers pericyte contraction by initiating the generation of reactive oxygen species and subsequent release of endothelin-1 in microvessels (Nortley et al., 2019). APOE4 was also shown to promote pericyte injury and BBB impairment in the hippocampus and medial temporal lobe of AD patients (Montagne et al., 2020). Thus, pericytes are damaged in AD brain and dysfunction of pericytes contributes to AD pathogenesis. The potential vascular contribution to AD pathogenesis sheds light on a novel way to develop vascular protection-oriented therapeutic methods for AD patients. However, the molecular mechanisms mediating vascular pathology in AD brain are largely unknown.

1.3 NLRP3 inflammasome

Innate immunity is the first barrier of the body's defense, which is affected by pattern recognition. The body recognizes pathogen-related molecular patterns, activates downstream signaling pathways, and causes inflammation react to resist the invasion of pathogens (Liu D et al., 2013). There are four main types of pattern recognition receptors in the body, including Toll-like receptor (TLR), NOD-like receptor (NLR), c-type coagulation agglutinin receptor and retinoic acid inducible gene 1 receptor. NOD-like receptors play a vital role in inherent immunity and host physiology (Maekawa T et al., 2012).

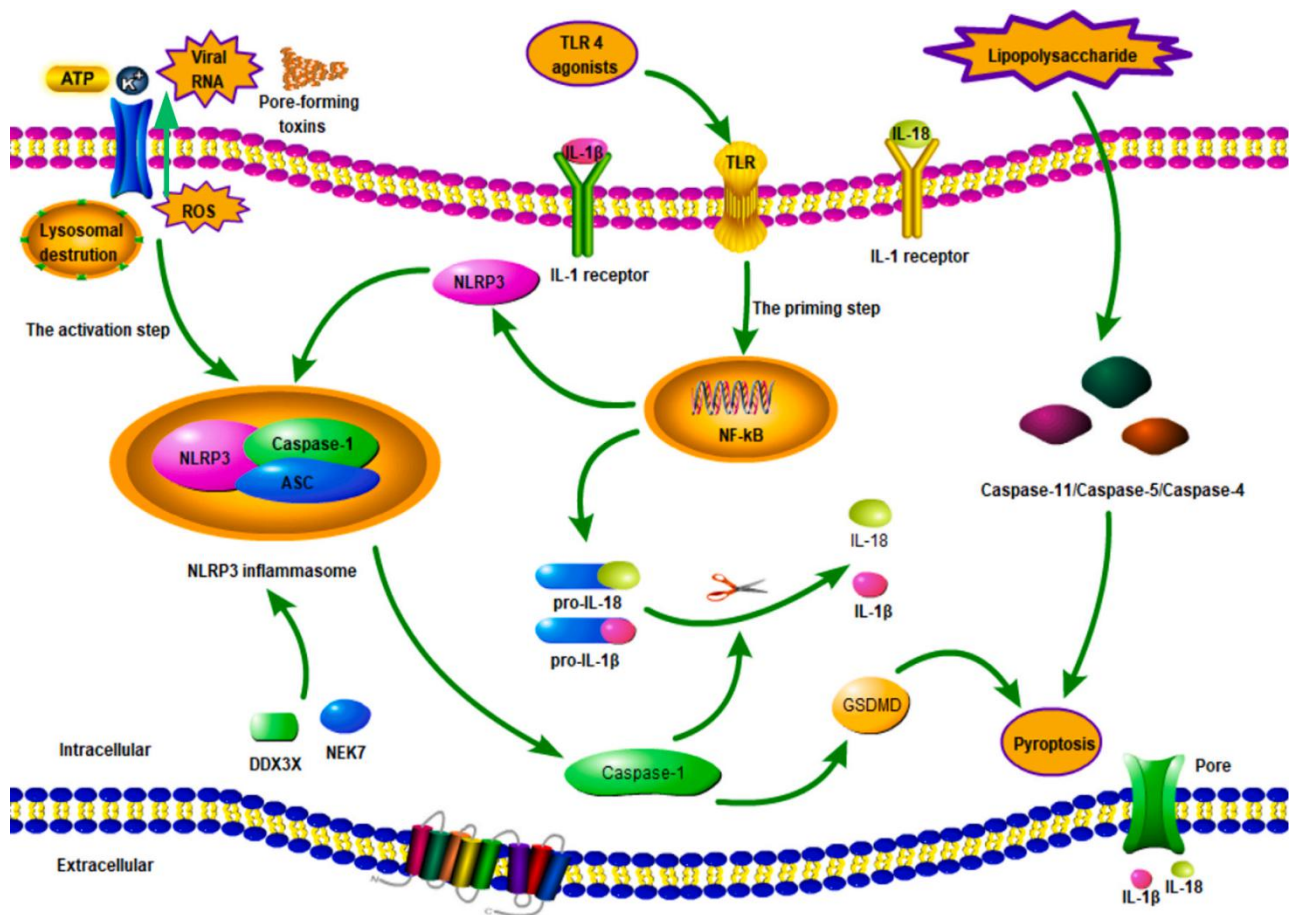


Fig1.3 The mechanisms of NLRP3 inflammasome activation. The activation of NLRP3 inflammasome is a complex regulatory process that requires two triggering steps: the initiation step and the activation step. The priming step is induced by the TLR4 agonist, which then activates the NF- κ B pathway by promoting the expression of NLRP3, pro-IL-18, and pro-IL-1 β . Then, the assembly of NLRP3 inflammasomes is activated by various triggers, such as viral RNA, pore-forming toxin, and ATP. In addition, the activation step of the NLRP3 inflammasome is mediated by K⁺ efflux, lysosomal destruction, and elevated ROS. Activated caspase-1 can further induce the maturation of IL-18 and IL-1 β and lyse GSDMD to form membrane pores, thereby mediating cell pyrolysis. Mature IL-1 β molecules can be released into the extracellular environment through membrane pores, amplifying the inflammatory effect. In addition, caspase-11 in mice (or caspase-4 and caspase-5 in humans) can induce the activation of non-classical NLRP3 inflammasomes, leading to pyrolysis and the secretion of pro-inflammatory cytokines. (Feng YS, Tan ZX, Wu LY, Dong F, Zhang F. *The involvement of NLRP3 inflammasome in the treatment of neurodegenerative diseases. Biomed Pharmacother.* 2021;138:111428.)

NLRP3 inflammasome is a protein complex that exists in the cytoplasm. It relies on the molecular platform of caspase 1 to promote the maturation and release of interleukin (IL) 1 β and

IL-18, and cause inflammation reaction(LatzE et al., 2010). Once the regulation of the NLRP3 inflammasome in the body is unbalanced, excessive IL-18 and IL-18 may be produced, which may cause a series of inflammatory diseases. Asc is an important adaptor protein of NLRP3 inflammasome, connecting upstream NLRP3 and downstream precursor caspase-1. Caspase-1 is the effector protein of NLRP3 inflammasome. The precursor caspase-1 has no catalytic activity and can be activated by autocatalysis. Once activated, it can convert the inactive pro-inflammatory cytokines IL-1 β and IL-1. The precursor of 18 is sheared into mature IL-1 β and IL-18. NLRP3 inflammasomes are mainly expressed in neutrophils, macrophages, monocytes and dendritic cells, and their expression induces an inflammatory response (Guarda et al., 2011). Data show that activating NLRP3 inflammasomes requires two steps: ①Initiating the signal, transcribe the precursors of NLRP3 inflammasome and IL-1 β through the NF κ B pathway; ②Activating the signal, pathogen-related molecular patterns directly activate the inflammasome(Feng YS et al., 2021).

1.4 NLRP3 is involved in AD pathogenesis

The pathogenesis of AD is associated with the formation of amyloid plaques and neurofibrillary tangles (NFTs), which result from the accumulation of A β and the intracellular deposition of hyperphosphorylated tau proteins (DeTure, M.A et al., 2019). However, other pathogenic factors are also involved in the etiology of AD (Freeman, LC et al., 2016). For example, many studies have indicated that neuroinflammation also plays a central role in the pathogenesis of AD (Swardfager, W et al., 2010 ; Huang, C et al., 2017). Moreover, the aggregation of NFTs, tau proteins and A β could activate a proinflammatory downstream cascade of astrocytes and microglia that leads to and exacerbates AD pathology (Liu Y et al., 2014). Numerous inflammatory markers have been found in the AD brain, including increased levels of inflammatory cytokines and chemokines, as well as the accumulation of activated microglia in damaged areas (Lee, Y. J et al., 2010). Furthermore, NLRP3 inflammasome is closely related to the pathogenesis of AD and other inflammasomes have been shown to induce neuroinflammation in the central nervous system (CNS) (Heneka, M. T et al., 2015; Heneka, M. T et al., 2013; dos Santos, G et al., 2012).

NLRP3 inflammasome, which is known to be associated with many chronic inflammatory and autoimmune diseases, consist of NLRP3, the adaptor molecule apoptosis-associated speck-like protein containing a CARD (ASC), and the cysteine protease caspase-1. There is more and more evidences to support the following view: NLRP3 inflammasome plays a vital role in the pathogenesis of AD, and is closely related to molecular events that are associated with AD (such as fibrous A β) (Heneka, M.T et al., 2015; Halle, A et al., 2008). Intracellular A β buildup activates the NLRP3 inflammasome in microglia, subsequently, caspase-1 self-cleavage forms active caspase-1, which in turn triggering pro-IL-1 β and pro-IL-18 mature, indicating that NLRP3 inflammasome activation may worsen neuroinflammation of AD (Venegas and Heneka 2019). Caspase-1 cleavage levels in the brains of patients with mild cognitive impairment and AD are elevated (Heneka, M.T et al., 2013). Increased expression of active IL-1 β has been found in the cerebrospinal fluid of patients with AD (Blum-Degen, D et al., 1995). In addition, AD models show that fibril A β can trigger the activation of NLRP3 inflammasomes in microglia, leading to the maturation of pro-IL-1 β and the production of IL-1 β (Heneka, MT et al., 2015; Halle, A et al. People, 2008). Recently, some studies have reported that amylin receptor can mediate the activation of A β -induced NLRP3 inflammasome pathway (Fu W et al., 2017). In addition, A β can trigger an increase in the expression of ROS (reactive oxygen species), which can activate the NLRP3 inflammasome pathway through the TRPM2 (transient receptor potential melatonin 2) pathway (Aminzadeh, M et al., 2017). Another research team found that tau seeds can activate the NLRP3-ASC inflammasome pathway and trigger the production of IL-1 β depends on ASC-dependent manner (AStancu, IC, etc., 2017). Therefore, understanding the NLRP3 inflammasome may help to understand the pathology of AD.

1.5 NLRP3 and Pericytes

Multiple studies have shown that cerebrovascular pericytes express pattern molecular recognition receptors (PRRs), such as Toll-like receptors, such as TLR2 and TLR4, and NOD (nucleotide binding oligomerization domain)-like receptor proteins, such as NLRP1 and NLRP3 (Guijarro-Munoz et al., 2014; Leaf et al., 2017; Nyul-Toth et al., 2017). After lipopolysaccharide (LPS) and TNF- α stimulation, and E. coli infection, cerebrovascular pericytes cultured in vitro will activate the expression of inflammatory genes, release cytokines (such as IL-1 β and TNF- α) and chemotactic. These inflammatory responses may change: 1) the

proliferation and migration of pericytes, 2) the interaction with other inflammatory cells, and 3) the expression of LRP1 related to A β endocytosis (Guijarro-Munoz et al., 2014; Kovac et al., 2011; Nyul-Toth et al., 2017). A mouse experiment conducted by the Shanghai Institute of Neuroscience found that cerebral vascular pericytes can sense the peripheral inflammation caused by intraperitoneal injection of LPS, and transmit peripheral inflammation information to the central nervous system by secreting CCL-2 to stimulate the central inflammatory process. Thereby changing the electrophysiological activity of nerve cells. These in vitro and in vivo research results suggest that the immune signal mechanism may regulate the activity and function of cerebral vascular pericytes. However, the specific role of the immune regulation mechanism of cerebrovascular pericytes in the pathogenesis of AD has not been reported yet, And it is interesting to ask whether innate immune signaling (like NLRP3 inflammasome) regulates cellular fate and functions of pericytes in the brain.

NLRP3-contained inflammasome has attracted great attention in AD researches, as it is activated in AD brain and potentially mediates microglial inflammatory responses, exaggerates A β and Tau protein aggregation in APP or Tau-transgenic mice (Heneka et al., 2013; Ising et al., 2019; Stancu et al., 2019; Venegas et al., 2017). NLRP3 is considered as a promising therapeutic target for AD patients (Dempsey et al., 2017). However, the effects of NLRP3 activation on pericytes and vascular dysfunction were not addressed. In this study, we used NLRP3-knockout mice and treated cultured pericytes with NLRP3 inhibitor, MCC950, or interleukin (IL)-1 β , a major product of NLRP3-contained inflammasome. We observed that NLRP3 might be essential for the maintenance of healthy pericytes in the brain, that AKT (also known as protein kinase B) might mediate the physiological effect of NLRP3 in pericytes. We further investigated effects of NLRP3 on the vasculature and pericyte survival in brains under both physiological and pathological conditions.

2. MATERIALS AND METHODS

2.1 Materials

Instruments, experimental materials and kits, unless otherwise specified, were the same as described in Part I.

2.2 Methods

2.1.1. Mice and Cross-breeding

NLRP3 knockout (NLRP3^{-/-}) mice were kindly provided by N. Fasel (University of Lausanne, Lausanne, Switzerland) (Martinon et al., 2006). MyD88 knockout (MyD88^{-/-}) mice were originally provided by S. Akira and K. Takeda (Osaka University, Osaka, Japan) (Adachi et al., 1998). Breeding between heterozygous mutants (+/-) on a C57BL/6 background were used to maintain mouse colonies. Mice were compared only between littermates. Animal experiments were performed in accordance with all relevant national rules and were authorized by the local research ethical committee. All animal experiments were approved by the regional ethical committee of the regional council in Saarland, Germany.

2.1.2. Tissue collection and isolation of blood vessels

Animals were euthanized by inhalation of isofluorane and perfused with ice-cold phosphate-buffered saline (PBS). The brain was removed and divided. The left hemisphere was immediately fixed in 4% paraformaldehyde (Sigma-Aldrich Chemie GmbH, Taufkirchen, Germany) in PBS and embedded in paraffin for immunohistochemistry. The cortex and hippocampus were carefully dissected from the right hemisphere, snap-frozen in liquid nitrogen and stored at -80°C for biochemical analysis. Cortex and hippocampus were also used for isolation of brain vessel fragments according to the published protocol (Boulay et al., 2015). Briefly, brain tissues were homogenized in HEPES-contained Hanks' balanced salt solution (HBSS) and centrifuged at 4,400 g in HEPES-HBSS buffer supplemented with dextran from *Leuconostoc* spp. (molecular weight ~ 70,000; Sigma-Aldrich) to delete myelin. The vessel pellet was re-suspended in HEPES-HBSS buffer supplemented with 1% bovine serum albumin

(Sigma-Aldrich) and filtered with 20 μm -mesh. The blood vessel fragments were collected on the top of filter and frozen at -80°C for further biochemical analysis.

2.1.3. Histological image acquisition and analysis

Serial 40- μm -thick sagittal sections were cut from the paraffin-embedded hemisphere. Four serial sections per mouse with 400 μm of interval between two neighboring sagittal sections were stained with rabbit anti-PDGFR β monoclonal antibody (clone: 28E1; Cell Signaling Technology Europe, Frankfurt am Main, Germany) and Alexa488-conjugated goat anti-rabbit IgG (Thermo Fisher Scientific, Darmstadt, Germany). The coverage of PDGFR β staining-positive cells in the whole hippocampus and cortex was estimated with the Cavalieri method on a Zeiss AxioImager.Z2 microscope (Carl Zeiss Microscopy GmbH, Göttingen, Germany) equipped with a Stereo Investigator system (MBF Bioscience, Williston, VT, USA). The grid size was set at 10 μm , which provided coefficient of error estimates of < 0.05 .

To quantify vasculature in the brain, our established protocol was used (Decker et al., 2018). Briefly, 4 serial paraffin-embedded sections per mouse were deparaffinized, heated at 80°C in citrate buffer (10mM, pH = 6) for 1 hour and digested with Digest-All 3 (Pepsin) (Thermo Fisher Scientific) for 20 minutes. Thereafter, brain sections were stained with rabbit anti-collagen IV polyclonal antibody (Catalog: # ab6586; Abcam, Cambridge, UK) and Alexa488-conjugated goat anti-rabbit IgG (Thermo Fisher Scientific). After being mounted, the whole brain including hippocampus and cortex was imaged with MicroLucida (MBF Bioscience). The length and branching points of collagen type IV staining-positive blood vessels were analyzed with a free software, *AngioTool* (<http://angiotool.nci.nih.gov>) (Zudaire et al., 2011). The parameters of analysis for all compared samples were kept constant. The length and branching points were adjusted with area of interest.

2.1.4. Western blot analysis of PDGFR β and CD13 in cerebral blood vessels

Isolated blood vessels were lysed in RIPA buffer (50mM Tris [pH 8.0], 150mM NaCl, 0.1% SDS, 0.5% sodiumdeoxy-cholate, 1% NP-40, and 5mM EDTA) supplemented with protease inhibitor cocktail (Roche Applied Science, Mannheim, Germany) on ice. The tissue lysate was sonicated before being loaded onto 10% SDS-PAGE. For Western blot detection, rabbit monoclonal antibodies against PDGFR β and CD13/APN (clone: 28E1 and D6V1W,

respectively; Cell Signaling Technology Europe) were used. In the same sample, β -actin was detected as a loading control using rabbit monoclonal antibody (clone: 13E5; Cell Signaling Technology Europe). Western blots were visualized via the ECL method (PerkinElmer LAS GmbH, Rodgau, Germany). Densitometric analysis of band densities was performed with ImageJ software (<https://imagej.nih.gov/ij/>). For each sample, the protein level was calculated as a ratio of target protein/ β -actin.

2.1.5. Culture of pericytes

Human primary brain vascular pericytes (HBPC) were immortalized by infecting cells with tsSV40T lentiviral particles (Umehara et al., 2018). The selected immortalized HBPC clone 37 (hereafter referred to as HBPC/ci37) was used for our study. HBPC/ci37 cells were cultured at 33 °C with 5% CO₂/ 95% air in pericyte medium (Catalog: # 1201; Sciencell Research Laboratories, Carlsbad, CA, USA) containing 2% (v/v) fetal bovine serum, 1% (w/v) pericyte growth factors, and penicillin-streptomycin. Culture flasks and plates were treated with Collagen Coating Solution (Catalog: # 125-50; Sigma-Aldrich). HBPC/ci37 cells were used at 40 ~ 60 passages in this study.

2.1.6. Analysis of pericyte proliferation and apoptosis

Pericytes were seeded at 1.0×10^4 cells on 96-well plate /100 μ l (day 0), and cultured in pericyte medium containing NLRP3 inhibitor, MCC950 (Catalog: # PZ0280; Sigma-Aldrich), at 0, 25, 50 and 100 nM. The cell survival was detected with MTT-based Cell Proliferation Kit I (Catalog: # 11465007001; Sigma-Aldrich) on days 1, 2, 3, 4, 5, 6 and 7. In order to further detect cell death and proliferation of pericytes, cells were cultured in 12-well plate at 5.0×10^5 cells/well, and treated with MCC950 as described in MTT assay. After 24 hours, pericytes were collected and lysed in RIPA buffer. Quantitative Western blot was used with rabbit monoclonal antibody against cleaved caspase-3 (clone: 5A1E; Cell Signaling Technology Europe), mouse monoclonal antibody against proliferating cell nuclear antigen (PCNA) (clone: PC10; Cell Signaling Technology Europe) and rabbit monoclonal antibody against Ki-67 (clone: SP6; Abcam). α -tubulin and β -actin were detected as an internal control with mouse monoclonal antibody (clone: DM1A; Abcam) and rabbit monoclonal antibody (clone: 13E5; Cell Signaling Technology Europe), respectively.

2.1.7. Treatments of pericytes for detection of PDGFR β and CD13 and phosphorylated AKT, ERK and NF κ B p65

Pericytes were cultured in 12-well plate at 5.0×10^5 cells/well. Before experiments, we replaced culture medium with serum-free pericyte medium and cultured cells at 37°C for 3 days to facilitate cell differentiation (Umehara et al., 2018). Thereafter, pericytes were treated for 24 hours with MCC950, at 0, 25, 50 and 100 nM, recombinant human IL-1 β (Catalog: # 201-LB; R&D Systems, Wiesbaden, Germany) at 0, 5, 10 and 50 ng/ml, or AKT Inhibitor VIII (Catalog: # 124018; Sigma-Aldrich) at 0, 0.5, 1 and 5 μ M. Cell lysate was prepared in RIPA buffer supplemented with protease inhibitor cocktail (Roche Applied Science) and phosphatase inhibitors (50 nM okadaic acid, 5 mM sodium pyrophosphate, and 50 mM NaF; Sigma-Aldrich). For Quantitative Western blot, the following antibodies were used: rabbit monoclonal antibodies against PDGFR β , CD13/APN, phosphorylated AKT (Ser473), phosphorylated ERK1/2 (Thr202/Tyr204), phosphorylated NF κ B p65 (S536), NF κ B p65, β -actin, GAPDH (clone: 28E1, D6V1W, D9E, D13.14.4E, 93H1, D14E12, 13E5, and 14C10, respectively; Cell Signaling Technology Europe), rabbit polyclonal antibodies against AKT and phosphorylated GSK-3 β (Ser9) (Catalog: # 9272 and Catalog: # 9336, respectively; Cell Signaling Technology Europe) and mouse monoclonal antibodies against ERK1/2 and GSK-3 β (clone: L34F12 and 3D10, respectively; Cell Signaling Technology Europe) and α -tubulin (clone: DM1A; Abcam).

2.1.8. Flow cytometric analysis of innate immune receptors in pericytes

In order to investigate the potential role of innate immune signaling in pericytes during AD pathogenesis, we detected innate immune receptors, TLR1, TLR2, TLR4 and CD14, on the cell surface of pericytes isolated from 9-month-old APP- transgenic and wild-type littermate mice. AD mice were sacrificed at the 9-month-old, and the cerebral cortex and hippocampus were harvested after phosphate-buffered saline perfusion. The tissue was carefully dissected to prepare a single-cell suspension, with myelin removed, using the Neural Tissue Dissociation Kit (papain based) and Myelin Removal Beads II (both from Miltenyi Biotec GmbH, Bergisch Gladbach, Germany), according to the manufacturer's protocols. After pelleting cells by centrifugation, we added 40 μ l of blocking buffer containing 25 mg/mL rat anti-mouse CD16/CD32 antibody (2.4G2; BD Biosciences) and 10% fetal calf serum to prevent nonspecific binding. Thirty minutes after

blocking at 4°C, cells were incubated with fluorophore-conjugated antibodies against mouse TLR1, TLR2, TLR4 and CD14 (eBioscience, Frankfurt, Germany). After thorough washing, different inflammatory cell populations were immediately analyzed using flow cytometry (BD FACSCanto II), and absolute numbers of cells were counted using BD Trucount absolute counting tubes (BD Biosciences).

2.1.9. Statistics

Data was presented as mean \pm SEM for mice and mean \pm SD for cells. For multiple comparisons, one-way or two-way ANOVA followed by Bonferroni or Tukey post hoc test. Two independent-samples Students t test was used to compare means for two groups of cases. All statistical analyses were performed with GraphPad Prism 5 version 5.01 for Windows (GraphPad Software, San Diego, CA, USA). Statistical significance was set at $p < 0.05$.

3. RESULTS

3.1 NLRP3 deficiency reduces pericyte cell coverage and decreases protein levels of PDGFR β and CD13 in the Brain

To the best of our knowledge, we are first to show the protein expression of NLRP3 in cerebral pericytes. As shown in Fig 3.1A, some brain cells were co-stained by NLRP3 and PDGFR β -specific antibodies. To explore effects of NLRP3 on the maintenance of pericytes in the brain, we estimated the coverage of PDGFR β -positive cells in brains from 9-month-old NLRP3-knockout (NLRP3^{-/-}) and wild-type (NLRP3^{+/+}) littermate mice. We observed that NLRP3 deficiency significantly decreased the coverage of PDGFR β -immune reactive cells in microvessels with < 6 μ m of diameter in a gene dose-dependent manner (Fig 3.1, B and C one-way ANOVA, $p < 0.05$). In isolated blood vessels from brains of 9-month-old NLRP3^{-/-}, NLRP3^{+/-} and NLRP3^{+/+} littermate mice, we similarly observed that deletion of NLRP3 significantly reduced PDGFR β and CD13 proteins, two pericyte markers, in the cerebral blood vessels also with a gene dose-dependent pattern (Fig 3.1, D and E; one-way ANOVA, $p < 0.05$).

In further experiments, we asked whether innate immune signaling serves a common effect on pericyte survival in the brain. We detected PDGFR β and CD13 proteins in cerebral blood vessels isolated from 6-month-old MyD88^{-/-}, MyD88^{+/-} and MyD88^{+/+} littermate mice. As shown in Fig 3.1, F and G, protein levels of CD13 and PDGFR β were both lower in MyD88-deficient mice than in MyD88-wildtype controls (one-way ANOVA, $p < 0.05$).

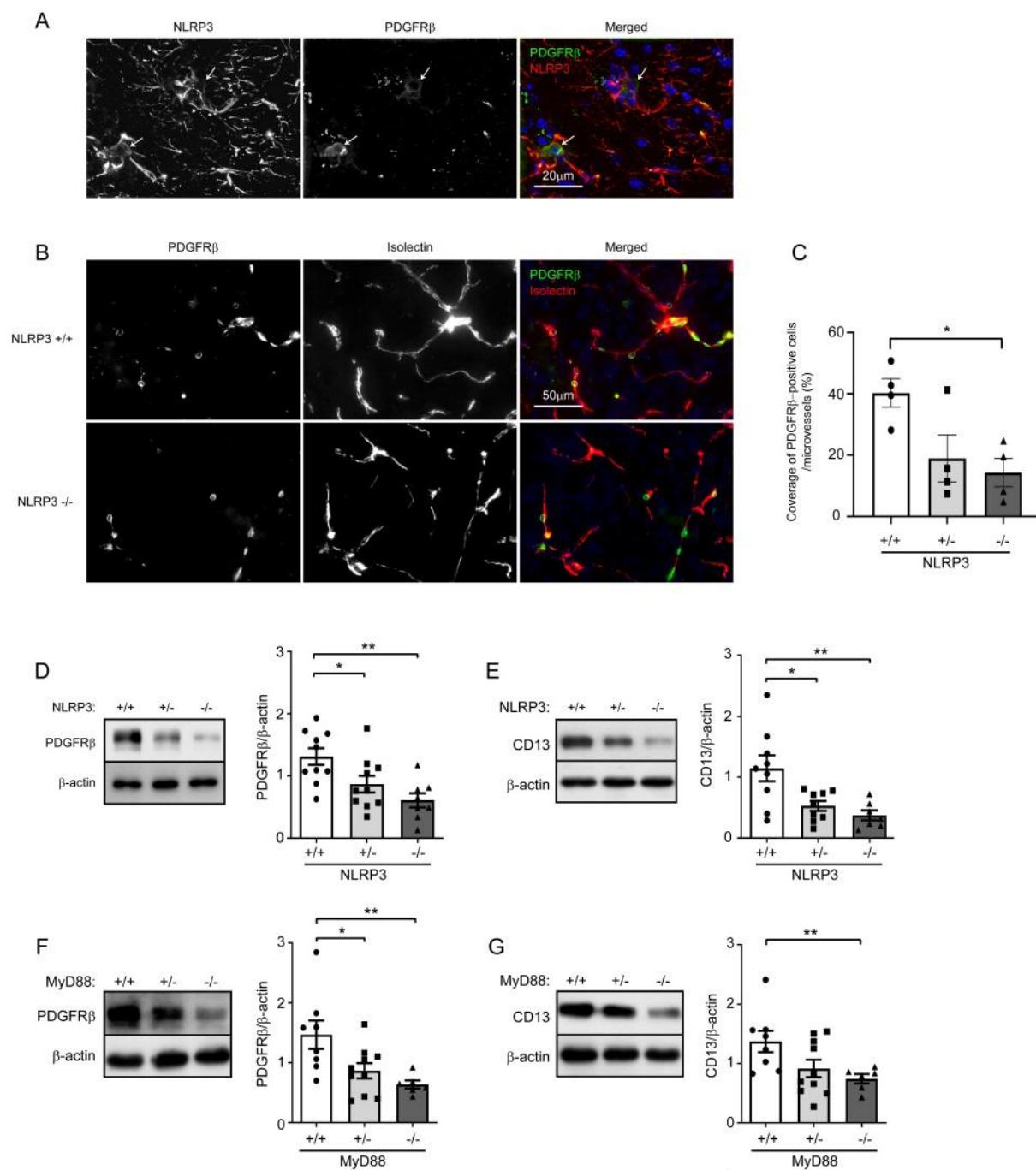


Fig 3.1 NLRP3 deficiency reduces pericyte cell coverage and decreases protein levels of PDGFR β and CD13 in the brain. A, 9-month-old mouse brains were co-stained for NLRP3 and PDGFR β . PDGFR β -immune reactive cell bodies (in green; marked with arrows) were stained by NLRP3-specific antibodies (in red). B, brain tissues from 9-month-old NLRP3-knockout (+/- and -/-) and wild-type (+/+) littermate mice were then co-stained for PDGFR β (with anti-PDGFR β antibodies, in green) and endothelial cells (with isolectin B4, in red). C, the coverage of PDGFR β -positive pericytes was calculated as a ratio of PDGFR β /isolectin B4-positive area. One-way ANOVA

followed by Tukey *post hoc* test, $n = 4$ per group. D-G, 9-month-old NLRP3 and 6-month-old MyD88 littermate mice with homozygous (-/-) and heterozygous (+/-) knockout, and wild-type (+/+) of *nlrp3* and *myd88* genes, respectively, were analyzed for protein levels of PDGFR β and CD13 in isolated cerebral blood vessels. One-way ANOVA followed by Bonferroni *post hoc* test, $n = 10, 10$ and 8 for NLRP3 (+/+, +/- and -/-) mice in PDGFR β detection and $n = 9, 9$ and 7 for NLRP3 (+/+, +/- and -/-) mice in CD13 detection; $n = 8, 10$ and 6 for MyD88 (+/+, +/- and -/-) mice in the detection of both PDGFR β and CD13. *: $p < 0.05$ and **: $p < 0.01$.

3.2 NLRP3 deficiency reduces vasculature in the brain

Pericytes are essential for the development of cerebral circulation. We asked whether NLRP3 deficiency affects the structure of cerebral blood vessels. We observed that, in 9-month-old mouse brains, deficiency of NLRP3 significantly reduced the total length and branching points of collagen type IV-positive blood vessels (Fig 3.2, A - C; one-way ANOVA, $p < 0.05$). The reduction of brain vasculature was dependent on the copies of NLRP3-encoding gene.

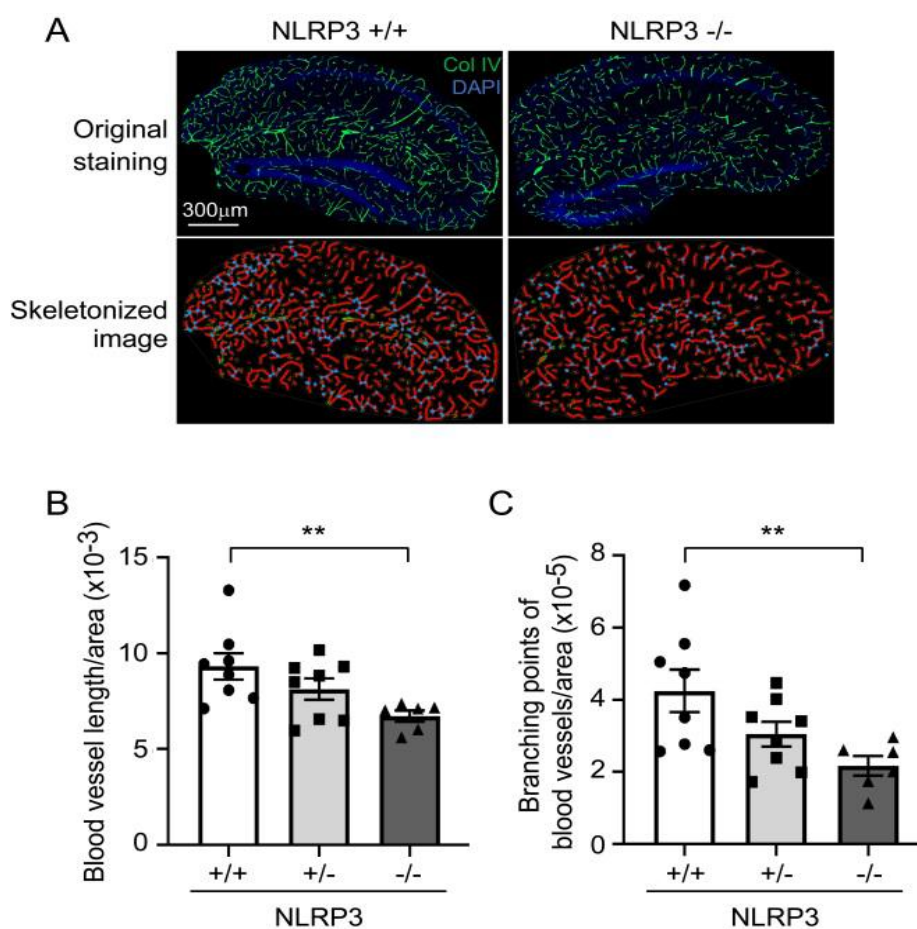


Fig 3.2 NLRP3 deficiency reduces vasculature in the brain. A, brains of 9-month-old littermate mice with homozygous (-/-), heterozygous (+/-) and wild-type (+/+) of *nlrp3* gene were stained for collagen type IV (Col IV).

The blood vessels in hippocampus were thresholded and skeletonized. The skeleton representation of vasculature is shown in red and branching points of blood vessels are in blue. B and C, the total length and branching points of blood vessels were calculated and adjusted by area of analysis. One-way ANOVA followed by Bonferroni *post hoc* test, $n = 8, 8$ and 6 for NLRP3 (+/+, +/- and -/-) mice, respectively. $**p < 0.01$.

3.3 NLRP3 inhibition attenuates cell proliferation in cultured pericytes

After we observed that NLRP3 deficiency decreased the number of pericytes in the brain, we continued to investigate underlying mechanisms mediating the effects of NLRP3 on pericytes. After treating cultured pericytes with NLRP3 inhibitor, MCC950, at different concentrations, we observed that NLRP3 inhibition significantly reduced the conversion of MTT into its colorful product in a dose-dependent manner (Fig3.3, A; one-way ANOVA, $p < 0.05$; $n = 4$ per group). In further experiments, we detected cell proliferation protein PCNA and Ki-67 in MCC950-treated cells. As it was shown in Fig3.3, B-D, MCC950 treatments significantly decreased protein levels of both PCNA (Fig. 3, B and C; one-way ANOVA, $p < 0.05$; $n = 3$ per group) and Ki-67 (Fig 3.3, B and D; one-way ANOVA, $p < 0.05$; $n = 4$ per group), two typical protein markers for cell proliferation. Thus, inhibition of NLRP3 potentially suppressed proliferation of pericytes.

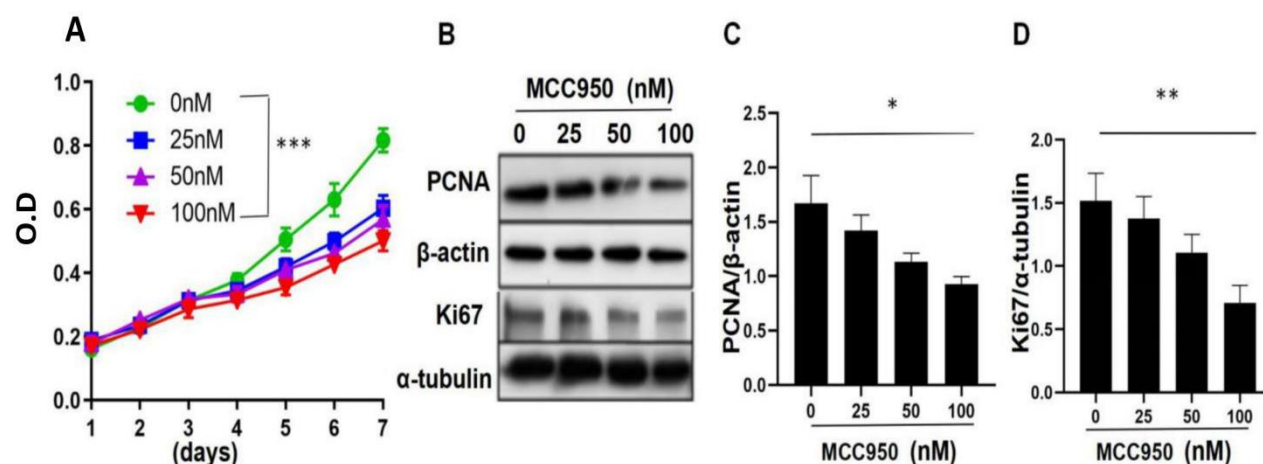
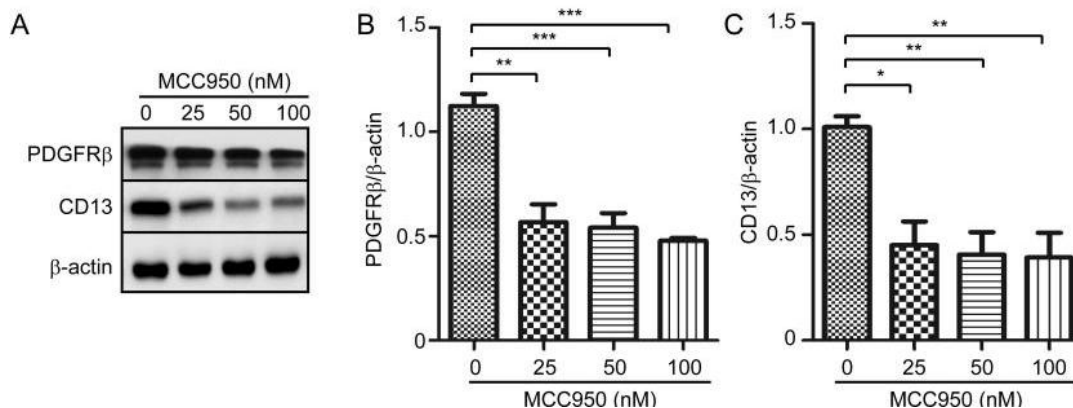


Fig3.3 NLRP3 inhibition attenuates cell proliferation in cultured pericytes. A, cultured pericytes were treated with NLRP3 inhibitor, MCC950, at 0, 25, 50 and 100 nM and analyzed for proliferation with MTT assay every day for 7 days. Two-way ANOVA followed by Tukey post-hoc *post hoc* test, $n = 4$ per group. $**p < 0.01$ and $**p < 0.001$. B, C and D, pericytes were cultured and treated with MCC950 at indicated concentrations for 24 hours. Cell lysate were detected for PCNA and Ki-67 with quantitative Western blot.

Inhibition of NLRP3 reduces protein levels of PCNA and Ki-67 in a dose-dependent manner. One-way ANOVA followed by Tukey post-hoc *post hoc* test, $n = 3$ per group for PCNA and $n = 4$ per group for Ki-67. $*p < 0.05$ and $**p < 0.01$.

3.4 NLRP3 inhibition attenuates expression of PDGFR β and CD13 in cultured pericytes

In order to examine the specific effects of NLRP3 on pericyte behavior, we detected protein levels of PDGFR β and CD13 in cultured pericytes after NLRP3 inhibition. PDGFR β and CD13 mediate both physiological and pathophysiological functions of pericytes (Lindahl et al., 1997; Rangel et al., 2007). We observed that treatments with MCC950 decreased expression of PDGFR β and CD13 in pericytes in a dose-dependent manner (Fig 3.4, A-C; One-way ANOVA, $p < 0.05$; $n = 4$ per group). To analyze underlying mechanisms, through which NLRP3 drives pericyte differentiation, we detected phosphorylation of AKT, ERK and NF- κ B in MCC950-treated cells. Activation of AKT and ERK is involved in pericyte proliferation and migration (Bonacchi et al., 2001; Yao et al., 2014). As shown in Fig 3.4, D-F, inhibition of NLRP3 reduced the protein levels of both phosphorylated AKT and ERK in a dose-dependent manner (One-way ANOVA, $p < 0.05$; $n = 4$ per group). However, phosphorylation of NF- κ B in pericytes was not significantly changed by treatments with MCC950 (Fig 3.4, G and H; One-way ANOVA, $p = 0.094$; $n = 3$ per group).



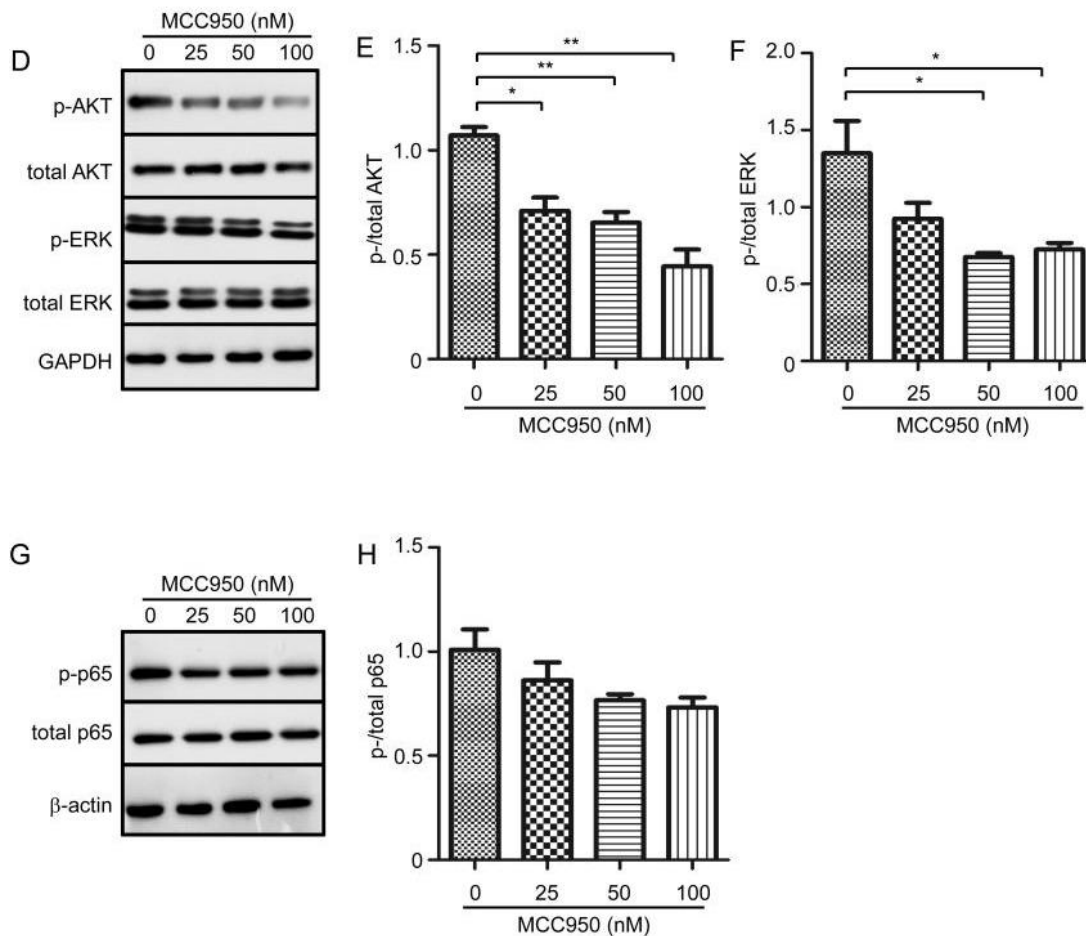


Fig3.4 NLRP3 inhibition attenuates protein expression of PDGFR β and CD13 and inhibits phosphorylation of AKT and ERK in cultured pericytes. Pericytes were cultured and treated with MCC950 at 0, 25, 50 and 100 nM for 24 hours. A, D and G, Western blot was used to detect PDGFR β and CD13, as well as phosphorylated and total protein levels of AKT, ERK and NF κ B p65. B, C, E and F, Inhibition of NLRP3 reduces protein levels of PDGFR β and CD13, and inhibits phosphorylation of AKT and ERK with a dose-dependent pattern. One-way ANOVA followed by Tukey *post hoc* test, n = 4 per group. * p < 0.05, **p < 0.01 and ***p < 0.001. G, Phosphorylation of NF κ B p65 is not significantly changed by inhibition of NLRP3. One-way ANOVA, n = 3 per group.

3.5 IL-1 β increases protein expression of PDGFR β and CD13 in cultured pericytes.

NLRP3-contained inflammasome activates caspase 1 and subsequently cleaves pro-IL-1 β into active IL-1 β (Gross et al., 2011). Due to the low level of IL-1 β released from non-activated pericytes, we could not detect reduction of IL-1 β secreted from NLRP3-deficient pericytes compared to NLRP3-wild-type pericytes (data not shown). However, we hypothesized that IL-1 β

affects differentiation of pericytes. We treated cultured pericytes with IL-1 β at different concentrations. Very interestingly, IL-1 β increases the protein expression of PDGFR β and CD13 also with a concentrations-dependent pattern (Fig 3.5, A-C; One-way ANOVA, $p < 0.05$; $n = 3$ per group). As potential regulating mechanisms, we observed that IL-1 β treatments significantly increased phosphorylation of AKT but of ERK (Fig 3.5, D-F; One-way ANOVA, $p < 0.05$; $n = 3$ per group).

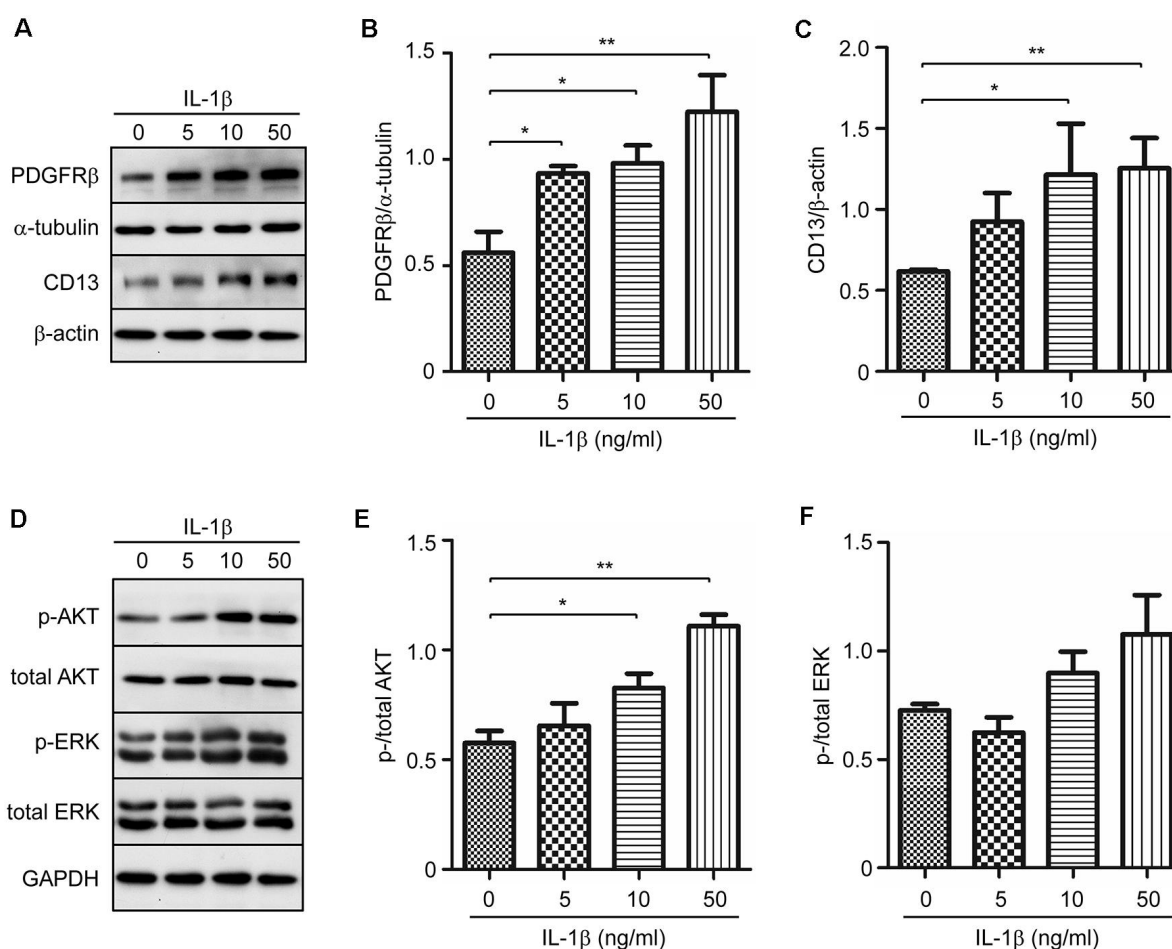


Fig 3.5 IL-1 β increases protein expression of PDGFR β and CD13 in cultured pericytes. Pericytes were cultured and treated with recombinant human IL-1 β at 0, 5, 10 and 50 ng/ml for 24 hours. A and D, Western blot was used to detect PDGFR β and CD13, as well as phosphorylated and total protein levels of AKT and ERK. B, C, E and F, stimulation of IL-1 β increases protein levels of PDGFR β and CD13, and activates phosphorylation of AKT, but not ERK, in a dose-dependent manner. One-way ANOVA followed by Tukey *post hoc* test, $n = 3$ per group. * $p < 0.05$ and ** $p < 0.01$.

3.6 Deficiency of NLRP3 increases pericytes and vasculature in the brain of Tau-transgenic AD mice

After we observed that deficiency of NLRP3 decreases pericytes and vasculature in the brain under the physiological condition (Quan et al., 2020), we continued to investigate the pathophysiological function of NLRP3 in an AD mouse model. Human Tau-transgenic mice (Yoshiyama et al., 2007) were cross-bred with NLRP3 knockout mice (Martinon et al., 2006). By 9 months of age, Tau-transgenic and wild-type with different expression of NLRP3 were analyzed for pericyte coverage and vasculature using the same protocol as we used in our previous study (Decker et al., 2018; Quan et al., 2020). As shown in Fig 3.6a, A and B, deficiency of NLRP3 increases the coverage of PDGFR β -positive pericytes in the micro-vessels of Tau-transgenic mice (one-way ANOVA, $p < 0.05$). Accordingly, NLRP3 deficiency increases the length and branching points of blood vessels in Tau-transgenic (Fig 3.6b, A and B; one-way ANOVA, $p < 0.05$). Deficiency of NLRP3 regulates both pericyte coverage and vasculature in a gene copies-dependent manner (Fig3.6a and Fig3.6b).

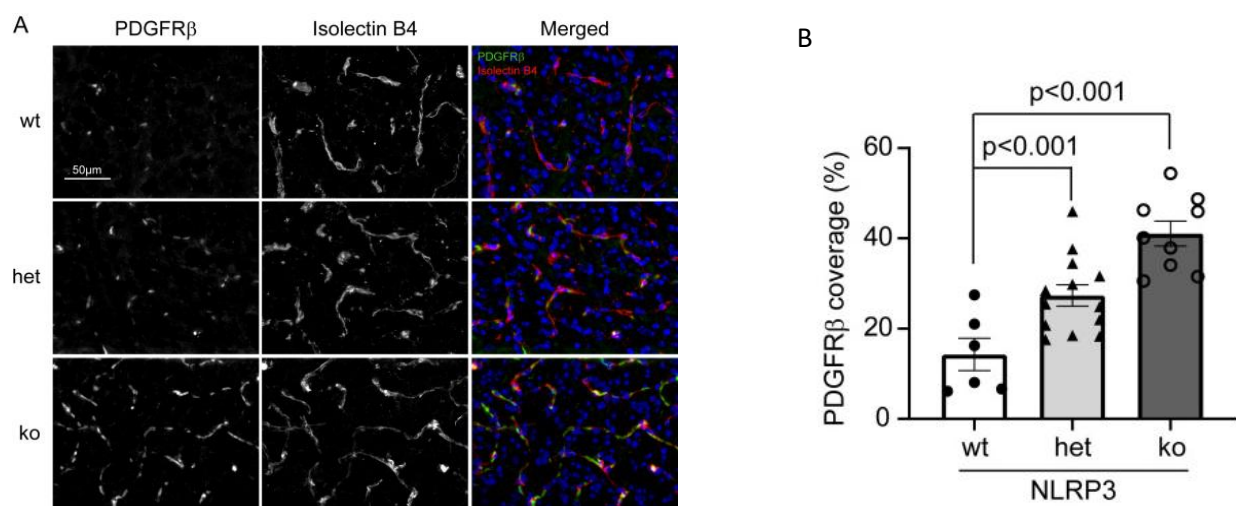


Fig 3.6a NLRP3 deficiency increases the pericyte cell coverage in cerebral blood vessels of Tau-transgenic mice. A, mouse brains from 9-month-old Tau-transgenic mice with wild-type [wt] NLRP3, and heterozygous [het] and homozygous [ko] knockout of NLRP3 were co-stained for PDGFR β (with anti-PDGFR β antibodies, in green) and endothelial cells (with isolectin B4, in red). B, the coverage of PDGFR β -positive pericytes calculated as a ratio of PDGFR β /isolectin B4-positive area is increased by deficiency of NLRP3 in a gene dose-dependent manner (One-way ANOVA followed by Bonferroni *post hoc* test, $n \geq 6$ per group).

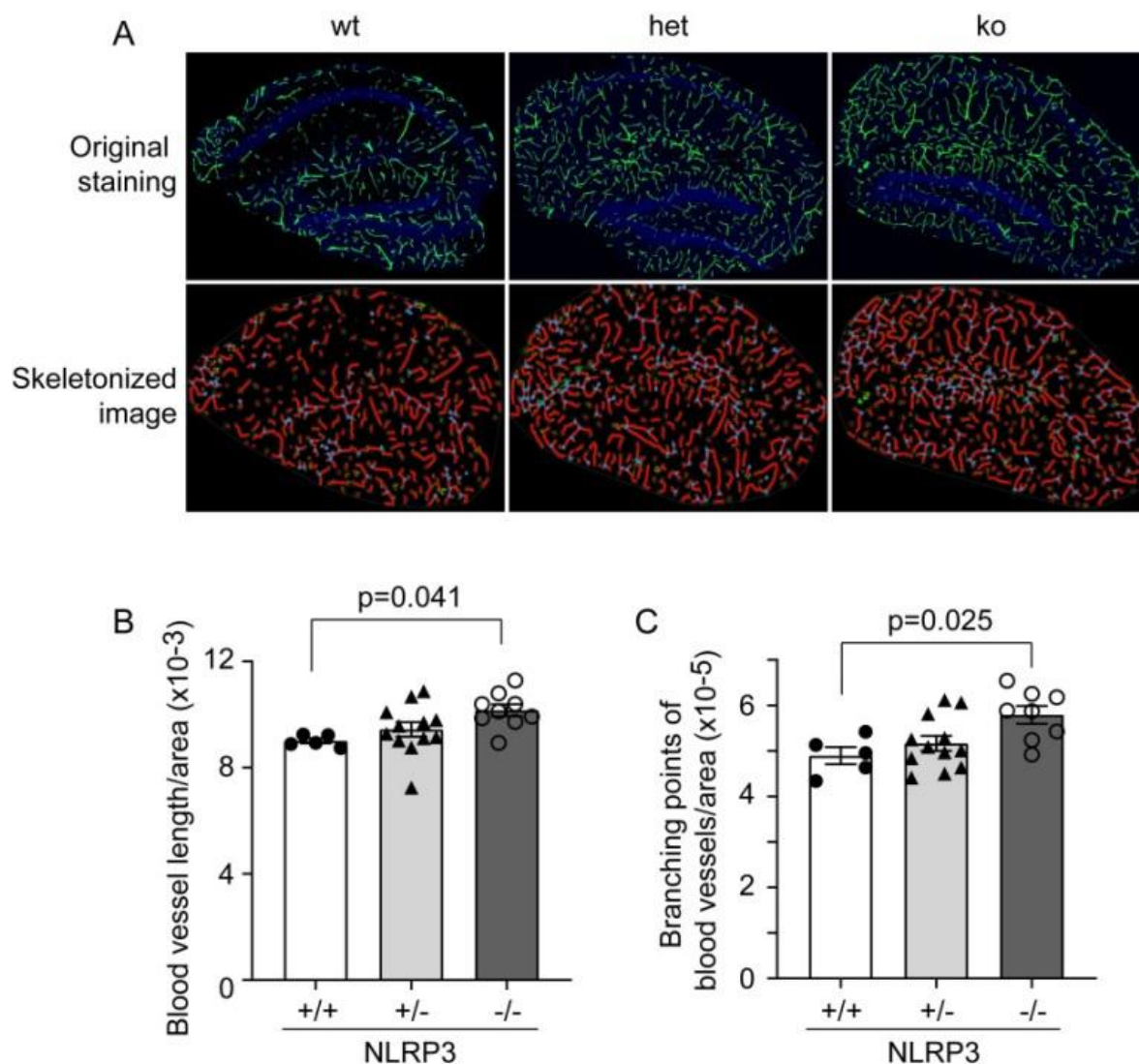


Fig 3.6b NLRP3 deficiency increases the vasculature in the brain of Tau-transgenic mice. A, brains of 9-month-old Tau-transgenic mice with homozygous (ko) and heterozygous (het) knockout of *nlrp3* and wild-type (wt) *nlrp3* gene were stained for collagen type IV. The blood vessels in hippocampus were thresholded and skeletonized. The skeleton representation of vasculature is shown in red and branching points of blood vessels are in blue. B and C, the total length and branching points of blood vessels were calculated and adjusted by brain area of analysis. Deficiency of NLRP3 increases the vasculature of the brain (One-way ANOVA followed by Bonferroni *post hoc* test, $n \geq 5$ per group).

3.7 Deletion of MyD88 specifically in pericytes attenuates amyloid pathology in

APP/PS1-transgenic mice

After we observed that NLRP3 deficiency regulates pericyte coverage and vasculature in the brain under physiological and pathological conditions (Quan et al., 2020), we continued to examine whether MyD88 in pericytes modulate AD pathogenesis. Expression of TLR1 and TLR2 is highly up-regulated on pericytes in APP-transgenic mouse brain. To explore the potential role of innate immune signaling in pericytes during AD pathogenesis, we detected innate immune receptors, TLR1, TLR2, TLR4 and CD14, on the cell surface of pericytes isolated from 9-month-old APP-transgenic and wild-type littermate mice (Radde et al., 2006). We observed that expression of TLR1, TLR2 and TLR4 is highly up-regulated in AD mice compared to wild-type controls (Fig. 3.7, A and B; t test, $p < 0.05$). Our previous study has shown that TLR2 in cooperation with TLR1 serves as a primary receptor for A β to trigger neuroinflammatory activation (Liu et al., 2012).

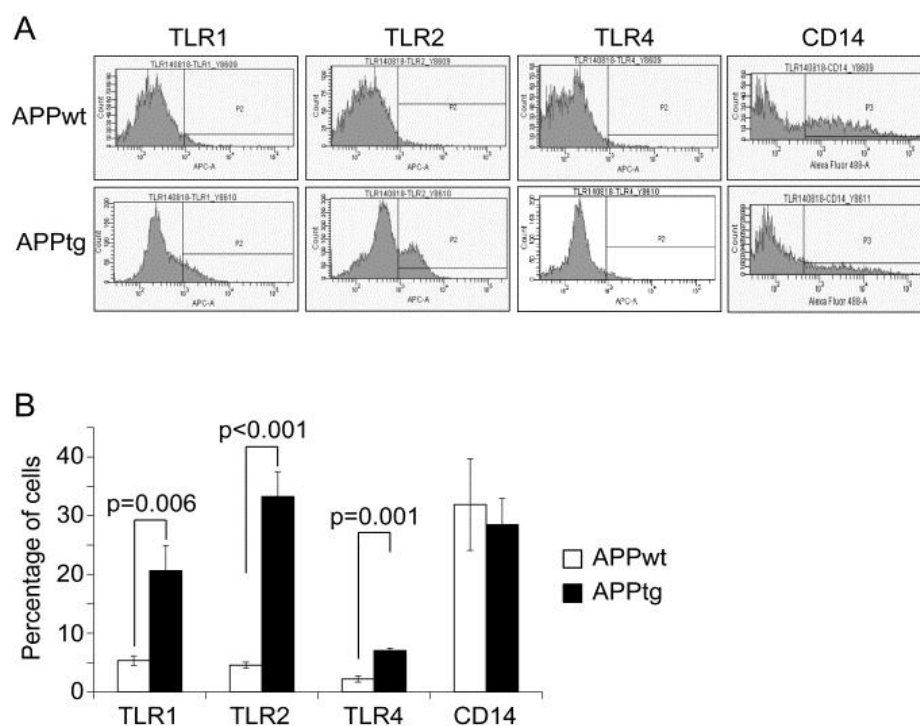
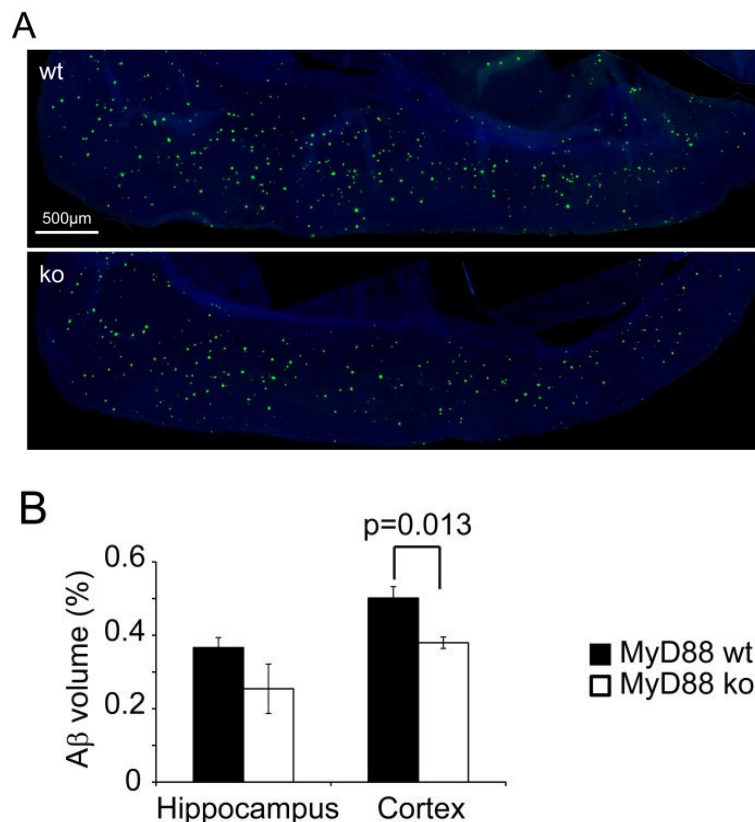


Fig 3.7 TLR1, TLR2 and TLR4 are highly expressed on pericytes in APP-transgenic mouse brain. 9 month-old APP-transgenic (APPtg) and wild-type (APPwt) littermate mice were analyzed for expression of innate immune receptors on brain pericytes. Cortex and hippocampus were carefully dissected and digested with Neural Tissue Dissociation Kit (papain-based; MiltenyiBiotec). Single-cell suspensions were prepared and

pericytes were selected with PE-conjugated anti-PDGFR β and MicroBeads-conjugated anti-PE antibodies (both from MiltenyiBiotec). The selected cells were further labelled with APC-conjugated antibodies against TLR1, TLR2 or TLR4, or Alexa488-conjugated antibody against CD14 (all antibodies from eBioscience) and thereafter detected with flow cytometry. Expression of TLR1, TLR2 and TLR4 is highly up-regulated in pericytes from APP^{tg} mice compared to APP^{wt} mice. Two-independent groups t test; n = 6 per group.

3.8 Deficiency of MyD88 in pericytes attenuates AD-associated pathology in APP-transgenic mice

To explore the potential effects of pericyte MyD88 on AD pathogenesis, we cross-bred APP-transgenic mice with *myd88*-floxed mice (Hou et al., 2008) and PDGFR β -CreERT2 transgenic mice (Gerl et al., 2015) to create AD mice with APP^{tg}/Myd88^{fl/fl}/Cre^{tg} and APP^{tg}/Myd88^{fl/fl}/Cre^{wt} of genotypes. By 2 months of age, mice were injected (i.p.) with tamoxifen for the deletion of MyD88 specifically in pericytes. In 5-month-old APP-transgenic mice, we observed that deficiency of MyD88 in pericytes reduces A β deposits in the brain parenchyma and increases the expression of pericyte markers, PDGFR β and CD13, in the cerebral microvessels (Fig3.8, t test, $p < 0.05$), which suggests that MyD88 in pericytes mediates AD pathogenesis.



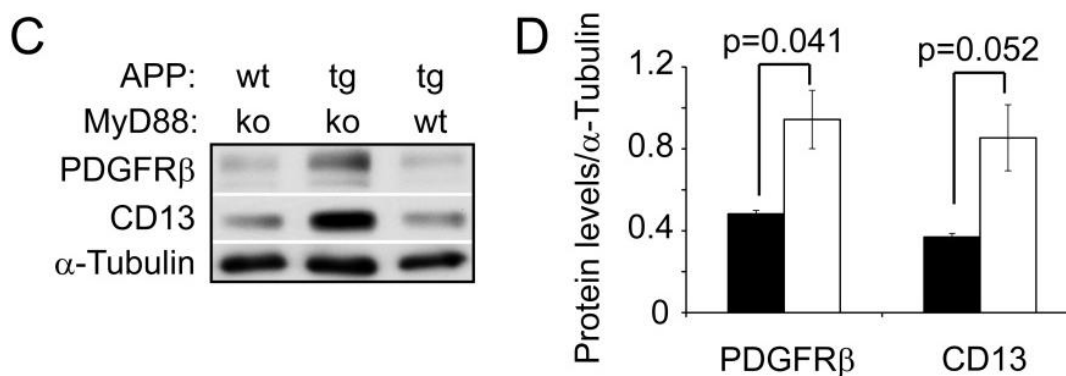


Fig3.8 Deficiency of MyD88 in pericytes reduces A β deposits in association with increased pericyte markers in the brain of APP-transgenic mice. Two-month-old AD mice with APP^{tg}/Myd88^{fl/fl}/Cre^{tg} and APP^{tg}/Myd88^{fl/fl}/Cre^{wt} of genotypes were injected with tamoxifen for the induction of MyD88 deletion in pericytes. By 5 months of age, the brain tissues from these two groups of mice were stained with methoxy-XO4 that specifically recognizes β -sheet secondary structure of A β . The area of methoxy-XO4-positive staining and the whole analyzed brain region was automatically calculated with *Image-J* (A and B; t test, n = 4 per group). Microvessels were also isolated from the brain tissues, lysed in RIPA buffer and detected for pericyte markers, PDGFR β and CD13, with quantitative Western blot (C and D; t test, n = 4 per group).

4. DISCUSSION

Pericytes play a central role in regulating microvascular circulation and BBB function in the brain (Sweeney et al., 2016). Our study demonstrated that general deletion of NLRP3 under physiological conditions decreases the coverage of pericytes and protein levels of PDGFR β and CD13 in cerebral blood vessels, which is correlated with a reduction of vasculature in the brain, which corroborates a recent observation that dysfunction of pericytes decreases the length of cerebral blood vessels in PDGFR β -mutated mouse brain (Montagne et al., 2018). However, we observed that general deficiency of NLRP3 increases the pericyte coverage and vasculature in Tau-transgenic AD mouse model. It appears that NLRP3 serves different effects on pericytes and vasculature under physiological and pathological conditions. As in our animal models, NLRP3 is deleted in both pericytes and non-pericytes, especially microglia, we supposed that 1) NLRP3 regulates neuroinflammatory activation, thereby modifying pericytes and angiogenesis; 2) NLRP3 directly regulates pericyte survival and activation; or 3) both.

Activation of NLRP3-contained inflammasome produces active IL-1 β (Gross et al., 2011). MyD88 mediates inflammatory activation after challenges of TLRs ligands and IL-1 β (O'Neill and Bowie, 2007). We observed that deficiency of either NLRP3 or MyD88 decreases protein levels of PDGFR β and CD13 in the cerebral micro-vessels, and attenuates the vasculature in the mouse brain. We supposed that NLRP3 drives a basal inflammatory activation in the brain under a physiological condition, although it was difficult to detect the changes of IL-1 β secretion in NLRP3 or MyD88-deficient brains. The basic inflammatory activation might promote the pericyte survival. However, in the AD brain, where the inflammatory activation is substantially exaggerated, the pro-angiogenic effects of inflammation are replaced by toxic effects on the vessels. We did observe that the vasculature is reduced in AD mice, over-expressing APP or Tau in neurons (Decker et al., 2018), which is recovered by the neuroinflammatory inhibition in APP-transgenic mice with haploinsufficiency of MyD88 specifically in microglia (Quan et al., 2021). Treatments with IL-1 β increase PDGFR β and CD13 expression in cultured pericytes within 24 hours (Quan et al., 2020 and 2021); however, it could not be excluded that a long-term

inflammatory activation induces cell death of pericytes (Quan et al., 2021). Moreover, other inflammatory mediators, especially oxidative stress, which is present in the brain of AD patients and mouse models (Berkowitz BA et al., 2017), might damage pericytes. It has been reported that A β -activated perivascular macrophages injure the neurovascular coupling through producing reactive oxygen species (Park et al., 2017). Oxygen free radicals produced in cerebral microvessels stimulate the secretion of endothelin 1 from endothelial cells, and subsequently cause pericyte contraction in APP-transgenic mice (Nortley R et al., 2019). Furthermore, inflammatory activation might also indirectly impair pericytes by altering endothelial cells and astrocytes (Maiuolo J et al., 2018; He JT et al., 2020; Yamazaki Y et al., 2017), as all these cells interact with each others in the AD brain.

Growing evidence shows that pericytes share innate signalling pathways with microglia and respond to extracellular inflammatory stimuli. We showed that NLRP3 is expressed in pericytes, which forms the structural basis for the inflammatory activation. In cultured pericytes, inhibition of NLRP3 attenuates phosphorylation of multiple inflammation-related kinases, such as AKT and ERK, and perhaps also NF- κ B ($p = 0.094$), and decreases cell proliferation and PDGFR β and CD13 expression. Treatments with IL-1 β increase PDGFR β and CD13 expression in our cultured pericytes. It is consistent with a report that TNF- α at 10ng/ml promotes cultured pericytes to proliferate and migrate (Tigges et al., 2013). It is not surprising that angiogenesis is activated with pericyte proliferation in inflammatory lesion sites of multiple sclerosis (Girolamo et al., 2014). During early wound healing, NLRP3 facilitates angiogenesis; however, production of IL-1 β appeared not to be always necessary for angiogenesis (Weinheimer-Haus et al., 2015).

AKT is a known kinase to regulate cell survival, proliferation, and angiogenesis in response to extracellular signals (Manning and Cantley, 2007). AKT activation prevents pericyte loss in diabetic retinopathy (Yun et al., 2018). In our experiments, AKT activation might mediate protective effects of NLRP3 on pericytes, as AKT phosphorylation is reduced by NLRP3 inhibition but enhanced by IL-1 β activation. Moreover, inhibition of AKT down-regulates expression of PDGFR β and CD13 in pericytes. Interestingly, PDGFR β activation induces

phosphorylation of AKT (Lehti et al., 2005). Thus, PDGFR β and AKT activate each other and form a potential positive feed-back to maintain healthy pericytes in the brain.

In additional experiments, we observed that TLR1 and TLR2 expression are up-regulated in cerebral vascular pericytes in APP-transgenic mice than in their wild-type littermate controls. TLR2 and TLR1 are the main receptors mediating A β activation in microglia (Liu et al., 2012). Therefore, we hypothesized that TLR2 might also mediate A β to activate cerebrovascular pericytes and play an important pathological role in AD brain. Thus, we knocked out MyD88 specifically in pericytes. We did observe that MyD88 deficiency in pericytes reduces A β deposition in the cortex, which is associated with an increase of PDGFR β and CD13 in the cerebral blood vessels. Thus, our exploratory studies strongly suggest that innate immune signalling pathways, i.e. NLRP3 or TLR2-MyD88, regulate the inflammatory responses of pericytes and their pathogenic role in AD brain.

In summary, our study suggested that NLRP3 activation maintains healthy pericytes in the brain perhaps through activating AKT signaling pathway in pericytes. However, NLRP3 deficiency protects pericytes and vasculature from AD-associated impairment in Tau-transgenic mice, although the underlying mechanisms need to be further investigated. Our studies also suggest that pericytes display microglia-like characters and innate immune signalling pathways modulate the pathogenic behaviour of pericytes in AD.

REFERENCES

- Abbott, N. J., A. A. Patabendige, D. E. Dolman, S. R. Yusof and D. J. Begley (2010). Structure and function of the blood-brain barrier. *Neurobiol Dis* 37(1): 13-25.
- Adams, J. N., A. Maass, T. M. Harrison, S. L. Baker and W. J. Jagust (2019). Cortical tau deposition follows patterns of entorhinal functional connectivity in aging. *Elife* 8.
- Adachi, O., Kawai, T., Takeda, K., Matsumoto, M., Tsutsui, H., Sakagami, M., Nakanishi, K., Akira, S., 1998. Targeted disruption of the MyD88 gene results in loss of IL-1- and IL-18-mediated function. *Immunity* 9, 143-150.
- Anastasia, A., Deinhardt, K., Wang, S., Martin, L., Nichol, D., Irmady, K., Trinh, J., Parada, L., Rafii, S., Hempstead, B.L., Kermani, P., 2014. Trkb signaling in pericytes is required for cardiac microvessel stabilization. *PLoS One* 9, e87406.
- Ajami, B., J. L. Bennett, C. Krieger, W. Tetzlaff and F. M. Rossi (2007). Local self-renewal can sustain CNS microglia maintenance and function throughout adult life. *Nat Neurosci* 10(12): 1538-1543.
- Akira, S., K. Takeda and T. Kaisho (2001). Toll-like receptors: critical proteins linking innate and acquired immunity. *Nat Immunol* 2(8): 675-680.
- Akira, S., S. Uematsu and O. Takeuchi (2006). Pathogen recognition and innate immunity. *Cell* 124(4): 783-801.
- Aminzadeh, M., Roghani, M., Sarfallah, A., & Riazi, G. H. (2018). TRPM2 dependence of ROS-induced NLRP3 activation in Alzheimer's disease. *International immunopharmacology*, 54, 78–85. <https://doi.org/10.1016/j.intimp.2017.10.024>
- Apostolova, L. G., S. L. Risacher, T. Duran, E. C. Stage, N. Goukasian, J. D. West, T. M. Do, J. Grotts, H. Wilhalme, K. Nho, M. Phillips, D. Elashoff, A. J. Saykin and I. Alzheimer's Disease Neuroimaging (2018). Associations of the Top 20 Alzheimer Disease Risk Variants With Brain Amyloidosis. *JAMA Neurol* 75(3): 328-341.
- Asai, H., S. Ikezu, S. Tsunoda, M. Medalla, J. Luebke, T. Haydar, B. Wolozin, O. Butovsky, S. Kugler and T. Ikezu (2015). Depletion of microglia and inhibition of exosome synthesis halt tau propagation. *Nat Neurosci* 18(11): 1584-1593.

-
- Aschenbrenner, A. J., B. A. Gordon, T. L. S. Benzinger, J. C. Morris and J. J. Hassenstab (2018). Influence of tau PET, amyloid PET, and hippocampal volume on cognition in Alzheimer disease. *Neurology* 91(9): e859-e866.
- Ballard, C., S. Gauthier, A. Corbett, C. Brayne, D. Aarsland and E. Jones (2011). Alzheimer's disease. *Lancet* 377(9770): 1019-1031.
- Baranello, R. J., K. L. Bharani, V. Padmaraju, N. Chopra, D. K. Lahiri, N. H. ...Pappolla and K. Sambamurti (2015). Amyloid-beta protein clearance and degradation (ABCD) pathways and their role in Alzheimer's disease. *Curr Alzheimer Res* 12(1): 32-46.
- Bayer, T. A., R. Cappai, C. L. Masters, K. Beyreuther and G. Multhaup (1999). It all sticks together--the APP-related family of proteins and Alzheimer's disease. *Mol Psychiatry* 4(6): 524-528.
- Bejanin, A., D. R. Schonhaut, R. La Joie, J. H. Kramer, S. L. Baker, N. Sosa, N. Ayakta, A. ... J. Jagust and G. D. Rabinovici (2017). Tau pathology and neurodegeneration contribute to cognitive impairment in Alzheimer's disease. *Brain* 140(12): 3286-3300.
- Bellia, F., V. Lanza, S. Garcia-Vinuales, I. M. M. Ahmed, A. Pietropaolo, C. Iacobucci, G. ... G. Grasso and D. Milardi (2019). Ubiquitin binds the amyloid beta peptide and interferes with its clearance pathways. *Chem Sci* 10(9): 2732-2742.
- Bennett, R. E., Robbins, A. B., Hu, M., Cao, X., Betensky, R. A., Clark, T., . . . Hyman, B. T. (2018). Tau induces blood vessel abnormalities and angiogenesis-related gene expression in P301L transgenic mice and human Alzheimer's disease. *Proc Natl Acad Sci U S A*, 115(6), E1289-E1298. doi:10.1073/pnas.1710329115.
- Berkowitz BA, Lenning J, Khetarpal N, et al. In vivo imaging of prodromal hippocampus CA1 subfield oxidative stress in models of Alzheimer disease and Angelman syndrome. *FASEB J*. 2017;31(9):4179-4186. doi:10.1096/fj.201700229R.
- Bintener C, M. o. (2020). Dementia in Europe Yearbook 2019: estimating the prevalence of dementia in Europe. *Alzheimer Europe*.
- Blum-Degen, D., Müller, T., Kuhn, W., Gerlach, M., Przuntek, H., & Riederer, P. (1995). Interleukin-1 beta and interleukin-6 are elevated in the cerebrospinal fluid of Alzheimer's and de novo Parkinson's disease patients. *Neuroscience letters*, 202(1-2), 17–20.

-
- Block, M. L., L. Zecca and J. S. Hong (2007). "Microglia-mediated neurotoxicity: uncovering the molecular mechanisms." *Nat Rev Neurosci* 8(1): 57-69.
- Bolmont, T., Haiss, F., Eicke, D., Radde, R., Mathis, C. A., Klunk, W. E., . . . Calhoun, M. E. (2008). Dynamics of the microglial/amyloid interaction indicate a role in plaque maintenance. *J Neurosci*, 28(16), 4283-4292. doi:10.1523/JNEUROSCI.4814-07.2008
- Bonacchi, A., Romagnani, P., Romanelli, R.G., Efsen, E., Annunziato, F., Lasagni, L., Francalanci, M., Serio, M., Laffi, G., Pinzani, M., Gentilini, P., Marra, F., 2001. Signal transduction by the chemokine receptor CXCR3: activation of Ras/ERK, Src, and phosphatidylinositol 3-kinase/Akt controls cell migration and proliferation in human vascular pericytes. *J Biol Chem* 276, 9945-9954.
- Boulay, A. C., Saubamea, B., Declèves, X., & Cohen-Salmon, M. (2015). Purification of Mouse Brain Vessels. *J Vis Exp*(105), e53208. doi:10.3791/53208
- Brandenburg, S., Muller, A., Turkowski, K., Radev, Y. T., Rot, S., Schmidt, C., . . . Vajkoczy, P. (2016). Resident microglia rather than peripheral macrophages promote vascularization in brain tumors and are source of alternative pro-angiogenic factors. *Acta Neuropathol*, 131(3), 365-378. doi:10.1007/s00401-015-1529-6
- Brown, G. C. and A. Vilalta (2015). How microglia kill neurons. *Brain Res* 1628(Pt B): 288-297.
- Bsibsi, M., R. Ravid, D. Gveric and J. M. van Noort (2002). Broad expression of Toll-like receptors in the human central nervous system. *J Neuropathol Exp Neurol* 61(11): 1013-1021.
- Buckley, R. F., B. Hanseeuw, A. P. Schultz, P. Vannini, S. L. Aghjayan, M. J. Properzi, J. D. Jackson, E. C. Mormino, D. M. Rentz, R. A. Sperling, K. A. Johnson and R. E. Amariglio (2017). Region-Specific Association of Subjective Cognitive Decline With Tauopathy Independent of Global beta-Amyloid Burden. *JAMA Neurol* 74(12): 1455-1463.
- Bulloj, A., M. C. Leal, E. I. Surace, X. Zhang, H. Xu, M. D. Ledesma, E. M. Castano and L. Morelli (2008). Detergent resistant membrane-associated IDE in brain tissue and cultured cells: Relevance to Abeta and insulin degradation. *Mol Neurodegener* 3: 22.
- Busche, M. A. and B. T. Hyman (2020). Synergy between amyloid-beta and tau in Alzheimer's disease. *Nat Neurosci* 23(10): 1183-1193.

-
- Byun, K., Y. Yoo, M. Son, J. Lee, G. B. Jeong, Y. M. Park, G. H. Salekdeh and B. Lee (2017). Advanced glycation end-products produced systemically and by macrophages: A common contributor to inflammation and degenerative diseases. *Pharmacol Ther* 177: 44-55.
- Cacace, R., K. Slegers and C. Van Broeckhoven (2016). Molecular genetics of early-onset Alzheimer's disease revisited. *Alzheimers Dement* 12(6): 733-748.
- Cameron, B., W. Tse, R. Lamb, X. Li, B. T. Lamb and G. E. Landreth (2012). Loss of interleukin receptor-associated kinase 4 signaling suppresses amyloid pathology and alters microglial phenotype in a mouse model of Alzheimer's disease. *J Neurosci* 32(43): 15112-15123.
- Capiralla, H., V. Vingthdeux, H. Zhao, R. Sankowski, Y. Al-Abed, P. Davies and P. Marambaud (2012). Resveratrol mitigates lipopolysaccharide- and Abeta-mediated microglial inflammation by inhibiting the TLR4/NF-kappaB/STAT signaling cascade. *J Neurochem* 120(3): 461-472.
- Chen, K., P. Iribarren, J. Hu, J. Chen, W. Gong, E. H. Cho, S. Lockett, N. M. Dunlop and J. M. Wang (2006). Activation of Toll-like receptor 2 on microglia promotes cell uptake of Alzheimer disease-associated amyloid beta peptide. *J Biol Chem* 281(6): 3651-3659.
- Chen, Z. and B. D. Trapp (2016). Microglia and neuroprotection. *J Neurochem* 136 Suppl1:10-17.
- Cole, S. L. and R. Vassar (2007). The Alzheimer's disease beta-secretase enzyme, BACE1. *Mol Neurodegener* 2: 22.
- Colton, C. A., Mott, R. T., Sharpe, H., Xu, Q., Van Nostrand, W. E., & Vitek, M. P. (2006). Expression profiles for macrophage alternative activation genes in AD and in mouse models of AD. *J Neuroinflammation*, 3, 27. doi:10.1186/1742-2094-3-27
- Condello, C., P. Yuan, A. Schain and J. Grutzendler (2015). Microglia constitute a barrier that prevents neurotoxic protofibrillar Abeta42 hotspots around plaques. *Nat Commun* 6: 6176.
- Congdon, E. E. and E. M. Sigurdsson (2018). Tau-targeting therapies for Alzheimer disease. *Nat Rev Neurol* 14(7): 399-415.
- Corrada, M. M., R. Brookmeyer, A. Paganini-Hill, D. Berlau and C. H. Kawas (2010). Dementia incidence continues to increase with age in the oldest old: the 90+ study. *Ann Neurol* 67(1): 114-121.

-
- Cortes-Canteli, M. and C. Iadecola (2020). Alzheimer's Disease and Vascular Aging: JACC Focus Seminar. *J Am Coll Cardiol* 75(8): 942-951.
- Costello, D. A., D. G. Carney and M. A. Lynch (2015). alpha-TLR2 antibody attenuates the Abeta-mediated inflammatory response in microglia through enhanced expression of SIGIRR. *Brain Behav Immun* 46: 70-79.
- Da Mesquita S, Fu Z, Kipnis J. The Meningeal Lymphatic System: A New Player in Neurophysiology. *Neuron*. 2018;100(2):375-388. doi:10.1016/j.neuron.2018.09.022.
- Da Mesquita, S., A. Louveau, A. Vaccari, I. Smirnov, R. C. Cornelison, K. M. Kingsmore, ...S. T. Acton and J. Kipnis (2018). Functional aspects of meningeal lymphatics in ageing and Alzheimer's disease. *Nature* 560(7717): 185-191.
- Dai, J., Peng, L., Fan, K., Wang, H., Wei, R., Ji, G., . . . Guo, Y. (2009). Osteopontin induces angiogenesis through activation of PI3K/AKT and ERK1/2 in endothelial cells. *Oncogene*, 28(38), 3412-3422. doi:10.1038/onc.2009.189.
- de Bruijn, R. F., J. Heeringa, F. J. Wolters, O. H. Franco, B. H. Stricker, A. Hofman, P. J. Koudstaal and M. A. Ikram (2015). Association Between Atrial Fibrillation and Dementia in the General Population. *JAMA Neurol* 72(11): 1288-1294.
- De Roeck, A., C. Van Broeckhoven and K. Sleegers (2019). The role of ABCA7 in Alzheimer's disease: evidence from genomics, transcriptomics and methylomics. *Acta Neuropathol* 138(2): 201-220.
- Deane, R., I. Singh, A. P. Sagare, R. D. Bell, N. T. Ross, B. LaRue, R. Love, ..., B. L. Miller and B. V. Zlokovic (2012). A multimodal RAGE-specific inhibitor reduces amyloid beta-mediated brain disorder in a mouse model of Alzheimer disease. *J Clin Invest* 122(4): 1377-1392.
- Decker, Y., Muller, A., Nemeth, E., Schulz-Schaeffer, W. J., Fatar, M., Menger, M. D., . . . Fassbender, K.(2018). Analysis of the vasculature by immunohistochemistry in paraffin-embedded brains. *Brain Struct Funct*, 223(2), 1001-1015.
- DeTure, M. A., & Dickson, D. W. (2019). The neuropathological diagnosis of Alzheimer's disease. *Molecular neurodegeneration*, 14(1), 32.

-
- De Luca C, Colangelo AM, Alberghina L, Papa M. Neuro-Immune Hemostasis: Homeostasis and Diseases in the Central Nervous System. *Front Cell Neurosci.* 2018;12:459. Published 2018 Nov 26. doi:10.3389/fncel.2018.00459.
- Dempsey, C., Rubio Araiz, A., Bryson, K.J., Finucane, O., Larkin, C., Mills, E.L., Robertson, A.A.B., Cooper, M.A., O'Neill, L.A.J., Lynch, M.A., 2017. Inhibiting the NLRP3 inflammasome with MCC950 promotes non-phlogistic clearance of amyloid-beta and cognitive function in APP/PS1 mice. *Brain Behav Immun* 61, 306-316.
- dos Santos, G., Kutuzov, M. A., & Ridge, K. M. (2012). The inflammasome in lung diseases. *American journal of physiology. Lung cellular and molecular physiology*, 303(8), L627–L633.
- DeVos, S. L., R. L. Miller, K. M. Schoch, B. B. Holmes, C. S. Kebodeaux, A. J. ... M. I. Diamond and T. M. Miller (2017). Tau reduction prevents neuronal loss and reverses pathological tau deposition and seeding in mice with tauopathy. *Sci Transl Med* 9(374).
- Eftekharzadeh, B., J. G. Daigle, L. E. Kapinos, A. Coyne, J. Schiantarelli, Y. Carlomagno, C. ...J. D. Rothstein and B. T. Hyman (2018). Tau Protein Disrupts Nucleocytoplasmic Transport in Alzheimer's Disease. *Neuron* 99(5): 925-940 e927.
- Engelhardt, B., R. O. Carare, I. Bechmann, A. Flugel, J. D. Laman and R. O. Weller (2016). "Vascular, glial, and lymphatic immune gateways of the central nervous system." *Acta Neuropathol* 132(3): 317-338.
- Erickson, M. A., Hansen, K., & Banks, W. A. (2012). Inflammation-induced dysfunction of the low-density lipoprotein receptor-related protein-1 at the blood-brain barrier: protection by the antioxidant N-acetylcysteine. *Brain Behav Immun*, 26(7), 1085-1094. doi:10.1016/j.bbi.2012.07.003
- Ewers, M., N. Franzmeier, M. Suarez-Calvet, E. Morenas-Rodriguez, M. A. A. Caballero, G. ... C. Haass and I. Alzheimer's Disease Neuroimaging (2019). Increased soluble TREM2 in cerebrospinal fluid is associated with reduced cognitive and clinical decline in Alzheimer's disease. *Sci Transl Med* 11(507).
- Fan, Z., A. A. Okello, D. J. Brooks and P. Edison (2015). Longitudinal influence of microglial activation and amyloid on neuronal function in Alzheimer's disease. *Brain* 138(Pt 12): 3685-3698.

-
- Farris, W., S. Mansourian, Y. Chang, L. Lindsley, E. A. Eckman, M. P. Frosch, C. B. Eckman, R. E. Tanzi, D. J. Selkoe and S. Guenette (2003). Insulin-degrading enzyme regulates the levels of insulin, amyloid beta-protein, and the beta-amyloid precursor protein intracellular domain in vivo. *Proc Natl Acad Sci U S A* 100(7): 4162-4167.
- figures, A. s. d. f. a. (2019). "2019 Alzheimer's disease facts and figures." *Alzheimer's & Dementia* 15(3): 321-387.
- figures, A. s. d. f. a. (2020). "2020 Alzheimer's disease facts and figures." *Alzheimers Dement*.
- Fernandez-Klett, F., Brandt, L., Fernandez-Zapata, C., Abuelnor, B., Middeldorp, J., Sluijs, J. A., . . . Priller, J. (2020). Denser brain capillary network with preserved pericytes in Alzheimer's disease. *Brain Pathol*, 30(6), 1071-1086. doi:10.1111/bpa.12897
- Freeman, L. C., & Ting, J. P. (2016). The pathogenic role of the inflammasome in neurodegenerative diseases. *Journal of neurochemistry*, 136 Suppl 1, 29–38. <https://doi.org/10.1111/jnc.13217>
- Focke, C., Blume, T., Zott, B., Shi, Y., Deussing, M., Peters, F., . . . Brendel, M. (2018). Early and longitudinal microglial activation but not amyloid accumulation predict cognitive outcome in PS2APP mice. *J Nucl Med*. doi:10.2967/jnumed.118.217703
- Gasparini, L. and H. Xu (2003). "Potential roles of insulin and IGF-1 in Alzheimer's disease." *Trends Neurosci* 26(8): 404-406.
- Gil-Martins, E., D. J. Barbosa, V. Silva, F. Remiao and R. Silva (2020). Dysfunction of ABC transporters at the blood-brain barrier: Role in neurological disorders. *Pharmacol Ther* 213: 107554.
- Ginhoux, F., M. Greter, M. Leboeuf, S. Nandi, P. See, S. Gokhan, M. F. Mehler, ...I. M. Samokhvalov and M. Merad (2010). Fate mapping analysis reveals that adult microglia derive from primitive macrophages. *Science* 330(6005): 841-845.
- Ginhoux, F., S. Lim, G. Hoeffel, D. Low and T. Huber (2013). "Origin and differentiation of microglia." *Front Cell Neurosci* 7: 45.
- Gjoneska, E., A. R. Pfenning, H. Mathys, G. Quon, A. Kundaje, L. H. Tsai and M. Kellis (2015). Conserved epigenomic signals in mice and humans reveal immune basis of Alzheimer's disease. *Nature* 518(7539): 365-369.

-
- Gogoleva, V. S., M. S. Drutskaya and K. S. N. Atretkhany (2019). "The Role of Microglia in the Homeostasis of the Central Nervous System and Neuroinflammation." *Molecular Biology* 53(5): 696-703.
- Gomez-Isla, T., R. Hollister, H. West, S. Mui, J. H. Growdon, R. C. Petersen, J. E. Parisi and B. T. Hyman (1997). Neuronal loss correlates with but exceeds neurofibrillary tangles in Alzheimer's disease. *Ann Neurol* 41(1): 17-24.
- Gong, C. X. and K. Iqbal (2008). Hyperphosphorylation of microtubule-associated protein tau: a promising therapeutic target for Alzheimer disease. *Curr Med Chem* 15(23): 2321-2328.
- Gosselin, D. and S. Rivest (2008). "MyD88 signaling in brain endothelial cells is essential for the neuronal activity and glucocorticoid release during systemic inflammation." *Mol Psychiatry* 13(5): 480-497.
- Guerreiro, R., A. Wojtas, J. Bras, M. Carrasquillo, E. Rogaeva, E. Majounie, C. Cruchaga, C. ... J. Hardy and G. Alzheimer Genetic Analysis (2013). "TREM2 variants in Alzheimer's disease." *N Engl J Med* 368(2): 117-127.
- Goldmann, T., Wieghofer, P., Muller, P. F., Wolf, Y., Varol, D., Yona, S., . . . Prinz, M. (2013). A new type of microglia gene targeting shows TAK1 to be pivotal in CNS autoimmune inflammation. *Nat Neurosci*, 16(11), 1618-1626. doi:10.1038/nn.3531.
- Goodman JR, Adham ZO, Woltjer RL, Lund AW, Iliff JJ. Characterization of dural sinus-associated lymphatic vasculature in human Alzheimer's dementia subjects. *Brain Behav Immun*. 2018;73:34-40. doi:10.1016/j.bbi.2018.07.020.
- Gonzalez-Prieto, M., Gutierrez, I. L., Garcia-Bueno, B., Caso, J. R., Leza, J. C., Ortega-Hernandez, A., . . . Madrigal, J. L. M. (2021). Microglial CX3CR1 production increases in Alzheimer's disease and is regulated by noradrenaline. *Glia*, 69(1), 73-90. doi:10.1002/glia.23885
- Gosselin, D., & Rivest, S. (2008). MyD88 signaling in brain endothelial cells is essential for the neuronal activity and glucocorticoid release during systemic inflammation. *Mol Psychiatry*, 13(5), 480-497. doi:10.1038/sj.mp.4002122
- Halle, A., Hornung, V., Petzold, G. C., Stewart, C. R., Monks, B. G., Reinheckel, T., Fitzgerald, K. A., Latz, E., Moore, K. J., & Golenbock, D. T. (2008). The NALP3 inflammasome is involved in the innate immune response to amyloid-beta. *Nature immunology*, 9(8), 857–865. <https://doi.org/10.1038/ni.1636>

-
- Halliday, M. R., S. V. Rege, Q. Ma, Z. Zhao, C. A. Miller, E. A. Winkler and B. V. Zlokovic (2016). "Accelerated pericyte degeneration and blood-brain barrier breakdown in apolipoprotein E4 carriers with Alzheimer's disease." *J Cereb Blood Flow Metab* 36(1): 216-227.
- Hao, W., Liu, Y., Liu, S., Walter, S., Grimm, M. O., Kiliaan, A. J., . . . Fassbender, K. (2011). Myeloid differentiation factor 88-deficient bone marrow cells improve Alzheimer's disease-related symptoms and pathology. *Brain*, 134(Pt 1), 278-292. doi:10.1093/brain/awq325
- Haruwaka, K., Ikegami, A., Tachibana, Y., Ohno, N., Konishi, H., Hashimoto, A., . . . Wake, H. (2019). Dual microglia effects on blood brain barrier permeability induced by systemic inflammation. *Nat Commun*, 10(1), 5816. doi:10.1038/s41467-019-13812-z.
- Harold D, Abraham R, Hollingworth P, et al. Genome-wide association study identifies variants at *CLU* and *PICALM* associated with Alzheimer's disease [published correction appears in *Nat Genet*. 2009 Oct;41(10):1156] [published correction appears in *Nat Genet*. 2013 Jun;45(6):712. Haun, Reinhard [added]]. *Nat Genet*. 2009;41(10):1088-1093. doi:10.1038/ng.440.
- He, Z., J. L. Guo, J. D. McBride, S. Narasimhan, H. Kim, L. Changolkar, B. Zhang, R. J. Gathagan, C. Yue, C. Dengler, A. Stieber, M. Nitla, D. A. Coulter, T. Abel, K. R. Brunden, J. Q. Trojanowski and V. M. Lee (2018). "Amyloid-beta plaques enhance Alzheimer's brain tau-seeded pathologies by facilitating neuritic plaque tau aggregation." *Nat Med* 24(1): 29-38.
- He JT, Zhao X, Xu L, Mao CY. Vascular Risk Factors and Alzheimer's Disease: Blood-Brain Barrier Disruption, Metabolic Syndromes, and Molecular Links. *J Alzheimers Dis*. 2020;73(1):39-58. doi:10.3233/JAD-190764.
- Heneka, M. T., Carson, M. J., El Khoury, J., Landreth, G. E., Brosseron, F., Feinstein, D. L., ... Kummer, M. P. (2015). Neuroinflammation in Alzheimer's disease. *Lancet Neurol*, 14(4), 388-405. doi:10.1016/S1474-4422(15)70016-5
- Heneka, M. T., Kummer, M. P., & Latz, E. (2014). Innate immune activation in neurodegenerative disease. *Nature reviews. Immunology*, 14(7), 463–477. <https://doi.org/10.1038/nri3705>

-
- Heneka, M. T., Golenbock, D. T., & Latz, E. (2015). Innate immunity in Alzheimer's disease. *Nature immunology*, 16(3), 229–236. <https://doi.org/10.1038/ni.3102>
- Heneka, M. T., Kummer, M. P., Stutz, A., Delekate, A., Schwartz, S., Vieira-Saecker, A., ... Golenbock, D. T. (2013). NLRP3 is activated in Alzheimer's disease and contributes to pathology in APP/PS1 mice. *Nature*, 493(7434), 674-678. doi:10.1038/nature11729
- Hickman, S. E., Allison, E. K., Coleman, U., Kingery-Gallagher, N. D., & El Khoury, J. (2019). Heterozygous CX3CR1 Deficiency in Microglia Restores Neuronal beta-Amyloid Clearance Pathways and Slows Progression of Alzheimer's Like-Disease in PS1-APP Mice. *Front Immunol*, 10, 2780. doi:10.3389/fimmu.2019.02780
- Holbrook JA, Jarosz-Griffiths HH, Caseley E, et al. Neurodegenerative Disease and the NLRP3 Inflammasome. *Front Pharmacol*. 2021;12:643254. Published 2021 Mar 10. doi:10.3389/fphar.2021.643254
- Hoover, B. R., M. N. Reed, J. Su, R. D. Penrod, L. A. Kotilinek, M. K. Grant, R. Pitstick, G. A. Carlson, L. M. Lanier, L. L. Yuan, K. H. Ashe and D. Liao (2010). "Tau mislocalization to dendritic spines mediates synaptic dysfunction independently of neurodegeneration." *Neuron* 68(6): 1067-1081.
- Hou, B., Reizis, B., & DeFranco, A. L. (2008). Toll-like receptors activate innate and adaptive immunity by using dendritic cell-intrinsic and -extrinsic mechanisms. *Immunity*, 29(2), 272-282. doi:10.1016/j.immuni.2008.05.016
- Huang, C., Dong, D., Jiao, Q., Pan, H., Ma, L., & Wang, R. (2017). Sarsasapogenin-AA13 ameliorates A β -induced cognitive deficits via improving neuroglial capacity on A β clearance and antiinflammation. *CNS neuroscience & therapeutics*, 23(6), 498–509. <https://doi.org/10.1111/cns.12697>
- Hughes, C., M. L. Choi, J. H. Yi, S. C. Kim, A. Drews, P. S. George-Hyslop, C. Bryant, S. Gandhi, K. Cho and D. Klenerman (2020). "Beta amyloid aggregates induce sensitised TLR4 signalling causing long-term potentiation deficit and rat neuronal cell death." *Commun Biol* 3(1): 79.
- Hung, Y. F., C. Y. Chen, Y. C. Shih, H. Y. Liu, C. M. Huang and Y. P. Hsueh (2018). "Endosomal TLR3, TLR7, and TLR8 control neuronal morphology through different transcriptional programs." *J Cell Biol* 217(8): 2727-2742.

-
- Hyman, B. T., G. W. Van Hoesen, A. R. Damasio and C. L. Barnes (1984). "Alzheimer's disease: cell-specific pathology isolates the hippocampal formation." *Science* 225(4667): 1168-1170.
- Hsu, H. W., Rodriguez-Ortiz, C. J., Zumkehr, J., & Kitazawa, M. (2021). Inflammatory Cytokine IL-1beta Downregulates Endothelial LRP1 via MicroRNA-mediated Gene Silencing. *Neuroscience*, 453, 69-80. doi:10.1016/j.neuroscience.2020.11.021
- Jacobs, H. I. L., T. Hedden, A. P. Schultz, J. Sepulcre, R. D. Perea, R. E. Amariglio, K. V. Papp, D. M. Rentz, R. A. Sperling and K. A. Johnson (2018). "Structural tract alterations predict downstream tau accumulation in amyloid-positive older individuals." *Nat Neurosci* 21(3): 424-431.
- Jay, T. R., Hirsch, A. M., Broihier, M. L., Miller, C. M., Neilson, L. E., Ransohoff, R. M., . . . Landreth, G. E. (2017). Disease Progression-Dependent Effects of TREM2 Deficiency in a Mouse Model of Alzheimer's Disease. *J Neurosci*, 37(3), 637-647.
- Jay, T. R., Miller, C. M., Cheng, P. J., Graham, L. C., Bemiller, S., Broihier, M. L., . . . Lamb, B. T. (2015). TREM2 deficiency eliminates TREM2+ inflammatory macrophages and ameliorates pathology in Alzheimer's disease mouse models. *J Exp Med*, 212(3), 287-295. doi:10.1084/jem.20142322
- Jiang, L., Mu, H., Xu, F., Xie, D., Su, W., Xu, J., . . . Hu, X. (2020). Transcriptomic and functional studies reveal undermined chemotactic and angiostimulatory properties of aged microglia during stroke recovery. *J Cereb Blood Flow Metab*, 40(1_suppl), S81-S97. doi:10.1177/0271678X20902542
- Jiang, T., J. T. Yu, N. Hu, M. S. Tan, X. C. Zhu and L. Tan (2014). "CD33 in Alzheimer's disease." *Mol Neurobiol* 49(1): 529-535.
- Kang, J. and S. Rivest (2007). "MyD88-deficient bone marrow cells accelerate onset and reduce survival in a mouse model of amyotrophic lateral sclerosis." *J Cell Biol* 179(6): 1219-1230.
- Kawai, T. and S. Akira (2010). "The role of pattern-recognition receptors in innate immunity: update on Toll-like receptors." *Nat Immunol* 11(5): 373-384.
- Keller, J. N., K. B. Hanni and W. R. Markesbery (2000). "Impaired proteasome function in Alzheimer's disease." *J Neurochem* 75(1): 436-439.

-
- Keren-Shaul, H., A. Spinrad, A. Weiner, O. Matcovitch-Natan, R. Dvir-Szternfeld, T. K. Ulland, E. David, K. Baruch, D. Lara-Astaiso, B. Toth, S. Itzkovitz, M. Colonna, M. Schwartz and I. Amit (2017). "A Unique Microglia Type Associated with Restricting Development of Alzheimer's Disease." *Cell* 169(7): 1276-1290 e1217.
- Kleinberger, G., Y. Yamanishi, M. Suarez-Calvet, E. Czirr, E. Lohmann, E. Cuyvers, H. Struyfs, N. Pettkus, ... M. Colonna and C. Haass (2014). "TREM2 mutations implicated in neurodegeneration impair cell surface transport and phagocytosis." *Sci Transl Med* 6(243): 243ra286.
- Koenigsknecht-Talboo, J., & Landreth, G. E. (2005). Microglial phagocytosis induced by fibrillar beta-amyloid and IgGs are differentially regulated by proinflammatory cytokines. *J Neurosci*, 25(36), 8240-8249. doi:10.1523/JNEUROSCI.1808-05.2005
- Krasemann, S., Madore, C., Cialic, R., Baufeld, C., Calcagno, N., El Fatimy, R., . . . Butovsky, O. (2017). The TREM2-APOE Pathway Drives the Transcriptional Phenotype of Dysfunctional Microglia in Neurodegenerative Diseases. *Immunity*, 47(3), 566-581 e569. doi:10.1016/j.immuni.2017.08.008
- Kuhnke, D., Jedlitschky, G., Grube, M., Krohn, M., Jucker, M., Mosyagin, I., . . . Vogelgesang, (2007). MDR1-P-Glycoprotein (ABCB1) Mediates Transport of Alzheimer's amyloid-beta peptides--implications for the mechanisms of Abeta clearance at the blood-brain barrier. *Brain Pathol*, 17(4), 347-353. doi:10.1111/j.1750-3639.2007.00075.x
- Labzin, L. I., M. T. Heneka and E. Latz (2018). "Innate Immunity and Neurodegeneration." *Annu Rev Med* 69: 437-449.
- Leaf, I.A., Nakagawa, S., Johnson, B.G., Cha, J.J., Mittelsteadt, K., Guckian, K.M., Gomez, I.G., Altemeier, W.A., Duffield, J.S., 2017. Pericyte MyD88 and IRAK4 control inflammatory and fibrotic responses to tissue injury. *J Clin Invest* 127, 321-334.
- Lee, C. Y. D., A. Daggett, X. Gu, L. L. Jiang, P. Langfelder, X. Li, N. Wang, Y. Zhao, C. S. Park, Y. Cooper, I. Ferando, I. Mody, G. Coppola, H. Xu and X. W. Yang (2018). "Elevated TREM2 Gene Dosage Reprograms Microglia Responsivity and Ameliorates Pathological Phenotypes in Alzheimer's Disease Models." *Neuron* 97(5): 1032-1048 e1035.

-
- Lee, S., Varvel, N. H., Konerth, M. E., Xu, G., Cardona, A. E., Ransohoff, R. M., & Lamb, B. (2010). CX3CR1 deficiency alters microglial activation and reduces beta-amyloid deposition in two Alzheimer's disease mouse models. *Am J Pathol*, 177(5), 2549-2562. doi:10.2353/ajpath.2010.100265
- Lee, Y. J., Han, S. B., Nam, S. Y., Oh, K. W., & Hong, J. T. (2010). Inflammation and Alzheimer's disease. *Archives of pharmacal research*, 33(10), 1539–1556.
- Leissring, M. A. (2016). "Abeta-Degrading Proteases: Therapeutic Potential in Alzheimer Disease." *CNS Drugs* 30(8): 667-675.
- Letiembre, M., Y. Liu, S. Walter, W. Hao, T. Pfander, A. Wrede, W. Schulz-Schaeffer and K. Fassbender (2009). "Screening of innate immune receptors in neurodegenerative diseases: a similar pattern." *Neurobiol Aging* 30(5): 759-768.
- Lehti, K., Allen, E., Birkedal-Hansen, H., Holmbeck, K., Miyake, Y., Chun, T.H., Weiss, S.J., 2005. An MT1-MMP-PDGF receptor-beta axis regulates mural cell investment of the microvasculature. *Genes Dev* 19, 979-991.
- Liebner, S., R. M. Dijkhuizen, Y. Reiss, K. H. Plate, D. Agalliu and G. Constantin (2018). "Functional morphology of the blood-brain barrier in health and disease." *Acta Neuropathol* 135(3): 311-336.
- Lewcock, J. W., Schlepckow, K., Di Paolo, G., Tahirovic, S., Monroe, K. M., & Haass, C. (2020). Emerging Microglia Biology Defines Novel Therapeutic Approaches for Alzheimer's Disease. *Neuron*. doi:10.1016/j.neuron.2020.09.029
- Lim, J. E., Kou, J., Song, M., Pattanayak, A., Jin, J., Lalonde, R., & Fukuchi, K. (2011). MyD88 deficiency ameliorates beta-amyloidosis in an animal model of Alzheimer's disease. *Am J Pathol*, 179(3), 1095-1103. doi:10.1016/j.ajpath.2011.05.045
- Lindahl, P., Johansson, B. R., Leveen, P., & Betsholtz, C. (1997). Pericyte loss and microaneurysm formation in PDGF-B-deficient mice. *Science*, 277(5323), 242-245.
- Liu Q, Yan L, Huang M, et al. Experimental alcoholism primes structural and functional impairment of the glymphatic pathway. *Brain Behav Immun*. 2020;85:106-119. doi:10.1016/j.bbi.2019.06.029.

-
- Liu, S., Liu, Y., Hao, W., Wolf, L., Kiliaan, A. J., Penke, B., . . . Fassbender, K. (2012). TLR2 is a primary receptor for Alzheimer's amyloid beta peptide to trigger neuroinflammatory activation. *J Immunol*, 188(3), 1098-1107. doi:10.4049/jimmunol.1101121.
- Liu, Y., Liu, X., Hao, W., Decker, Y., Schomburg, R., Fulop, L., . . . Fassbender, K. (2014). IKKbeta deficiency in myeloid cells ameliorates Alzheimer's disease-related symptoms and pathology. *J Neurosci*, 34(39), 12982-12999. doi:10.1523/JNEUROSCI.1348-14.2014.
- Liu, Z., Condello, C., Schain, A., Harb, R., & Grutzendler, J. (2010). CX3CR1 in microglia regulates brain amyloid deposition through selective protofibrillar amyloid-beta phagocytosis. *J Neurosci*, 30(50), 17091-17101. doi:10.1523/JNEUROSCI.4403-10.2010
- Long, J. M. and D. M. Holtzman (2019). "Alzheimer Disease: An Update on Pathobiology and Treatment Strategies." *Cell* 179(2): 312-339.
- Love, S., Miners, J.S., 2016. Cerebrovascular disease in ageing and Alzheimer's disease. *Acta Neuropathol* 131, 645-658.
- Louveau A, Plog BA, Antila S, Alitalo K, Nedergaard M, Kipnis J. Understanding the functions and relationships of the glymphatic system and meningeal lymphatics. *J Clin Invest*. 2017;127(9):3210-3219. doi:10.1172/JCI90603.
- Ma, Q., Zhao, Z., Sagare, A. P., Wu, Y., Wang, M., Owens, N. C., . . . Zlokovic, B. V. (2018). Blood-brain barrier-associated pericytes internalize and clear aggregated amyloid-beta42 by LRP1-dependent apolipoprotein E isoform-specific mechanism. *Mol Neurodegener*, 13(1), 57. doi:10.1186/s13024-018-0286-0.
- Maiuolo J, Gliozzi M, Musolino V, et al. The "Frail" Brain Blood Barrier in Neurodegenerative Diseases: Role of Early Disruption of Endothelial Cell-to-Cell Connections. *Int J Mol Sci*. 2018;19(9):2693. Published 2018 Sep 10. doi:10.3390/ijms19092693.
- Manning, B.D., Cantley, L.C., 2007. AKT/PKB signaling: navigating downstream. *Cell* 129, 1261-1274.
- Martinon, F., Petrilli, V., Mayor, A., Tardivel, A., Tschopp, J., 2006. Gout-associated uric acid crystals activate the NALP3 inflammasome. *Nature* 440, 237-241.

-
- Massey, A. C., S. Kaushik, G. Sovak, R. Kiffin and A. M. Cuervo (2006). "Consequences of the selective blockage of chaperone-mediated autophagy." *Proc Natl Acad Sci U S A* 103(15): 5805-5810.
- Masters, C. L., G. Multhaup, G. Simms, J. Pottgiesser, R. N. Martins and K. Beyreuther (1985). "Neuronal origin of a cerebral amyloid: neurofibrillary tangles of Alzheimer's disease contain the same protein as the amyloid of plaque cores and blood vessels." *EMBO J* 4(11): 2757-2763.
- Mastorakos, P., Mihelson, N., Luby, M., Burks, S. R., Johnson, K., Hsia, A. W., . . . McGavern, D. B. (2021). Temporally distinct myeloid cell responses mediate damage and repair after cerebrovascular injury. *Nat Neurosci*, 24(2), 245-258. doi:10.1038/s41593-020-00773-6
- McDermott, J. R. and A. M. Gibson (1997). "Degradation of Alzheimer's beta-amyloid protein by human and rat brain peptidases: involvement of insulin-degrading enzyme." *Neurochem Res* 22(1): 49-56.
- McKhann, G. M. (2011). "Changing concepts of Alzheimer disease." *JAMA* 305(23): 2458-2459.
- Meyer-Luehmann, M., Spiess-Jones, T. L., Prada, C., Garcia-Alloza, M., de Calignon, A., Rozkalne, A., Hyman, B. T. (2008). Rapid appearance and local toxicity of amyloid-beta plaques in a mouse model of Alzheimer's disease. *Nature*, 451(7179), 720-724.
- Mhatre, S. D., C. A. Tsai, A. J. Rubin, M. L. James and K. I. Andreasson (2015). "Microglial malfunction: the third rail in the development of Alzheimer's disease." *Trends Neurosci* 38(10): 621-636.
- Michaud, J. P., Halle, M., Lampron, A., Theriault, P., Prefontaine, P., Filali, M., . . . Rivest, S. (2013). Toll-like receptor 4 stimulation with the detoxified ligand monophosphoryl lipid A improves Alzheimer's disease-related pathology. *Proc Natl Acad Sci U S A*, 110(5), 1941-1946. doi:10.1073/pnas.1215165110
- Michaud, J. P., Richard, K. L., & Rivest, S. (2011). MyD88-adaptor protein acts as a preventive mechanism for memory deficits in a mouse model of Alzheimer's disease. *Mol Neurodegener*, 6(1), 5. doi:10.1186/1750-1326-6-5
- Michaud, J. P., Richard, K. L., & Rivest, S. (2012). Hematopoietic MyD88-adaptor protein acts as a natural defense mechanism for cognitive deficits in Alzheimer's disease. *Stem Cell Rev Rep*, 8(3), 898-904. doi:10.1007/s12015-012-9356-9

-
- Miller, D. S. (2015). "Regulation of ABC transporters blood-brain barrier: the good, the bad, and the ugly." *Adv Cancer Res* 125: 43-70.
- Miners, J. S., S. Baig, J. Palmer, L. E. Palmer, P. G. Kehoe and S. Love (2008). "Abeta-degrading enzymes in Alzheimer's disease." *Brain Pathol* 18(2): 240-252.
- Montagne, A., Nation, D. A., Sagare, A. P., Barisano, G., Sweeney, M. D., Chakhoyan, A., . . . Zlokovic, B. V. (2020). APOE4 leads to blood-brain barrier dysfunction predicting cognitive decline. *Nature*, 581(7806), 71-76. doi:10.1038/s41586-020-2247-3.
- Montagne A, Barnes SR, Sweeney MD, et al. Blood-brain barrier breakdown in the aging human hippocampus. *Neuron*. 2015;85(2):296-302. doi:10.1016/j.neuron.2014.12.032.
- Montagne, A., Nikolakopoulou, A. M., Zhao, Z., Sagare, A. P., Si, G., Lazic, D., . . . Zlokovic, B. V. (2018). Pericyte degeneration causes white matter dysfunction in the mouse central nervous system. *Nat Med*, 24(3), 326-337. doi:10.1038/nm.4482.
- Mucke, L., & Selkoe, D. J. (2012). Neurotoxicity of amyloid beta-protein: synaptic and network dysfunction. *Cold Spring Harb Perspect Med*, 2(7), a006338.
- Naert, G., N. Laflamme and S. Rivest (2009). "Toll-like receptor 2-independent and MyD88-dependent gene expression in the mouse brain." *J Innate Immun* 1(5): 480-493.
- Natale G, Limanaqi F, Busceti CL, et al. Glymphatic System as a Gateway to Connect Neurodegeneration From Periphery to CNS. *Front Neurosci*. 2021;15:639140. Published 2021 Feb 9. doi:10.3389/fnins.2021.639140.
- Nation, D. A., Sweeney, M. D., Montagne, A., Sagare, A. P., D'Orazio, L. M., Pachicano, M.,... Zlokovic, B. V. (2019). Blood-brain barrier breakdown is an early biomarker of human cognitive dysfunction. *Nat Med*, 25(2), 270-276. doi:10.1038/s41591-018-0297- y.
- Nilsson, P., K. Loganathan, M. Sekiguchi, Y. Matsuba, K. Hui, S. Tsubuki, M. Tanaka, N. Iwata, T. Saito and T. C. Saido (2013). "Abeta secretion and plaque formation depend on autophagy." *Cell Rep* 5(1): 61-69.
- Nixon, R. A. and D. S. Yang (2011). "Autophagy failure in Alzheimer's disease--locating the primary defect." *Neurobiol Dis* 43(1): 38-45.

-
- Nortley, R., N. Korte, P. Izquierdo, C. Hirunpattarasilp, A. Mishra, Z. Jaunmuktane, V. Kyrargyri, T. Pfeiffer, L. Khenouf, C. Madry, H. Gong, A. Richard-Loendt, W. Huang, T. Saito, T. C. Saido, S. Brandner, H. Sethi and D. Attwell (2019). "Amyloid beta oligomers constrict human capillaries in Alzheimer's disease via signaling to pericytes." *Science* 365(6450).
- Nyul-Toth, A., Kozma, M., Nagyoszi, P., Nagy, K., Fazakas, C., Hasko, J., Molnar, K., Farkas, A.E., Vegh, A.G., Varo, G., Galajda, P., Wilhelm, I., Krizbai, I.A., 2017. Expression of pattern recognition receptors and activation of the non-canonical inflammasome pathway in brain pericytes. *Brain Behav Immun* 64, 220-231.
- O'Neill, L. A., D. Golenbock and A. G. Bowie (2013). "The history of Toll-like receptors - redefining innate immunity." *Nat Rev Immunol* 13(6): 453-460.
- Parhizkar, S., Arzberger, T., Brendel, M., Kleinberger, G., Deussing, M., Focke, C., . . . Haass, (2019). Loss of TREM2 function increases amyloid seeding but reduces plaque-associated ApoE. *Nat Neurosci*. doi:10.1038/s41593-018-0296-9
- Park, L., Uekawa, K., Garcia-Bonilla, L., Koizumi, K., Murphy, M., Pistik, R., ... Iadecola, C. (2017). Brain Perivascular Macrophages Initiate the Neurovascular Dysfunction of Alzheimer Abeta Peptides. *Circ Res*, 121(3), 258-269. doi:10.1161/CIRCRESAHA.117.311054
- Pooler, A. M., M. Polydoro, E. A. Maury, S. B. Nicholls, S. M. Reddy, S. Wegmann, C. William, L. Saqran, O. Cagsal-Getkin, R. Pitstick, D. R. Beier, G. A. Carlson, T. L. Spires-Jones and B. T. Hyman (2015). "Amyloid accelerates tau propagation and toxicity in a model of early Alzheimer's disease." *Acta Neuropathol Commun* 3: 14.
- Qin, Y., Liu, Y., Hao, W., Decker, Y., Tomic, I., Menger, M. D., Fassbender, K. (2016). Stimulation of TLR4 Attenuates Alzheimer's Disease-Related Symptoms and Pathology in Tau-Transgenic Mice. *J Immunol*, 197(8), 3281-3292. doi:10.4049/jimmunol.1600873
- Quan, W., Luo, Q., Tang, Q., Furihata, T., Li, D., Fassbender, K., & Liu, Y. (2020). NLRP3 Is Involved in the Maintenance of Cerebral Pericytes. *Frontiers in Cellular Neuroscience*, 14(276). doi:10.3389/fncel.2020.00276
- Radde, R., Bolmont, T., Kaeser, S. A., Coomaraswamy, J., Lindau, D., Stoltze, L., Jucker,

-
- M. (2006). Abeta42-driven cerebral amyloidosis in transgenic mice reveals early and robust pathology. *EMBO Rep*, 7(9), 940-946. doi:10.1038/sj.embor.7400784
- Raj, A., E. LoCastro, A. Kuceyeski, D. Tosun, N. Relkin, M. Weiner and I. Alzheimer's Disease Neuroimaging (2015). "Network Diffusion Model of Progression Predicts Longitudinal Patterns of Atrophy and Metabolism in Alzheimer's Disease." *Cell Rep* 10(3): 359-369.
- Rangasamy, S. B., Jana, M., Roy, A., Corbett, G. T., Kundu, M., Chandra, S., Pahan, K. (2018). Selective disruption of TLR2-MyD88 interaction inhibits inflammation and attenuates Alzheimer's pathology. *J Clin Invest*, 128(10), 4297-4312.
- Rangel, R., Sun, Y., Guzman-Rojas, L., Ozawa, M. G., Sun, J., Giordano, R. J., Pasqualini, R. (2007). Impaired angiogenesis in aminopeptidase N-null mice. *Proc Natl Acad Sci U S A*, 104(11), 4588-4593. doi:10.1073/pnas.0611653104
- Rapoport, M., H. N. Dawson, L. I. Binder, M. P. Vitek and A. Ferreira (2002). "Tau is essential to beta -amyloid-induced neurotoxicity." *Proc Natl Acad Sci U S A* 99(9): 6364-6369.
- Reed-Geaghan, E. G., Q. W. Reed, P. E. Cramer and G. E. Landreth (2010). "Deletion of CD14 attenuates Alzheimer's disease pathology by influencing the brain's inflammatory milieu." *J Neurosci* 30(46): 15369-15373.
- Reed-Geaghan, E. G., J. C. Savage, A. G. Hise and G. E. Landreth (2009). "CD14 and toll-like receptors 2 and 4 are required for fibrillar A{beta}-stimulated microglial activation." *J Neurosci* 29(38): 11982-11992.
- Roberts, K. F., Elbert, D. L., Kasten, T. P., Patterson, B. W., Sigurdson, W. C., Connors, R. E.,... Bateman, R. J. (2014). Amyloid-beta efflux from the central nervous system into the plasma. *Ann Neurol*, 76(6), 837-844. doi:10.1002/ana.24270
- Roher, A. E., C. Esh, T. A. Kokjohn, W. Kalback, D. C. Luehrs, J. D. Seward, L. I. Sue and T. G. Beach (2003). "Circle of willis atherosclerosis is a risk factor for sporadic Alzheimer's disease." *Arterioscler Thromb Vasc Biol* 23(11): 2055-2062.
- Roher, A. E., C. Esh, A. Rahman, T. A. Kokjohn and T. G. Beach (2004). "Atherosclerosis of cerebral arteries in Alzheimer disease." *Stroke* 35(11 Suppl 1): 2623-2627.

-
- Sagare, A. P., Bell, R. D., Zhao, Z., Ma, Q., Winkler, E. A., Ramanathan, A., & Zlokovic, B.V. (2013). Pericyte loss influences Alzheimer-like neurodegeneration in mice. *Nat Commun*, 4, 2932. doi:10.1038/ncomms3932.
- Satoh JI, Kino Y, Yanaizu M, Ishida T, Saito Y. Microglia express gamma-interferon-inducible lysosomal thiol reductase in the brains of Alzheimer's disease and Nasu-Hakola disease. *Intractable Rare Dis Res*. 2018;7(4):251-257. doi:10.5582/irdr.2018.01119.
- Sarlus, H. and M. T. Heneka (2017). "Microglia in Alzheimer's disease." *J Clin Invest* 127(9): 3240-3249.
- Scheltens, P., B. De Strooper, M. Kivipelto, H. Holstege, G. Chételat, C. E. Teunissen, J. Cummings and W. M. van der Flier (2021). "Alzheimer's disease." *The Lancet*.
- Schnöder, L., Gasparoni, G., Nordstrom, K., Schottek, A., Tomic, I., Christmann, A., Liu, Y. (2020). Neuronal deficiency of p38alpha-MAPK ameliorates symptoms and pathology of APP or Tau-transgenic Alzheimer's mouse models. *FASEB J*. doi:10.1096/fj.201902731RR
- Schnöder, L., Hao, W., Qin, Y., Liu, S., Tomic, I., Liu, X., . . . Liu, Y. (2016). Deficiency of Neuronal p38alpha MAPK Attenuates Amyloid Pathology in Alzheimer Disease Mouse and Cell Models through Facilitating Lysosomal Degradation of BACE1. *J Biol Chem*, 291(5), 2067-2079. doi:10.1074/jbc.M115.695916
- Scholtzova, H., Chianchiano, P., Pan, J., Sun, Y., Goñi, F., Mehta, P. D., & Wisniewski, T. (2014). Amyloid β and Tau Alzheimer's disease related pathology is reduced by Toll-like receptor 9 stimulation. *Acta Neuropathologica Communications*, 2(1), 101. doi:10.1186/s40478-014-0101-2
- Schroeder, P., Rivalan, M., Zaqout, S., Kruger, C., Schuler, J., Long, M., . . . Lehnardt, S. (2021). Abnormal brain structure and behavior in MyD88-deficient mice. *Brain Behav Immun*, 91, 181-193. doi:10.1016/j.bbi.2020.09.024
- Sengillo, J. D., Winkler, E. A., Walker, C. T., Sullivan, J. S., Johnson, M., & Zlokovic, B. V. (2013). Deficiency in mural vascular cells coincides with blood-brain barrier disruption in Alzheimer's disease. *Brain Pathol*, 23(3), 303-310. doi:10.1111/bpa.12004

-
- Shankar, G. M., Li, S., Mehta, T. H., Garcia-Munoz, A., Shepardson, N. E., Smith, I., . . . Selkoe, D. J. (2008). Amyloid-beta protein dimers isolated directly from Alzheimer's brains impair synaptic plasticity and memory. *Nat Med*, 14(8), 837-842. doi:10.1038/nm1782
- Shen, Y., H. Qin, J. Chen, L. Mou, Y. He, Y. Yan, H. Zhou, Y. Lv, Z. Chen, J. Wang and Y. D. Zhou (2016). "Postnatal activation of TLR4 in astrocytes promotes excitatory synaptogenesis in hippocampal neurons." *J Cell Biol* 215(5): 719-734.
- Shi, H., Y. Koronyo, A. Rentsendorj, G. C. Regis, J. Sheyn, D. T. Fuchs, A. A. Kramerov, A. V. Ljubimov, O. M. Dumitrascu, A. R. Rodriguez, E. Barron, D. R. Hinton, K. L. Black, C. A. Miller, N. Mirzaei and M. Koronyo-Hamaoui (2020). "Identification of early pericyte loss and vascular amyloidosis in Alzheimer's disease retina." *Acta Neuropathol* 139(5): 813-836.
- Shibata, M., Yamada, S., Kumar, S. R., Calero, M., Bading, J., Frangione, B., . . . Zlokovic, B. V. (2000). Clearance of Alzheimer's amyloid-ss(1-40) peptide from brain by LDL receptor-related protein-1 at the blood-brain barrier. *J Clin Invest*, 106(12), 1489-1499. doi:10.1172/JCI10498.
- Shinohara, M., Tachibana, M., Kanekiyo, T., & Bu, G. (2017). Role of LRP1 in the pathogenesis of Alzheimer's disease: evidence from clinical and preclinical studies. *J Lipid Res*, 58(7), 1267-1281. doi:10.1194/jlr.R075796.
- Skillbäck T, Delsing L, Synnergren J, et al. CSF/serum albumin ratio in dementias: a cross-sectional study on 1861 patients. *Neurobiol Aging*. 2017;59:1-9. doi:10.1016/j.neurobiolaging.2017.06.028.
- Silva J, Ferreira R, Trigo D. Glymphatic system, AQP4, and their implications in Alzheimer's disease. *Neurol Res Pract*. 2021;3(1):5. Published 2021 Jan 19. doi:10.1186/s42466-021-00102-7.
- Song, M., Jin, J., Lim, J. E., Kou, J., Pattanayak, A., Rehman, J. A., . . . Fukuchi, K. (2011). TLR4 mutation reduces microglial activation, increases Abeta deposits and exacerbates cognitive deficits in a mouse model of Alzheimer's disease. *J Neuroinflammation*, 8, 92. doi:10.1186/1742-2094-8-92.
- Spangenberg, E., P. L. Severson, L. A. Hohsfield, J. Crapser, J. Zhang, E. A. Burton, Y. Zhang, W. ... B. L. West and K. N. Green (2019). "Sustained microglial depletion with CSF1R

- inhibitor impairs parenchymal plaque development in an Alzheimer's disease model." *Nat Commun* 10(1): 3758.
- Spangenberg, E. E., Lee, R. J., Najafi, A. R., Rice, R. A., Elmore, M. R., Blurton-Jones, M., ... Green, K. N. (2016). Eliminating microglia in Alzheimer's mice prevents neuronal loss without modulating amyloid-beta pathology. *Brain*, 139(Pt 4), 1265-1281.
- Stakos, D. A., Stamatelopoulos, K., Bampatsias, D., Sachse, M., Zormpas, E., Vlachogiannis, N. I., ... Stellos, K. (2020). The Alzheimer's Disease Amyloid-Beta Hypothesis in Cardiovascular Aging and Disease: JACC Focus Seminar. *J Am Coll Cardiol*, 75(8), 952-967. doi:10.1016/j.jacc.2019.12.033
- Stancu, I. C., Cremers, N., Vanrusselt, H., Couturier, J., Vanoosthuyse, A., Kessels, S., Lodder, C., Brône, B., Huaux, F., Octave, J. N., Terwel, D., & Dewachter, I. (2019). Aggregated Tau activates NLRP3-ASC inflammasome exacerbating exogenously seeded and non-exogenously seeded Tau pathology in vivo. *Acta neuropathologica*, 137(4), 599–617.
- Stern, R. A., C. H. Adler, K. Chen, M. Navitsky, J. Luo, D. W. Dodick, M. L. Alosco, Y. Tripodis, D. D. Goradia, B. Martin, D. Mastroeni, N. G. Fritts, J. Jarnagin, M. D. Devous, Sr., M. A. Mintun, M. J. Pontecorvo, M. E. Shenton and E. M. Reiman (2019). "Tau Positron-Emission Tomography in Former National Football League Players." *N Engl J Med* 380(18): 1716-1725.
- Stewart, C. R., L. M. Stuart, K. Wilkinson, J. M. van Gils, J. Deng, A. Halle, K. J. Rayner, L. Boyer, R. Zhong, W. A. Frazier, A. Lacy-Hulbert, J. El Khoury, D. T. Golenbock and K. J. Moore (2010). "CD36 ligands promote sterile inflammation through assembly of a Toll-like receptor 4 and 6 heterodimer." *Nat Immunol* 11(2): 155-161.
- Storck, S. E., Meister, S., Nahrath, J., Meissner, J. N., Schubert, N., Di Spiezio, A., . . . Pietrzik, C. U. (2016). Endothelial LRP1 transports amyloid-beta(1-42) across the blood-brain barrier. *J Clin Invest*, 126(1), 123-136.
- Sweeney, M. D., Ayyadurai, S., & Zlokovic, B. V. (2016). Pericytes of the neurovascular unit: key functions and signaling pathways. *Nat Neurosci*, 19(6), 771-783.
- Sun, X., W. D. Chen and Y. D. Wang (2015). "beta-Amyloid: the key peptide in the pathogenesis of Alzheimer's disease." *Front Pharmacol* 6: 221.

-
- Sweeney, M. D., S. Ayyadurai and B. V. Zlokovic (2016). "Pericytes of the neurovascular unit: key functions and signaling pathways." *Nat Neurosci* 19(6): 771-783.
- Sweeney, M. D., A. Montagne, A. P. Sagare, D. A. Nation, L. S. Schneider, H. C. Chui, M. G. Harrington, ... J. M. Wardlaw and B. V. Zlokovic (2019). "Vascular dysfunction-The disregarded partner of Alzheimer's disease." *Alzheimers Dement* 15(1): 158-167.
- Sweeney, M. D., A. P. Sagare and B. V. Zlokovic (2018). "Blood-brain barrier breakdown in Alzheimer disease and other neurodegenerative disorders." *Nat Rev Neurol* 14(3): 133-150.
- Swardfager, W., Lanctôt, K., Rothenburg, L., Wong, A., Cappell, J., & Herrmann, N. (2010). A meta-analysis of cytokines in Alzheimer's disease. *Biological psychiatry*, 68(10), 930–941. <https://doi.org/10.1016/j.biopsych.2010.06.012>
- Tahara, K., H. D. Kim, J. J. Jin, J. A. Maxwell, L. Li and K. Fukuchi (2006). "Role of toll-like receptor signalling in Abeta uptake and clearance." *Brain* 129(Pt 11): 3006-3019.
- Tanifum, E. A., Starosolski, Z. A., Fowler, S. W., Jankowsky, J. L., & Annapragada, A. V. (2014). Cerebral vascular leak in a mouse model of amyloid neuropathology. *J Cereb Blood Flow Metab*, 34(10), 1646-1654. doi:10.1038/jcbfm.2014.125
- Tanzi, R. E., R. D. Moir and S. L. Wagner (2004). "Clearance of Alzheimer's Abeta peptide: the many roads to perdition." *Neuron* 43(5): 605-608.
- Tarasoff-Conway, J. M., R. O. Carare, R. S. Osorio, L. Glodzik, T. Butler, E. Fieremans, L. Axel, H. Rusinek, C. Nicholson, B. V. Zlokovic, B. Frangione, K. Blennow, J. Menard, H. Zetterberg, T. Wisniewski and M. J. de Leon (2015). "Clearance systems in the brain-implications for Alzheimer disease." *Nat Rev Neurol* 11(8): 457-470.
- Thomas JL, Jacob L, Boisserand L. Système lymphatique et cerveau [Lymphatic system in central nervous system]. *Med Sci (Paris)*. 2019;35(1):55-61. doi:10.1051/medsci/2018309.
- Timmers, M., I. Tesseur, J. Bogert, H. Zetterberg, K. Blennow, A. Borjesson-Hanson, M. Baquero, M. Boada, C. Randolph, L. Tritsmans, L. Van Nueten, S. Engelborghs and J. R. Streffer (2019). "Relevance of the interplay between amyloid and tau for cognitive impairment in early Alzheimer's disease." *Neurobiol Aging* 79: 131-141.

-
- Ulland, T. K., Song, W. M., Huang, S. C., Ulrich, J. D., Sergushichev, A., Beatty, W. L., . . . Colonna, M. (2017). TREM2 Maintains Microglial Metabolic Fitness in Alzheimer's Disease. *Cell*, 170(4), 649-663 e613. doi:10.1016/j.cell.2017.07.023
- Umehara, K., Sun, Y., Hiura, S., Hamada, K., Itoh, M., Kitamura, K., . . . Furihata, T. (2018). A New Conditionally Immortalized Human Fetal Brain Pericyte Cell Line: Establishment and Functional Characterization as a Promising Tool for Human Brain Pericyte Studies. *Molecular Neurobiology*, 55(7), 5993-6006. doi:10.1007/s12035-017-0815-9
- Vannella, K. M., & Wynn, T. A. (2017). Mechanisms of Organ Injury and Repair by Macrophages. *Annu Rev Physiol*, 79, 593-617. doi:10.1146/annurev-physiol-022516-034356
- Van Gool, B., S. E. Storck, S. M. Reekmans, B. Lechat, P. Gordts, L. Pradier, C. U. Pietrzik and A. J. M. Roebroek (2019). "LRP1 Has a Predominant Role in Production over Clearance of Abeta in a Mouse Model of Alzheimer's Disease." *Mol Neurobiol* 56(10): 7234-7245.
- Venegas, C. and M. T. Heneka (2019). "Inflammasome-mediated innate immunity in Alzheimer's disease." *FASEB J* 33(12): 13075-13084.
- Vilchez, D., I. Saez and A. Dillin (2014). "The role of protein clearance mechanisms in organismal ageing and age-related diseases." *Nat Commun* 5: 5659.
- Wang, D. S., N. Iwata, E. Hama, T. C. Saido and D. W. Dickson (2003). "Oxidized neprilysin in aging and Alzheimer's disease brains." *Biochem Biophys Res Commun* 310(1): 236-241.
- Wang, J. Z. and F. Liu (2008). "Microtubule-associated protein tau in development, degeneration and protection of neurons." *Prog Neurobiol* 85(2): 148-175.
- Wang, L., T. L. Benzinger, Y. Su, J. Christensen, K. Friedrichsen, P. Aldea, J. McConathy, N. J. Cairns, A. M. Fagan, J. C. Morris and B. M. Ances (2016). "Evaluation of Tau Imaging in Staging Alzheimer Disease and Revealing Interactions Between beta-Amyloid and Tauopathy." *JAMA Neurol* 73(9): 1070-1077.
- Wang, S., F. He and Y. Wang (2015). "Association Between Polymorphisms of the Insulin-Degrading Enzyme Gene and Late-Onset Alzheimer Disease." *Journal of Geriatric Psychiatry and Neurology* 28(2): 94-98.

-
- Wang, Y., Cella, M., Mallinson, K., Ulrich, J. D., Young, K. L., Robinette, M. L., . . . Colonna, M. (2015). TREM2 lipid sensing sustains the microglial response in an Alzheimer's disease model. *Cell*, 160(6), 1061-1071. doi:10.1016/j.cell.2015.01.049
- Wang, Y. and E. Mandelkow (2016). "Tau in physiology and pathology." *Nat Rev Neurosci* 17(1): 5-21.
- Wardlaw, J. M., S. J. Makin, M. C. V. Hernandez, P. A. Armitage, A. K. Heye, F. M. Chappell, S. Munoz-Maniega, E. Sakka, K. Shuler, M. S. Dennis and M. J. Thruppelton (2017). "Blood-brain barrier failure as a core mechanism in cerebral small vessel disease and dementia: evidence from a cohort study." *Alzheimers & Dementia* 13(6): 634-643.
- Watanabe, C., Imaizumi, T., Kawai, H., Suda, K., Honma, Y., Ichihashi, M., . . . Mizutani, K.I. (2020). Aging of the Vascular System and Neural Diseases. *Front Aging Neurosci*, 12, 557384. doi:10.3389/fnagi.2020.557384
- Weitz, T. M., D. Gate, K. Rezai-Zadeh and T. Town (2014). "MyD88 is dispensable for cerebral amyloidosis and neuroinflammation in APP/PS1 transgenic mice." *Am J Pathol* 184(11): 2855-2861.
- Wildsmith, K. R., M. Holley, J. C. Savage, R. Skerrett and G. E. Landreth (2013). "Evidence for impaired amyloid beta clearance in Alzheimer's disease." *Alzheimers Res Ther* 5(4): 33.
- Wolters, F. J., H. I. Zonneveld, A. Hofman, A. van der Lugt, P. J. Koudstaal, M. W. Vernooij, M. A. Ikram and G. Heart-Brain Connection Collaborative Research (2017). "Cerebral Perfusion and the Risk of Dementia: A Population-Based Study." *Circulation* 136(8): 719-728.
- Yamazaki Y, Kanekiyo T. Blood-Brain Barrier Dysfunction and the Pathogenesis of Alzheimer's Disease. *Int J Mol Sci*. 2017;18(9):1965. Published 2017 Sep 13. doi:10.3390/ijms18091965.
- Yao, Q., Renault, M.A., Chapouly, C., Vandierdonck, S., Belloc, I., Jaspard-Vinassa, B., Daniel-Lamaziere, J.M., Laffargue, M., Merched, A., Desgranges, C., Gadeau, A.P., 2014. Sonic hedgehog mediates a novel pathway of PDGF-BB-dependent vessel maturation. *Blood* 123, 2429-2437.

-
- Yasojima, K., E. G. McGeer and P. L. McGeer (2001). Relationship between beta amyloid peptide generating molecules and neprilysin in Alzheimer disease and normal brain. *Brain Res* 919(1): 115-121.
- Yoo HS, Lee EC, Chung SJ, et al. Effects of Alzheimer's disease and Lewy body disease on subcortical atrophy. *Eur J Neurol*. 2020;27(2):318-326. doi:10.1111/ene.14080.
- Yu, W. H., A. M. Cuervo, A. Kumar, C. M. Peterhoff, S. D. Schmidt, J. H. Lee, P. S. Mohan, M. Mercken, M. R. Farmery, L. O. Tjernberg, Y. Jiang, K. Duff, Y. Uchiyama, J. Naslund, P. M. Mathews, A. M. Cataldo and R. A. Nixon (2005). "Macroautophagy--a novel Beta-amyloid peptide-generating pathway activated in Alzheimer's disease." *J Cell Biol* 171(1): 87-98.
- Yuan, P., C. Condello, C. D. Keene, Y. Wang, T. D. Bird, S. M. Paul, W. Luo, M. Colonna, D. Baddeley and J. Grutzendler (2016). "TREM2 Haplodeficiency in Mice and Humans Impairs the Microglia Barrier Function Leading to Decreased Amyloid Compaction and Severe Axonal Dystrophy." *Neuron* 90(4): 724-739.
- Yun, J.H., Jeong, H.S., Kim, K.J., Han, M.H., Lee, E.H., Lee, K., Cho, C.H., 2018. beta-Adrenergic receptor agonists attenuate pericyte loss in diabetic retinas through Akt activation. *FASEB J* 32, 2324-2338.
- Zhao, Z., A. R. Nelson, C. Betsholtz and B. V. Zlokovic (2015). "Establishment and Dysfunction of the Blood-Brain Barrier." *Cell* 163(5): 1064-1078.
- Zilka, N., Z. Kazmerova, S. Jadhav, P. Neradil, A. Madari, D. Obetkova, O. Bugos and M. Novak (2012). Who fans the flames of Alzheimer's disease brains? Misfolded tau on the crossroad of neurodegenerative and inflammatory pathways. *J Neuroinflammation* 9: 47.
- Zudaire, E., Gambardella, L., Kurcz, C., & Vermeren, S. (2011). A computational tool for quantitative analysis of vascular networks. *PLoS One*, 6(11), e27385.

LIST OF FIGURES AND COOPERATIONS

PART I	
PART I Figure 1.1	Imaging of AD patients. From: Scheltens, De Strooper et al. 2021.
PART I Figure 1.2	APP processing and Aβ toxicity. From: Sun, Chen et al. 2015.
PART I Figure 1.3	Various pathways involved in removal of Aβ in the brain. From: Tanzi, Moir et al. 2004.
PART I Figure 1.4	Glymphatic system, neurovascular unit (NVU), and the blood-brain-barrier(BBB). From: Natale G, et al.Front Neurosci 2021.
PART I Figure 1.5	Microglia ontogeny and their physiological role in normal and pathological conditions. From: Gogoleva, Drutskaya et al. 2019.
PART I Figure 1.6	TLRs signaling pathway involved in innate immunity. From: Kawai and Akira ,2010
PART I Figure 3.1	APP/PS1-transgenic mice with deficiency of myd88 in microglia. Picture from: Alex Liu
PART I Figure 3.2	Morris water maze test. From: De Castell, S et al. 2015.
PART I Figure 3.3	Schematic figure of brain sample sections preparation. Picture from: Shirong Liu
PART I Figure 3.4	Summary Scheme of the Brain Vessel Purification Protocol From: Boulay, A.C et al. 2015.
PART I Figure 3.5	AngioTool's GUI and analysis flow. From: Zudaire E, et al. 2011.
PART I Figure 4.1	Establishment of APP/PS1-transgenic mice with haploinsufficiency of MyD88 in microglia. Tamoxifen injection:Wenqiang Quan and Alex Liu
PART I Figure 4.2	Haploinsufficiency of microglial MyD88 improves cognitive function in APP/PS1-transgenic mice. Water Maze and analysis: Wenqiang Quan and Alex Liu
PART I Figure 4.3	Haploinsufficiency of microglial MyD88 attenuates AD-associated loss of synaptic proteins in APP/PS1-transgenic mice. Western blot and analysis:Wenqiang Quan
PART I Figure 4.4	Haploinsufficiency of microglial MyD88 reduces cerebral Aβ load in APP/PS1-transgenic mice. Tissue collection and cutting; Immunohistochemistry and Immunofluorescence; Data analysis: Wenqiang Quan; Western blot: Inge Tomic; Data analysis: Alex Liu
PART I Figure 4.5	Haploinsufficient expression of MyD88 in microglia reduces Aβ load in the brain blood vessels of APP/PS1-transgenic mice. Blood vessles isolation; Western blot and analysis:Wenqiang Quan; Immunofluorescence:Qinghua Luo
PART I Figure 4.6	Haploinsufficient expression of MyD88 in microglia inhibits inflammatory activation in the brain of APP-transgenic mice. Realtime PCR:Wenqiang Quan and Alex Liu; Immunofluorescence:Qinghua Luo
PART I Figure 4.7	Haploinsufficient expression of MyD88 inhibits pro-inflammatory activation in microglia and enhances microglial responses to Aβ deposits in the brain of APP-

LIST OF FIGURES AND COOPERATIONS

	<p>transgenic mice. Realtime PCR:Wenqiang Quan and Alex Liu;Immunofluorescence and analysis:Wenqiang Quan and Qinghua Luo</p>
PART I Figure 4.8	<p>Haploinsufficiency of microglial MyD88 in microglia increases cerebral vasculature of APP/PS1-transgenic mice. Immunofluorescence and blood vessels analysis:Wenqiang Quan</p>
PART I Figure 4.9a	<p>Haploinsufficiency of microglial MyD88 significantly increased the distribution of microglia around blood vessels of APP/PS1-transgenic mice. Immunofluorescence and analysis: Wenqiang Quan and Qinghua Luo</p>
PART I Figure 4.9b	<p>Haploinsufficiency of MyD88 in microglia did not change the integrity of BBB in APP/PS1-transgenic mice. Western blot: Inge Tomic; Data analysis: Alex Liu</p>
PART I Figure 4.10	<p>Haploinsufficiency of microglial MyD88 increases LRP1 in cerebral microvessels of APP/PS1-transgenic mice. Blood vessels isolation; Western blot and analysis:Wenqiang Quan</p>
PART I Figure 4.11	<p>IL-1β treatment decreases LRP1 in cultured pericytes. Cell culture ; Western blot and analysis:Wenqiang Quan</p>
PART I Figure 4.12	<p>Haploinsufficiency of MyD88 in microglia decreases β- and γ-secretase activity, but does not affect the transcription of neprilysin and ide genes in the brain of APP/PS1-transgenic mice. Secretase activity assay and data analysis: Wenqiang Quan</p>
PART II	
PART II Figure 1.1	<p>Pathology of Alzheimer's disease. From: Lane CA,et al. 2018.</p>
PART II Figure 1.2	<p>The multifunctional role of pericytes in the CNS. From: Sweeney, Ayyadurai et al. 2016.</p>
PART II Figure 1.3	<p>The mechanisms of NLRP3 inflammasome activation. From: Feng YS et al. 2021.</p>
PART II Figure 3.1	<p>NLRP3 deficiency reduces pericyte cell coverage and decreases protein levels of PDGFRβ and CD13 in the brain. Immunofluorescence ; blood vessels isolation and Western blot analysis:Wenqiang Quan and Qinghua Luo</p>
PART II Figure 3.2	<p>NLRP3 deficiency reduces vasculature in the brain. Immunofluorescence and vessels analysis:Wenqiang Quan</p>
PART II Figure 3.3	<p>NLRP3 inhibition attenuates cell proliferation in cultured pericytes. Cell culture ; Western blot and analysis:Wenqiang Quan</p>
PART II Figure 3.4	<p>NLRP3 inhibition attenuates protein expression of PDGFRβ and CD13 and inhibits phosphorylation of AKT and ERK in cultured pericytes.. Cell culture ; Western blot and analysis:Wenqiang Quan</p>
PART II Figure 3.5	<p>IL-1β increases protein expression of PDGFRβ and CD13 in cultured pericytes. Cell culture ; Western blot and analysis:Wenqiang Quan</p>
PART II Figure 3.6a	<p>NLRP3 deficiency increases the pericyte cell coverage in cerebral blood vessels of Tau-transgenic mice. Immunofluorescence and blood vessels analysis:Wenqiang Quan and Alex Liu</p>
PART II Figure 3.6b	<p>NLRP3 deficiency increases the vasculature in the brain of Tau-transgenic mice. Immunofluorescence and blood vessels analysis:Wenqiang Quan and Alex Liu</p>

LIST OF FIGURES AND COOPERATIONS

PART II Figure 3.7	TLR1, TLR2 and TLR4 are highly expressed on pericytes in APP-transgenic mouse brain. FACS and analysis:Wenqiang Quan and Alex Liu
PART II Figure 3.8	Deficiency of MyD88 in pericytes reduces Aβ deposits in association with increased pericyte markers in the brain of APP-transgenic mice. Immunofluorescence ; Western blot and analysis:Wenqiang Quan

PUBLICATIONS

1. **Quan W**, Luo Q, Hao W, Tomic I, Furihata T, Schulz-Schäffer W, Menger MD, Fassbender K, Liu Y. Haploinsufficiency of microglial MyD88 ameliorates Alzheimer's pathology and vascular disorders in APP/PS1-transgenic mice. *Glia*. 2021;69(8):1987-2005. doi:10.1002/glia.24007.
2. **Quan W**, Luo Q, Tang Q, Furihata T, Li D, Fassbender K, Liu Y. NLRP3 Is Involved in the Maintenance of Cerebral Pericytes. *Front Cell Neurosci*. 2020 Aug 21;14:276. doi: 10.3389/fncel.2020.00276.
3. Liu W, Yang D, Chen L, Liu Q, Wang W, Yang Z, Shang A, **Quan W**(Co- corresponding author), Li D. Plasma Exosomal miRNA-139-3p is a Novel Biomarker of Colorectal Cancer. *J Cancer*. 2020 Jun 15;11(16):4899–906. doi: 10.7150/jca.45548.
4. Yang D, **Quan W**(Co-first authorship), Wu J, Ji X, Dai Y, Xiao W, Chew H, Sun Z, Li D. The value of red blood cell distribution width in diagnosis of patients with colorectal cancer. *Clin Chim Acta*. 2018 Apr;479:98-102. doi: 10.1016/j.cca.2018.01.022.
5. Shang A, Gu C, Wang W, Wang X, Sun J, Zeng B, Chen C, Chang W, Ping Y, Ji P, Wu J, **Quan W**, Yao Y, Zhou Y, Sun Z, Li D. Exosomal circPACRGL promotes progression of colorectal cancer via the miR-142-3p/miR-506-3p- TGF- β 1 axis. *Mol Cancer*. 2020 Jul 27;19(1):117.
6. Wang X, Shao QH, Zhou H, Wu JL, **Quan WQ**, Ji P, Yao YW, Li D, Sun ZJ. Ginkgolide B inhibits lung cancer cells promotion via beclin-1-dependent autophagy. *BMC Complement Med Ther*. 2020 Jun 23;20(1):194. doi: 10.1186/s12906-020-02980-x.
7. Shang A, Wang X, Gu C, Liu W, Sun J, Zeng B, Chen C, Ji P, Wu J, **Quan W**, Yao Y, Wang W, Sun Z, Li D. Exosomal miR-183-5p promotes angiogenesis in colorectal cancer by regulation of FOXO1. *Aging (Albany NY)*. 2020 May 3;12(9):8352-8371. doi: 10.18632/aging.103145.

-
8. Wang X, Sun ZJ, Wu JL, **Quan WQ**, Xiao WD, Chew H, Jiang CM, Li D. Naloxone attenuates ischemic brain injury in rats through suppressing the NIK/IKK α /NF- κ B and neuronal apoptotic pathways. *Acta Pharmacol Sin.* 2019 Feb;40(2):170-179. doi: 10.1038/s41401-018-0053-3.
9. Ji P, Zhou Y, Yang Y, Wu J, Zhou H, **Quan W**, Sun J, Yao Y, Shang A, Gu C, Zeng B, Firman J, Xiao W, Bals R, Sun Z, Li D. Myeloid cell-derived LL-37 promotes lung cancer growth by activating Wnt/ β -catenin signaling. *Theranostics.* 2019 Apr 12;9(8):2209-2223. doi: 10.7150/thno.30726.
10. Yang Y, Ji P, Wang X, Zhou H, Wu J, **Quan W**, Shang A, Sun J, Gu C, Firman J, Xiao W, Sun Z, Li D. Bronchoalveolar Lavage Fluid-Derived Exosomes: A Novel Role Contributing to Lung Cancer Growth. *Front Oncol.* 2019 Apr 2;9:197. doi: 10.3389/fonc.2019.00197.
11. Xie L, Jiang X, Li Q, Sun Z, **Quan W**, Duan Y, Li D, Chen T. Diagnostic Value of Methylated *Septin9* for Colorectal Cancer Detection. *Front Oncol.* 2018 Jul 2;8:247. doi: 10.3389/fonc.2018.00247.
12. Li D, Sun J, Liu W, Wang X, Bals R, Wu J, **Quan W**, Yao Y, Zhang Y, Zhou H, Wu K. Rig-G is a growth inhibitory factor of lung cancer cells that suppresses STAT3 and NF- κ B. *Oncotarget.* 2016 Oct 4;7(40):66032-66050. doi: 10.18632/oncotarget.11797.
13. Li D, Liu W, Wang X, Wu J, **Quan W**, Yao Y, Bals R, Ji S, Wu K, Guo J, Wan H. Cathelicidin, an antimicrobial peptide produced by macrophages, promotes colon cancer by activating the Wnt/ β -catenin pathway. *Oncotarget.* 2015 Feb 20;6(5):2939-50. doi: 10.18632/oncotarget.2845.
14. Wang X, Jiang CM, Wan HY, Wu JL, **Quan WQ**, Wu KY, Li D. Neuroprotection against permanent focal cerebral ischemia by ginkgolides A and B is associated with obstruction of the mitochondrial apoptotic pathway via inhibition of c-Jun N-terminal kinase in rats. *J Neurosci Res.* 2014 Feb;92(2):232-42. doi: 10.1002/jnr.23306.

15. Li D, Wang X, Wu JL, **Quan WQ**, Ma L, Yang F, Wu KY, Wan HY. Tumor-produced versican V1 enhances hCAP18/LL-37 expression in macrophages through activation of TLR2 and vitamin D3 signaling to promote ovarian cancer progression in vitro. *PLoS One*. 2013;8(2):e56616. doi: 10.1371/journal.pone.0056616.

16. Wang X, Jiang CM, Wan HY, Wu JL, **Quan WQ**, Bals R, Wu KY, Li D. CDA-2, a urinary preparation, inhibits lung cancer development through the suppression of NF-kappaB activation in myeloid cell. *PLoS One*. 2012;7(12):e52117. doi: 10.1371/journal.pone.0052117.

ACKNOWLEDGEMENTS

Those who love drinking water will cherish the origin as the people always think of their teachers when succeed. More than four years of doctoral career will come to an end, at this moment, all sincere gratitude is so pale and feeble in words. But silent words always have the meaning of recording friendship. In the past four years, there have been so many people and things worthy of my gratitude and touch in Homburg.

First and foremost I place my sincerest gratitude and respect to my advisors Dr. Yang Liu , Prof. Dr. Klaus Fassbender and Prof. Dr. Matthias Laschke for their outstanding guidance in accomplishing this work. I express my grateful thanks to Dr. Yang Liu for his intelligence, motivation and patience in supporting my scientific career as well as personal life. I would also like to acknowledge Prof. Dr. Klaus Fassbender, who inspired the projects with his enthusiasm and immense knowledge. I am grateful to both of my mentors for their time and valuable discussions throughout the development of this dissertation.

Regarding this thesis, from the design of the subject to the completion of the guidance and the finalization of this thesis, all the hard work of Dr. Liu Yang has been condensed. During the most important four years of my research literacy growth, I was able to spend the harmonious and loving Dr. Liu's team, which was my most regretless choice. I was able to cultivate good thinking and working habits, and learn to communicate effectively with others and work together. When faced with any doubts and difficulties, I would not panic, but patiently discover, analyze and solve problems. Dr. Yang Liu's rigorous academic attitude and meticulous dedication to scientific research have deeply infected me, inspired me, and benefited me for life! Here, I not only gained a more perceptual and three-dimensional understanding of scientific research, but also gained a life-long friendship between teachers and students and a precious "partnership" relationship. Dr. Liu not only taught me how to do academic work, but also taught me how to be a kind, wise, humble, brave and grateful person.

If the teacher's grace is eternal, then Dr. Wenlin Hao, Dr. Laura Schnöder, Tomic Inge, Andrea Schottek, and Dr. Yann Decker, who are also teachers and friends, are like the most refreshing pot of wine, Dr Wenlin Hao's erudition and seriousness, Dr. Laura Schnöder's humor and warm heart, Tomic Inge and Andrea Schottek's rigorous and vigorous work Efficiency, Dr. Yann Decker's meticulous,...always fragrant and full of flavor. At the same time, I am also very

grateful to my first research teacher, Professor Dong Li from Tongji Hospital of Tongji University. Thank him for taking me into the door of scientific research and giving me the opportunity to work with these outstanding colleagues. I also would like to credit my friendly and cheerful colleagues in AG Fassbender for making a joy experience in the last four years. Special thanks must go to Dr. Laura Schnöder, who introduced me into this lab and assisted me in my German translation works. Dr. Yang Liu provided daily supportive guidance with his knowledge and experience. Dr. Wenlin Hao, Mrs. Andrea Schottek and Mrs. Inge Tomic provided the skillful technical support for the progress of the projects. Ms Qinghua Luo, Dr. Yann Decker, Mr. Axel Chemla and Ms. Kathrin Litzenburger, were my best neighbors in the office and offered me their supportive discussions and suggestions. I express my thanks to all my lab mates.

I also have to thank everyone I met in Homburg, Qinghua Luo, Yiwen Yao, Xiaoyu Cai, Weikun Meng, Qilin Guo, Xiangda Zhou, Qing Liu, Jia Guo, Xianshu Bai, Wenhui Huang.....thank you for your company over the past four years, we are together spent countless beautiful days, and we even went to every corner of Homburg. Time has made us our closest friends, thank you for having you in my life.

If friendship is a dazzling firework, and the flashes of that flash can illuminate my distant galaxy, then I will definitely walk incessantly and follow the freedom of dreams. Well, I also want to thank myself. For the past four years, I am grateful for my persistence and not giving up. I am grateful that every time a person wanders behind, I can find a reason for myself to still believe in the rainbow after the storm. If you spend it alone, should you like yourself and thank you for your growth? I want to thank myself for slowly learning to take care of myself, and slowly learning to listen to my inner voice. Everyone needs to keep getting to know their unknown self, and so do I. I am grateful that I have not stopped exploring myself in the annual ring of the years, and I am grateful that I have always believed in becoming a better version of myself.

Speaking of thanks, I always have endless words. There are many people to thank, and many things to thank. Finally, I want to deeply thank my family for their understanding and support

over these several years. It was your silent dedication, selfless dedication, and meticulous care that relieved my worries and enabled me to successfully complete my studies.

I would also like to appreciate Dr M. Jucker (Hertie Institute for Clinical Brain Research, Tübingen) for providing APP/PS1-transgenic mice and Dr M. Prinz (Department of Neuropathology, University of Freiburg, Freiburg) for Cx3Cr1-CreERT2 mice. I appreciate Elisabeth Gluding and Isabel Euler for their excellent technical assistance.

I want to gratefully acknowledge the sufficient financial support on my thesis projects from “SNOWBALL” , an EU Joint Programme for Neurodegenerative Disease (JPND; 01ED1617B; to YL and KF); Alzheimer Forschung Initiative e.V. (#18009; to YL) and Medical Faculty of Saarland University through HOMFOR2016 (to Y.L.).

Furthermore, I offer my regards to my wife for her love, kindness and support. Lastly, and most importantly, I owe my deepest gratitude to my parents for giving birth to me at the first place and supporting me spiritually throughout my life. To them I dedicate this dissertation.